

Spontaneous Article

Stratigraphic architecture of the Cenozoic Dugong Supersequence: implications for the late post-breakup development of the Eucla Basin, southern Australian continental margin

Martyn S. STOKER* , Simon P. HOLFORD and Jennifer M. TOTTERDELL

Australian School of Petroleum and Energy Resources, University of Adelaide, Adelaide, SA 5005, Australia.

*Corresponding author. Email: martyn.stoker@adelaide.edu.au

ABSTRACT: This study presents an appraisal of the Middle Eocene–Quaternary Dugong Supersequence of the Eucla Basin, offshore southern Australia. It combines details of the rock record with seismic-stratigraphical information, and the resulting stratigraphic framework provides constraints on the nature of the late post-breakup development of the southern Australian continental margin. It is well established that the onshore-to-mid-shelf succession comprises a predominantly aggrading-to-prograding unconformity-bounded succession of carbonate platform deposits; however, our analysis of the outer shelf–upper slope section challenges the widely held view that this shelf-margin wedge represents a distally steepened prograding carbonate ramp primarily modulated by global eustasy. Instead, our results show that the Middle Eocene–Quaternary succession is punctuated by a series of unconformities that reflect a persistent tectonic instability and differential vertical movements throughout the late post-breakup period, the genesis of which is most closely related to tectonic events. Moreover, the upper slope clinoform succession was constructed and shaped predominantly by alongslope processes, and four different contourite drift types are recognised based on their seismic-stratigraphic expression: elongate mounded drift (Quaternary); infill drift (Pliocene); plastered drift (Oligocene); and separated drift (Middle–Upper Eocene). The Quaternary drift – herein termed the ‘Eyre Terrace Drift’ – is a spectacular basin-scale deposit, over 500 m thick and traced for up to 200 km along the upper slope Eyre Terrace. Upslope-migrating sediment waves are associated with this drift. Key sedimentary attributes consistent with a contourite origin include fine-grained sediment, multi-scale gradational bed contacts and pervasive bioturbation. There is also evidence of episodic downslope mass-movement processes ranging from the large-scale Late Neogene Slide, which extends downslope for 15–20 km, to sporadic slumped beds and turbidites recovered in boreholes. The interaction of alongslope and downslope processes indicates a more dynamic sedimentary setting than previously assumed along the outer margin of the Eucla Basin.

KEY WORDS: carbonate platform, contourite drift, Eyre Terrace, Great Australian Bight, Late Neogene Slide, outer shelf, upper slope.

The Cenozoic Eucla Basin is a large onshore–offshore sedimentary basin located along the western and central parts of the southern Australian passive continental margin (Fig. 1). It extends approximately 2000 km E–W and up to 700 km N–S, reaching southwards from inland of the Nullarbor Plain onto and across the continental shelf, slope and rise, commonly referred to as the Great Australian Bight (GAB) (Bradshaw *et al.* 2003; Clarke *et al.* 2003). The continental shelf offshore southern Australia is at its widest (up to 200 km) in the GAB where it is termed the Nullarbor Shelf (Bradshaw *et al.* 2003) (Fig. 1). The shelfbreak is generally located between 130 and 180 m water depth. The adjacent slope is divided into a gently dipping (up to 1°) upper slope, including the Eyre and Ceduna terraces, and a steeper dipping (up to 4°) lower slope (a zone of sediment bypass) that flattens onto the continental rise (the Yalata Sub-basin of Bradshaw *et al.* 2003). Submarine canyons are a common feature of much of the continental

slope of the GAB and are especially prevalent on its eastern side, extending upslope from the continental rise across the Ceduna Terrace up to the present-day shelfbreak (Talukder *et al.* 2021) (Fig. 2a).

The Middle Eocene–Pleistocene Dugong Supersequence represents the bulk of the fill of the Eucla Basin (Totterdell *et al.* 2000; Totterdell & Krassay 2003). This includes a highly distinctive, aggrading, Middle Eocene–Middle Miocene cool-water carbonate platform succession that has been traced continuously from the Bunda Plateau and Nullarbor Plain onto the Nullarbor Shelf and includes a spectacular buried Mid-Miocene reef (the ‘Little Barrier Reef’) up to 300 m high (Feary & James 1995, 1998). Seaward of the buried reef, the Dugong Supersequence comprises several unconformity-bounded Neogene–Quaternary depositional sequences that are exclusive to the outer shelf and upper slope; these have been described, collectively, as a southward-prograding package of



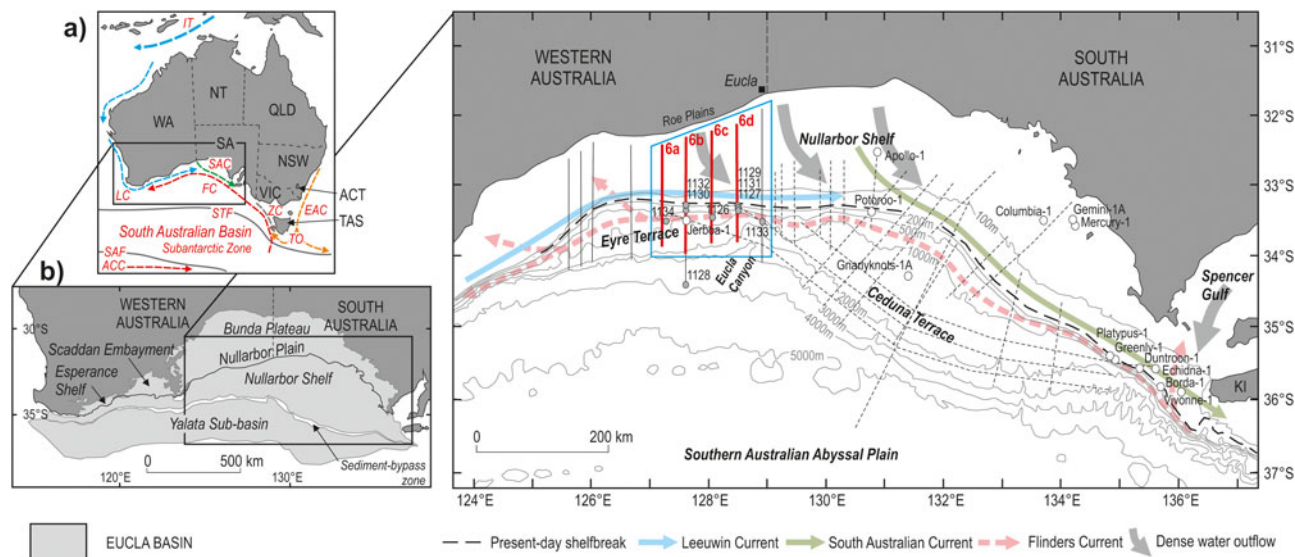


Figure 1 GAB location map showing geographic locations, bathymetry, wells (white circles), ODP boreholes (grey circles) and seismic lines used (solid black and red lines – JNOC 1990 survey) or referred to (dashed lines) in this study, as well as the main oceanographic elements that are potentially sedimentologically significant on the outer shelf and upper slope. Inset (a) shows regional setting of the Eucla Basin (oceanographic abbreviations (red text): ACC, Antarctic Circumpolar Current; EAC, East Australian Current; FC, Flinders Current; LC, Leeuwin Current; SAC, South Australian Current; SAF, Subantarctic Front; STF, Subtropical Front; TO, Tasman Outflow; ZC, Zeehan Current); inset (b) shows the onshore–offshore extent and structural subdivision of the Eucla Basin as defined by Bradshaw *et al.* (2003). Oceanographic data based on James *et al.* (2001), Ridgeway & Condie (2004), Middleton & Bye (2007), Anderskov *et al.* (2010) and Richardson *et al.* (2019). Bathymetric contours were generated from GeoMapApp (<http://www.geomapp.org>) using the Global Multi-Resolution Topography (GMRT) Synthesis (Ryan *et al.* 2009). Seismic data were supplied by PGS (as part of their Southern Australian Margin Digital Atlas), which we gratefully acknowledge. Bold red lines show location of profiles in Figure 6a–d. Blue box represents main area of study.

sigmoidal clinoforms that form a distally steepened carbonate ramp (James & von der Borch 1991; James *et al.* 1994; Feary & James 1995, 1998; Feary *et al.* 2004). The established view is that growth of this prograding package was controlled by the episodic delivery of sediment directly from the Nullarbor Shelf onto the upper slope, primarily in response to eustatic sea-level fluctuations, albeit complicated by local tectonics (James & von der Borch 1991; Feary & James 1995, 1998; Li *et al.* 2004).

By way of contrast, there is increasing evidence that the overall mounded geometry and internal characteristics of the predominantly Pleistocene upper-slope sedimentary wedge are more reminiscent of contourite sediment drifts (Huuse & Feary 2005). Characteristic features include shelfward-migrating sediment waves formerly and variably interpreted as slumps (James & von der Borch 1991), biogenic (bryozoan) mounds (Feary & James 1995, 1998) and, more recently, sediment waves (Anderskov *et al.* 2010). Contourite drifts characteristically form by upslope (shelfward) accretion of sediment driven by contour-following oceanic bottom currents (Stow *et al.* 2002). Eustatic sea-level fluctuations may influence the growth of contourite drifts to some degree, as they partly control the nature and volume of sediment supply, the nature and generation of different water masses (shallow and deep) and the oceanic circulation pattern; however, there are no unequivocal data that causally link sea level with rates of drift accumulation (Faugères & Stow 2008). Whereas Feary & James (1998) interpret the mounded Pleistocene upper slope deposits as a lowstand sequence resulting from repeated high-amplitude short-period sea-level fluctuations, a contourite-drift interpretation that involves upslope progradation does not neatly fit a highstand, lowstand or intermediate position in a eustasy-driven model (Faugères *et al.* 1999; Faugères & Stow 2008). Based on biostratigraphic data, it has been suggested that ocean current activity in the GAB was initiated in the Mid-Eocene (e.g., McGowran *et al.* 1997) – a scenario supported by the recent discovery of probable Mid-Eocene contourites on seismic reflection data from the Ceduna Terrace, in the eastern GAB (Jackson

et al. 2019). Thus, ocean currents might have played a greater role in shaping this margin than previously acknowledged.

These conflicting ideas on the development of the shelf-margin wedge suggest that a complete and convincing explanation of the stratigraphic architecture of the Dugong Supersequence remains to be established. To address this issue, this paper presents an appraisal of the stratigraphy of the Dugong Supersequence with a focus on its seismic-stratigraphic expression on the shelf and upper slope of the western GAB. We have concentrated on the identification and description of depositional sequences that are potentially ‘mappable’ across the entire GAB. Our revised stratigraphic framework is based on the reinterpretation of regional 2D seismic reflection profiles, and an appraisal of the rock record provided both by boreholes drilled on Leg 182 of the Ocean Drilling Programme (ODP) and petroleum exploration wells. Our analysis indicates that the development of the shelf-margin of the western GAB has been influenced by both downslope and alongslope processes since the Mid-Eocene, with alongslope processes being most pronounced during the Quaternary.

1. Regional setting of the Eucla Basin

1.1. Structure

The Eucla Basin developed as part of the Late Cretaceous–Cenozoic stepwise process of passive margin development offshore southern Australia, following the commencement of breakup of Australia and Antarctica at about 83 Ma (Totterdell *et al.* 2000; Norvick & Smith 2001; Sayers *et al.* 2003; Totterdell & Bradshaw 2004; Robson *et al.* 2017). The Eucla Basin unconformably overlies the Bight Basin, one of the major rift basins of the ‘Southern Rift System’ that had controlled extension throughout the entire protracted process of Mesozoic breakup in eastern Gondwana (Stagg *et al.* 1990). The present-day terraced shelf-margin physiography (Figs 2, 3) is a consequence of

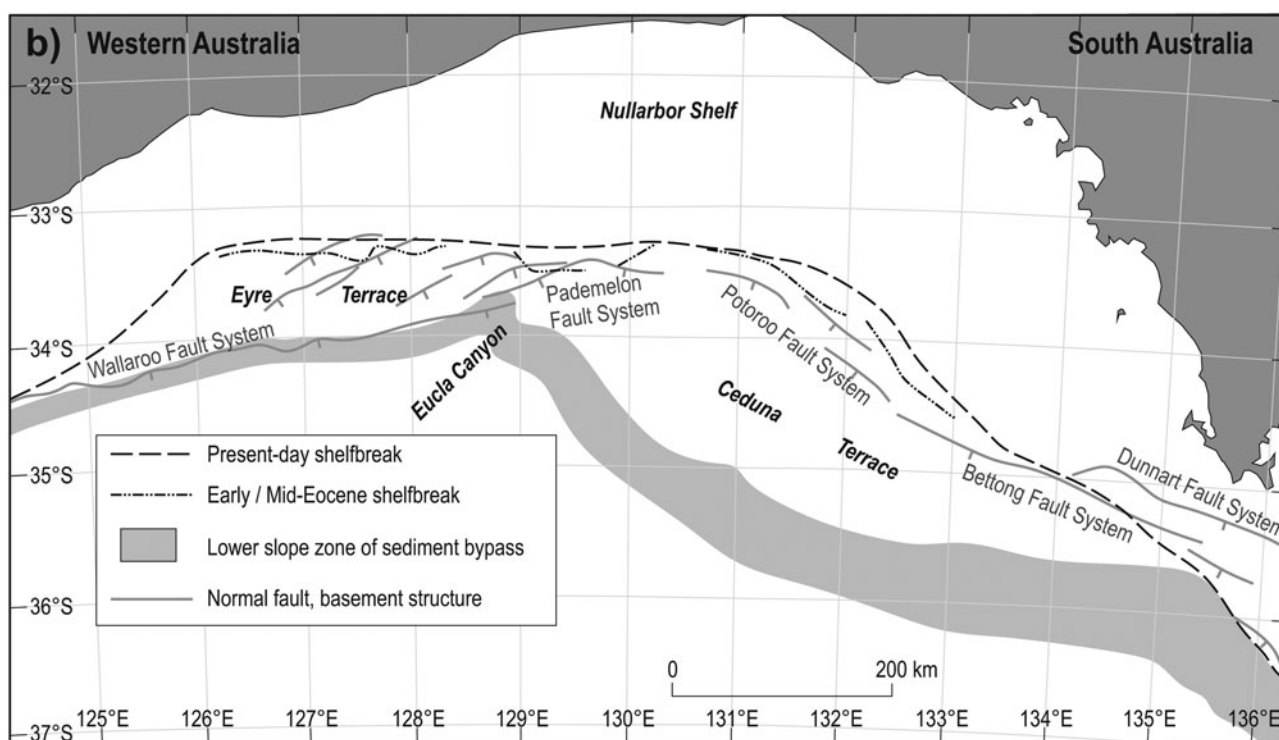
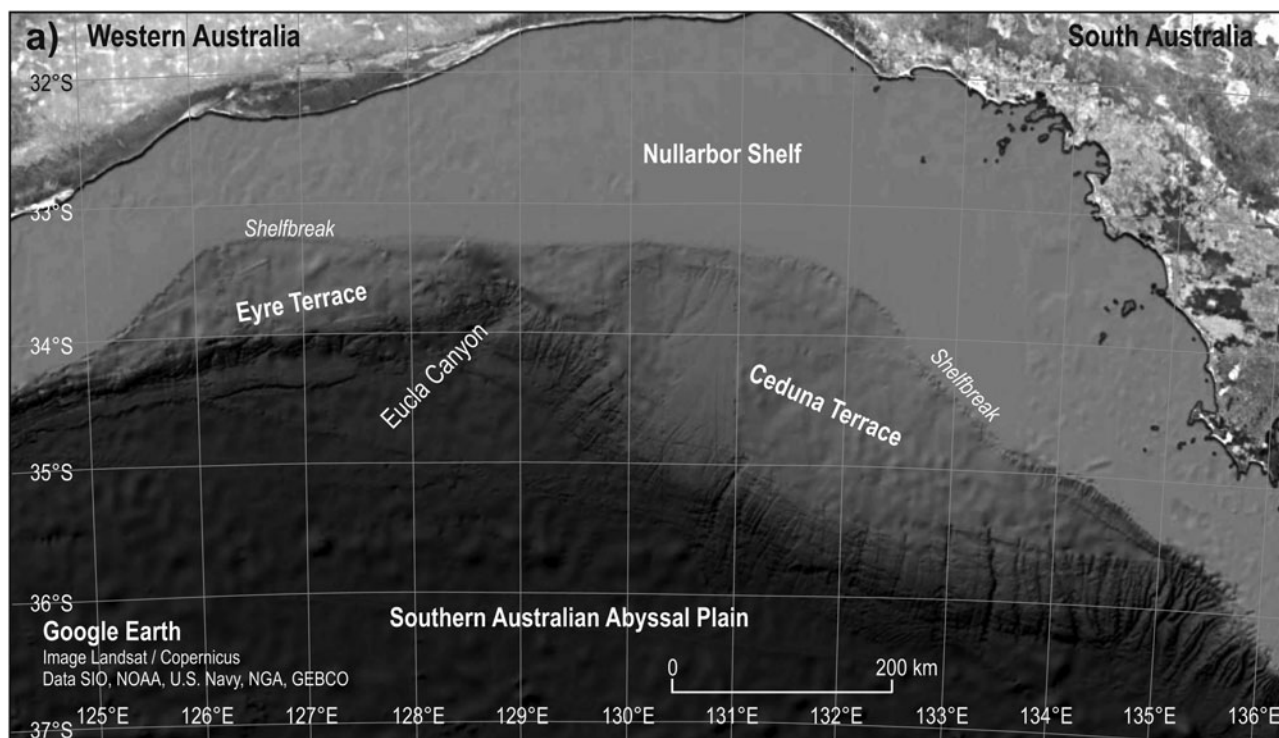


Figure 2 Maps showing (a) bathymetry of the GAB contrasting the gently shelving character of the upper slope (Eyre and Ceduna terraces) with the steeper lower slope where submarine canyons are clearly observed and facilitate the transport of sediment from the upper slope to the continental rise, bypassing the lower slope; (b) the Early/Mid-Eocene and present-day positions of the shelfbreak in relation to the margin-shaping network of basement lineaments (after Bradshaw *et al.* 2003).

the end-Cretaceous flexure, faulting and gravitational collapse of the early post-breakup, Campanian–Maastrichtian, passive margin – represented by the Hammerhead Supersequence of the Bight Basin – and formed the foundation upon which the unconformably overlying Palaeocene–Early Eocene Wobbecong Supersequence, the oldest part of the Eucla Basin succession, was deposited (Totterdell *et al.* 2000, 2005; Totterdell & Krassay 2003; Totterdell & Bradshaw 2004). A hiatus of 5–7 My is

envisaged to separate these two phases of passive margin development (Totterdell *et al.* 2000). Whereas the Campanian–Maastrichtian passive margin was strongly influenced by reactivation of structural elements formed during the pre-breakup phase of the Bight Basin (Hill 1995; Totterdell *et al.* 2000, 2005; Totterdell & Bradshaw 2004) (Fig. 3), the Eucla Basin and its fill represents increased tectonic stability during the Cenozoic.

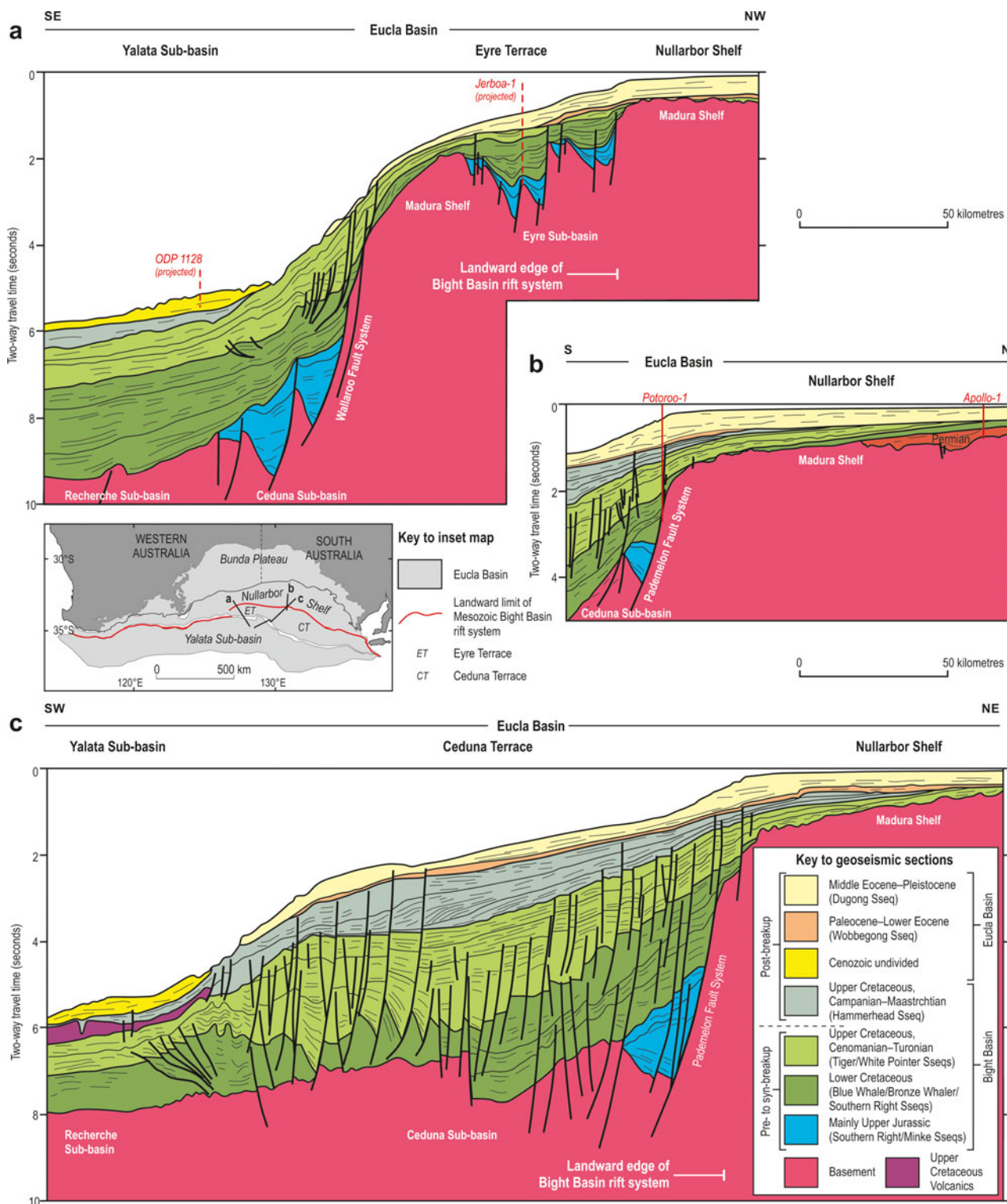


Figure 3 Geoseismic profiles showing the generalised structural and stratigraphic framework of the GAB, highlighting the distinction between the Cenozoic Eucla Basin and the Mesozoic Bight Basin rift system, as well as the separation between the pre-to-syn-breakup and post-breakup successions. Line drawings are modified after Bradshaw *et al.* (2003). Inset map shows location of profiles (a–c), and the landward extent of both basins. Structural elements associated with the Bight Basin and adjacent contemporary shelf are shown in white text. Sequence-stratigraphic (Sseq, supersequence) terminology is after Totterdell *et al.* (2000). Positions of commercial wells used in this study are also indicated together with foot-of-slope ODP site 1128.

An increase in the rate of seafloor spreading in the Mid-Eocene (~44–40 Ma) (Tikku & Cande 1999; Norvick & Smith 2001; Sayers *et al.* 2003; Li *et al.* 2004), accompanied by volcanism associated with the Bight Basin Igneous Complex (BBIC) (Schofield & Totterdell 2008; Reynolds *et al.* 2017), instigated rapid and widespread subsidence of the GAB that resulted in a regional unconformity between the Wobbegong Supersequence and the overlying Mid-Eocene–Quaternary Dugong

Supersequence (Totterdell *et al.* 2000, 2008). Since the Mid-Eocene, the location of the shelfbreak has remained relatively constant, controlled by a hinge-line that follows the well-established basement fault system associated with the Mesozoic Bight Basin (Figs 2b, 3). Whereas the southern Australian margin, in general, has been subject to compressional forces since the Mid-Eocene (Holford *et al.* 2011a, 2014), the Eucla Basin has remained largely tectonically stable with only minimal

subsidence of the margin (Hegarty *et al.* 1988; Brown *et al.* 2001; Bradshaw *et al.* 2003; Totterdell *et al.* 2005). Nevertheless, significant disparities in the elevations of correlative nearshore sequences across the basin suggest that it has been subject to differential vertical movements expressed as long-wavelength tilting (west-side-up, east-side-down tilting of ~100–200 m) since the Late Eocene (Hou *et al.* 2008 and references therein). Some of this relative vertical motion occurred after the Mid-Miocene causing exposure of the Nullarbor Plain and general seaward tilting of the Eucla Basin (Feary & James 1998). Further mild tectonic deformation is manifest onshore by numerous Late Miocene–Early Pliocene faults that displace the Nullarbor surface between 10 and 30 m (Hillis *et al.* 2008; Hou *et al.* 2008; Mounsher 2016).

1.2. Stratigraphy

A stacked succession of Middle Eocene to Pleistocene marine siliciclastic and carbonate rocks extends from the Bunda Plateau onto the Nullarbor Shelf (Lowry 1970; Cockshell *et al.* 1990; Hocking 1990; Benbow *et al.* 1995; Smith & Donaldson 1995; Messent *et al.* 1996; Feary & James 1998; Totterdell & Krassay 2003) (Fig. 3). On the Bunda Plateau, the stratigraphy of this succession is uniform across much of the basin and comprises a basal, transgressive, shallow-marine sandstone, the Middle

Eocene Hampton Sandstone, up to 30 m thick, conformably overlain by the Middle to Upper Eocene Wilson Bluff Limestone; the latter forms part of an up-to-300-m-thick aggrading succession of carbonate-platform rocks that also includes the Upper Oligocene–Lower Miocene Abrakurrie Limestone, the Lower to Middle Miocene Nullarbor Limestone and the ? Upper Pliocene–Lower Pleistocene Roe Calcarene (Lowry 1970; Hocking 1990; Benbow *et al.* 1995; Clarke *et al.* 2003; Hou *et al.* 2006, 2008; James *et al.* 2006) (Fig. 4). Collectively, these units represent the preserved onshore assemblage of the Dugong Supersequence (Totterdell & Krassay 2003). On the eastern margin of the Eucla Basin, the carbonate succession partially interdigitates with marginal- and non-marine deposits of the Lower to Upper Eocene Pidinga Formation (Benbow *et al.* 1995; Alley *et al.* 1999; Clarke & Hou 2000; Hou *et al.* 2006, 2008) (Fig. 4). The main characteristics of all these formations are summarised in Table 1.

On the Nullarbor Shelf, the Dugong Supersequence forms the bulk of a Cenozoic sedimentary wedge that gradually thickens up to 600 milliseconds (msecs) two-way travel time (TWTT) towards the shelf-edge, and locally exceeds 1000 msecs TWTT, beyond which it thins towards the edge of the Eyre and Ceduna terraces (Figs 3, 5). This is equivalent to a near-maximum estimated thickness of 1 km at the shelf-edge based on an interval

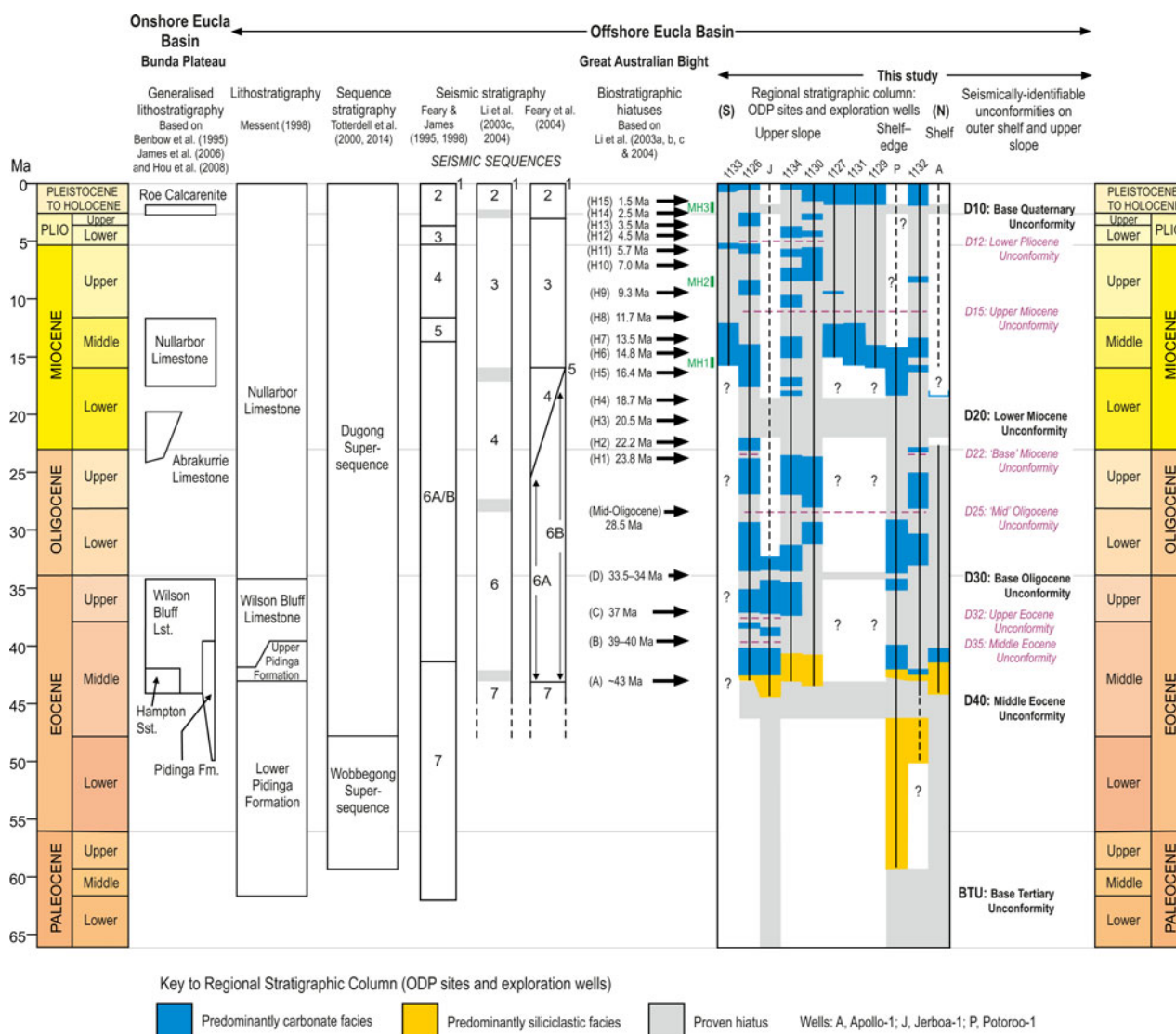


Figure 4 Comparison of stratigraphic schemes for Cenozoic siliciclastic and carbonate rocks for the Eucla Basin, from the Bunda Plateau–GAB region. Regional stratigraphic column summarised from stratigraphic-range chart in Figure 7, including major unconfomities (black, bold) mappable from the shelf to the upper slope, and minor unconfomities (purple, italics) that are largely restricted to the upper slope. Timescale is from Gradstein *et al.* (2012).

Table 1 Summary of the lithology, thickness, depositional environment and age of the main marine–paralic/non-marine stratigraphic units of the Eucla Basin preserved onshore, beneath the Bunda Plateau. Information derived from Lowry (1970), Hocking (1990), James & Bone (1991), Benbow *et al.* (1995), Li *et al.* (1996), Feary & James (1998), Clarke *et al.* (2003), Hou *et al.* (2006, 2008), James *et al.* (2006), Fairclough *et al.* (2007), O’Connell (2011), O’Connell *et al.* (2012), Mounsher (2016), Jagodzinski *et al.* (2019).

Lithostratigraphy	Lithology and thickness	Depositional environment	Age
Roe Calcarenite	Medium- to coarse-grained bioclastic sandy limestone; grainstone to rudstone texture; richly fossiliferous with diverse assemblage of molluscs, large benthic foraminifera and coralline algae. Thickness: generally 2–3 m; up to 8 m max.	Warm–temperate; subtidal, shoreface to inner shelf; seagrass-dominated.	Latest Pliocene–Early Pleistocene (Piacenzian–Gelasian)
Nullarbor Limestone	Pale brown, bioclastic, micritic limestone; wackestone to packstone texture; sporadic, very thin, basal lag of mud, sand and grit; highly fossiliferous with ubiquitous coralline algae, large benthic foraminifera, molluscs and local concentrations of zooxanthellate corals. Thickness: generally 20–35 m; 45 m max.	Warm–temperate to sub-tropical, stable, epeiric shelf; aggradation of limestone on shoreface; deposition occurred in water depths up to 50 m.	Early to Mid-Miocene (Burdigalian–Serravallian)
Abrakurrie Limestone	Yellow-brown, bryozoan-rich limestone; wackestone to rudstone texture; distinctly cyclical vertical sequence punctuated by numerous hardgrounds; top is lithified and weathered. Thickness: <10 m in east; up to 120 m in west.	Cool–temperate deep offshore shelf swept by open ocean swells; deposition occurred in water depths from >50 to >70 m.	Late Oligocene–Early Miocene (Chattian–Aquitainian)
Wilson Bluff Limestone	White to grey, thin-to-thickly-bedded, muddy, bioclastic limestone and calcareous mudstone; variable texture including wackestone, skeletal mudstone, rudstone and minor packstone; abundant bryozoans, scattered echinoids, bivalves, brachiopods, planktonic foraminifers and sponge spicules; base is locally a sandy, glauconitic marl. Thickness: <150 m in east; ~300 m in west.	Cool–temperate deep offshore shelf open to ocean currents; water depth >100 m; limestone deposition occurred over a series of neritic transgressive cycles.	Mid- to Late Eocene (late Lutetian–Priabonian)
Hampton Sandstone	Limonite-stained, medium- to coarse-grained quartz-rich sandstone, variably calcareous, partly clayey at base, glauconitic and fossiliferous at top; subordinate conglomerate and siltstone. Thickness: 25–85 m.	Predominantly shallow marine transgressive deposit.	Mid-Eocene (Lutetian)
Pidinga Formation	Well sorted, fine- to coarse-grained sandstone and interbedded siltstone and clay, generally carbonaceous, minor lignite; basal sediments in palaeovalleys are commonly coarse sand and gravel. Thickness: 30–100 m.	Fluvial, lacustrine and estuarine environments landward of the Ooldea coastal sand barrier; paralic–marginal marine seaward of NE basin margin.	Early to Late Eocene (late Ypresian–Priabonian)

velocity of 2 kms⁻¹ (see section 2, Data and methods). On seismic profiles, the base of the Dugong Supersequence is a sharp, planar, angular unconformity that truncates the Wobbegong Supersequence and older Mesozoic and Upper Palaeozoic rocks (Totterdell *et al.* 2000) (Figs 3, 6). Beneath the Ceduna Terrace, intrusions, volcanogenic edifices and lava flows of the BBIC locally overlie the unconformity and are themselves overlapped by the Dugong Supersequence (Reynolds *et al.* 2017). Despite its regional extent, the Dugong Supersequence represents a relatively sediment-starved continental margin succession. Its maximum drilled thickness occurs along the south-eastern shelf-margin (e.g., Cockshell *et al.* 1990; Bein & Taylor 1991; Smith & Donaldson 1995; Bradshaw *et al.* 2003; Totterdell & Bradshaw 2004) where it exceeds 1000 m in the Greenly-1, Platypus-1, Duntroon-1, Echidna-1 and Vivonne-1 wells and 2000 m in Borda-1 (Fig. 5; Table 2). Farther west, the drilled thickness of the shelf-margin wedge flanking the Eyre Terrace and NW Ceduna Terrace is commonly <1000 m thick as evidenced by the Potoroo-1 and Jerboa-1 wells and the ODP boreholes (Table 2).

Offshore, the basal transgressive sandstone was termed the Upper Pidinga Formation (Smith & Donaldson 1995; Messent 1998) whereas the overlying carbonate succession currently comprises the previously defined seismic-stratigraphic sequences 1–6 of Feary & James (1995, 1998) and Feary *et al.* (2004) (Fig. 4). The current structural disposition of the Dugong Supersequence – a seaward-dipping homocline – has facilitated the exposure of

rocks associated with the Middle Eocene–Middle Miocene carbonate platform (currently assigned as sequence 6B in the scheme of Feary & James 1995, 1998) on the inner part of the Nullarbor Shelf. Seabed sampling has recovered limestone fragments correlatable with the Eocene Wilson Bluff Limestone Formation to about 35 km from the coastline; however, the interpretation of ‘Miocene’ limestone fragments as belonging to the Abrakurrie Limestone and/or Nullarbor Limestone formations is ambiguous due to the lack of diagnostic biomarkers (Feary *et al.* 1993; James *et al.* 1994). This lack of stratigraphic resolution also prevails on seismic reflection profiles. Whereas the carbonate platform succession is generally well-imaged, the lower stratigraphic resolution of these data has resulted in a simplified two-fold lithostratigraphic subdivision generally being applied to this succession, particularly in the eastern GAB, where the Nullarbor Limestone is commonly represented as unconformably overlying the Wilson Bluff Limestone (Cockshell *et al.* 1990; Smith & Donaldson 1995; Messent *et al.* 1996; Messent 1998) (Fig. 4).

In the western GAB, a tentative subdivision of the carbonate platform succession beneath the inner shelf was proposed by Feary & James (1995, 1998), who described the lower part of the platform as a carbonate ramp correlatable with the Middle–Upper Eocene Wilson Bluff Limestone Formation, whereas the upper section of the platform is interpreted as a carbonate rimmed shelf and assigned as equivalent to the upper Lower–Middle Miocene Nullarbor Limestone Formation (Fig. 6).

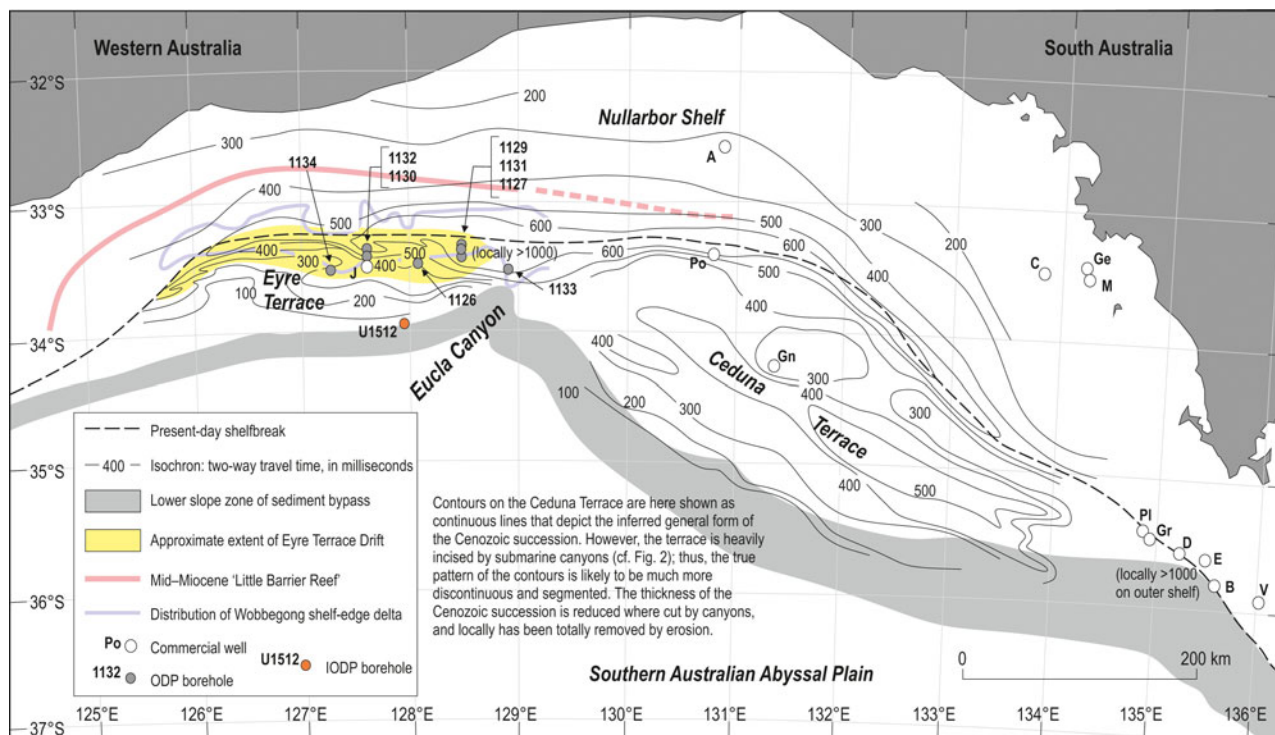


Figure 5 Isochron map showing the variation in difference (vertical thickness) of the TWTT between the seabed and basal Cenozoic reflections on the shelf and upper slope. Position of Mid–Miocene ‘Little Barrier Reef’ and distribution of Wobbecong shelf-edge delta, in western GAB, based on Feary & James (1995, 1998). Well abbreviations: A, Apollo-1; B, Borda-1; C, Columbia-1; D, Duntroon-1; E, Echidna-1; Ge, Gemini-1A; Gn, Gnarlyknots-1/1A; Gr, Greenly-1; J, Jerboa-1; M, Mercury-1; Pl, Platypus-1; Po, Potoroo-1; V, Vivonne-1.

They further speculated, initially, that the offshore equivalent of the Upper Oligocene–Lower Miocene Abrakurrie Limestone Formation correlated with the uppermost part of the ramp

Table 2 Drilled thicknesses (in metres) of the Dugong Supersequence in ODP boreholes and exploration wells in the GAB. ODP data based on information derived from this study’s appraisal of the individual site reports in Feary *et al.* (2000). Information for exploration wells derived from Messent (1998) combined with an appraisal of the well completion reports. All ODP sites, except 1126 and 1132, terminated (TD) within the Dugong Supersequence; sites 1126, 1132 and all wells penetrated the supersequence. The borehole and well sites are defined in Figure 1.

Borehole/well	Dugong Supersequence (m)
1126	396
1127	510 (TD)
1128	452 (TD)
1129	604 (TD)
1130	395 (TD)
1131	617 (TD)
1132	560
1133	152 (TD)
1134	397 (TD)
Apollo-1	~343
Borda-1	1964
Columbia-1	179
Duntroon-1	≥1459
Echidna-1	1003
Gemini-1/1A	~209
Gnarlyknots	~252
Greenly-1	1688
Jerboa-1	376
Mercury-1	194
Platypus-1	1493
Potoroo-1	679
Vivonne-1	977

phase (Feary & James 1995); subsequently, it was proposed that the basal unconformity of the Abrakurrie Limestone Formation corresponded to the transition from the ramp phase to the rim phase (Feary & James 1998). However, given the relatively restricted occurrence of the Abrakurrie Limestone Formation onshore (Lowry 1970; Hou *et al.* 2008), its offshore extent – whilst generally assumed (Feary & James 1995, 1998) – might be equally limited and/or absent. For example, in the Apollo-1 well (Figs 1, 7), biostratigraphic data indicate that the limestone directly overlying the Middle–Upper Eocene Wilson Bluff Limestone Formation is no older than 18.7 Ma, and thus correlated with the Nullarbor Limestone Formation (Messent 1998).

Seaward of the Mid-Miocene ‘Little Barrier Reef’, the Middle Eocene–Middle Miocene carbonate platform succession on the outer shelf and upper slope is described as a deep-water carbonate sediment apron (sequences 4–6A of Feary & James 1995, 1998), which is capped by a Neogene–Quaternary arrangement of aggradational to sigmoidal sequences (1–3 of Feary & James 1995, 1998) (Fig. 6). Based on ODP leg 182 boreholes, Li *et al.* (2003a, b, c, 2004) reported up to 20 biostratigraphic hiatuses from within this Middle Palaeogene (Eocene A–D, Mid Oligocene) to Neogene–Quaternary (H1–H15) shelf-margin succession (Fig. 4), each lasting ~0.5 Myr or more, and all interpreted to coincide with major third-order sequence boundaries. This series of unconformities was interpreted to reflect a eustasy-driven model of continental margin sedimentation (Li *et al.* 2003a, 2004). In addition, three ‘mega-hiatuses’ at about 15–16 Ma, 8–9 Ma and 1.5–2.5 Ma, each inferred to last >5 Myr (at selected sites), have been attributed to large-scale slope failure (Li *et al.* 2004).

On the lower slope, the Cenozoic succession is commonly thin-to-absent; site U1512 of the International Ocean Discovery Program (IODP) (Fig. 5) proved a 10-m-thick section of Upper Pleistocene sediments unconformable on Upper Cretaceous rocks (Huber *et al.* 2019). By way of contrast, at the foot of the slope, an up-to-500–600-m-thick sequence is locally preserved

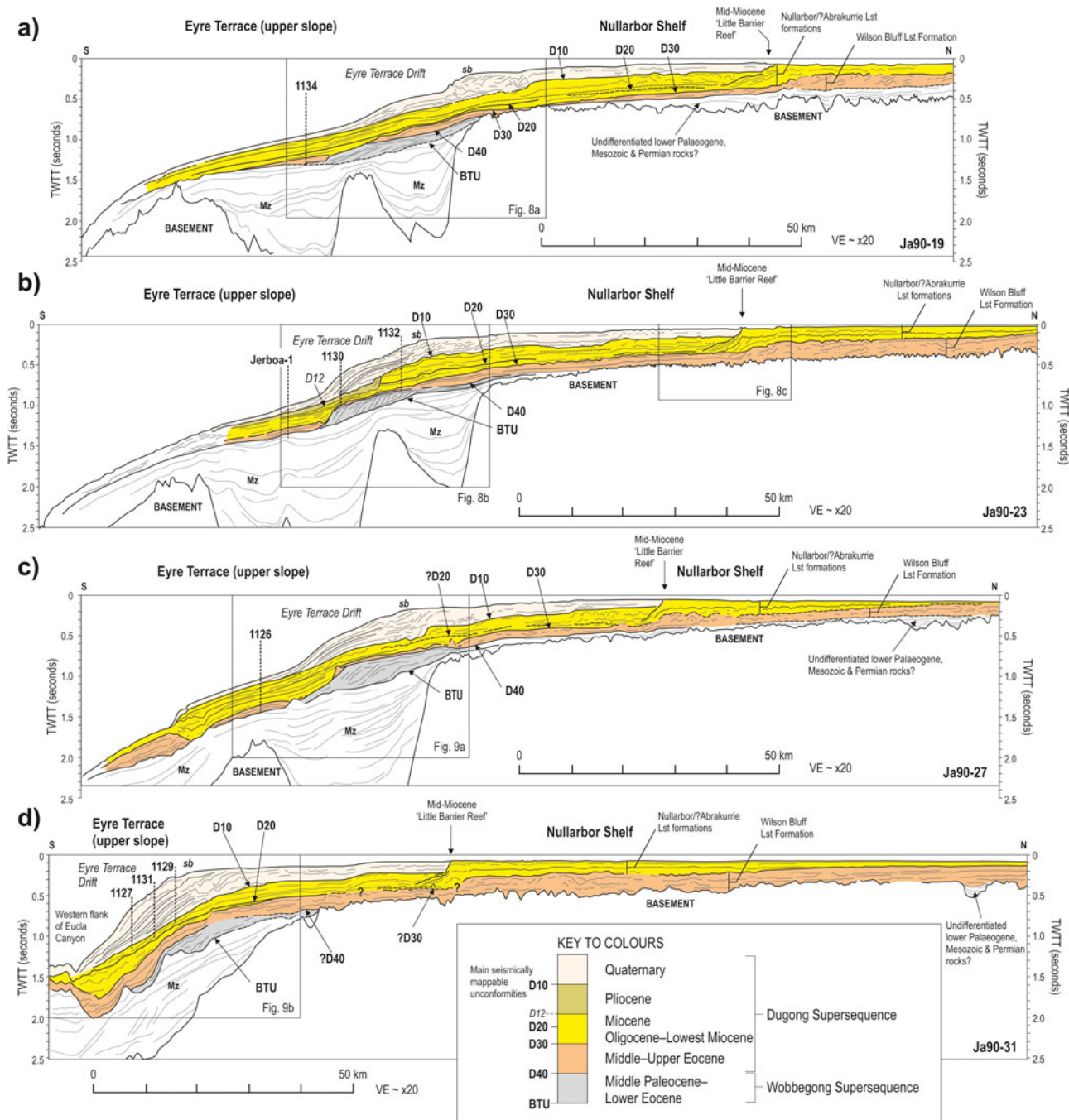


Figure 6 Interpreted seismic reflection profiles showing the generalised Cenozoic seismic-stratigraphical framework across the western GAB, the main seismically mappable unconformable boundaries (D10–D40 and the BTU, Base Tertiary Unconformity; D12, upper slope only), and the internal seismic reflection configuration of the Wobbecong and Dugong supersequences. Abbreviations: Mz, Mesozoic; sb, shelfbreak. Location of profiles shown in Figure 1. Inset boxes expanded in Figures 8 and 9 provide further details of the outer shelf–upper slope stratigraphy calibrated with ODP boreholes and the Jerboa-1 well. Vertical exaggeration (VE) at seabed ~×20.

(Bradshaw *et al.* 2003; Totterdell & Bradshaw 2004) (Fig. 3). ODP site 1128 proved at least 452 m of Middle Eocene–Quaternary sediments, including mass-flow deposits, in the upper part of the foot-of-slope succession (Shipboard Scientific Party 2000d). Whereas these deposits are correlatable with the Dugong Supersequence (Shipboard Scientific Party 2000d), regional studies (Bradshaw *et al.* 2003; Totterdell & Bradshaw 2004; Sauermilch *et al.* 2019) suggest that slope sediments attributable to both Wobbecong and Dugong supersequences are probably preserved along the foot of the slope, albeit largely undivided.

1.3. Modern oceanographic setting

The present-day shelf and slope of the GAB are influenced by two northern boundary currents: (1) an eastward-flowing

shelfbreak surface-current system including the Leeuwin and South Australian currents; and (2) the wider and deeper-reaching counter-flowing westward Flinders Current (Richardson *et al.* 2019; Duran *et al.* 2020) (Fig. 1). The main characteristics of these currents are presented in Table 3. The Leeuwin Current originates off NW Australia and flows southward, transporting subtropical surface water to Cape Leeuwin and then eastward along the shelfbreak and uppermost slope into the western GAB (124°E), beyond which the South Australian Current runs in extension of the Leeuwin Current from the central GAB to Kangaroo Island (Fig. 1). The Leeuwin Current exhibits a seasonal behaviour, being strongest in winter but effectively disappearing from the GAB in the summer, retarded by westward summer winds (Middleton & Bye 2007; Duran *et al.* 2020).

Table 3 Summary of the characteristics of the main modern-day southern Australian currents that bathe the shelf and slope of the GAB. Information derived from Cresswell & Petersen (1993), James *et al.* (2001), Middleton & Cirano (2002), Cirano & Middleton (2004), Cresswell & Griffin (2004), Ridgeway & Condie (2004), McCartney & Donohue (2007), Middleton & Bye (2007), Cresswell & Dominguez (2009), Feng *et al.* (2009), Petrusевич *et al.* (2009), Yao & Shi (2017), Wijeratne *et al.* (2018), Richardson *et al.* (2019) and Duran *et al.* (2020).

Current	Zone of influence (water depth, metres)	Current velocity	Notes
Leeuwin Current	0–250 m	0.3–0.5 ms ⁻¹	Eastward-flowing seasonal shelfbreak current; intensified by eastwards winter winds; retarded by westward summer winds, when effectively disappears from the GAB.
South Australian Current	0–300 m	Up to 0.5 ms ⁻¹	Eastward-flowing shelfbreak current; forms in shallow shelf waters of GAB as a gravity outflow of high-salinity warm water that is injected into the eastwards-flowing shelfbreak current; probably contributes to dense water cascades over the shelfbreak.
Flinders Current	Core of current 300–800 m adjacent to upper slope; 0–2000 m farther offshore	0.08 ms ⁻¹ for most of year between 300 and 800 m; strongest in summer with speeds up to 0.2 ms ⁻¹ in western GAB; 0.04 ms ⁻¹ at 1000 m	Westward-flowing dual-structured current that flows along the slope as an undercurrent trapped beneath the Leeuwin and South Australia shelfbreak currents, and as a surface-to-deep current farther offshore, particularly the central and western GAB, where it may form the dominant flow down to 2000 m; upwelling favourable bottom boundary layer that moves onto shelf when Leeuwin Current weakens in summer.

The Flinders Current is forced by the general anticyclonic circulation in the South Australia Basin, with the eastward-flowing Antarctic Circumpolar Current (ACC) forming the southern limb and the westward-flowing Flinders Current forming the northern limb (Middleton & Cirano 2002; McCartney & Donohue 2007; Wijeratne *et al.* 2018) (Fig. 1a). The Flinders Current emerges southwest of Tasmania and entrains and transports cold shallow-to-intermediate Subantarctic water masses equatorward from within the Subantarctic Zone, as well as via the Tasman Outflow (Richardson *et al.* 2019) (Fig. 1a). Adjacent to the southern Australian continental margin, the Flinders Current flows along the upper slope, including the Eyre Terrace, and is strongest and most continuous in summer, increasing in magnitude from E to W (Cresswell & Petersen 1993; Middleton & Bye 2007; Richardson *et al.* 2019) (Table 3). This cold and nutrient-rich water can move upwards onto the shelf when the Leeuwin Current weakens during summer months (James *et al.* 2001; Richardson *et al.* 2019).

1.4. Palaeoceanography

Reconstruction of the palaeocirculation during the Cenozoic is still a matter of considerable discussion. A warm-water microfauna in Middle–Upper Eocene rocks in the Eucla Basin led McGowran *et al.* (1997) to speculate the early presence (35–42 Ma) of a ‘proto-Leeuwin Current’ that transported this fauna from warm low latitudes to the southern Australian margin, then situated at about 60°S (Norvick & Smith 2001; Bijl *et al.* 2013). However, a pre-Oligocene initiation of a Leeuwin Current-type ‘current’ is disputed given that a circum-circular oceanic circulation that facilitated eastward flow of warm ocean waters probably did not occur until the Early Oligocene following the deepening of the Tasmanian Gateway (Stickley *et al.* 2004; Wyrwoll *et al.* 2009; Scher *et al.* 2015). Further incursions of anomalously warm water into the GAB, as revealed by the later Paleogene–Neogene biostratigraphic record at third-order scale, have also been attributed to a proto-Leeuwin Current (McGowran *et al.* 1997; Stickley *et al.* 2004). In contrast, Wyrwoll *et al.* (2009) have suggested that the Leeuwin Current *sensu stricto* was only established around 3–4 Ma when the Indonesian Gateway took on its present form and provided a passageway for Indonesian Throughflow – a major contributor to the source region of the Leeuwin Current.

The association of the Flinders Current with the ACC as part of the general anticyclonic circulation in the South Australia Basin suggests that it is no older than Early Oligocene following the deepening of the Tasmanian Gateway and the establishment of the circum-Antarctic currents (Exon *et al.* 1999; Norvick & Smith 2001). Sangiorgi *et al.* (2018) state that the modern Southern Ocean circulation possibly developed during the Mid-Miocene Climatic Optimum (17–14.8 Ma). However, in common with the ACC, the Flinders Current may not have attained its present-day strength until after the Mid-Miocene (~11 Ma) (Bijl *et al.* 2018; Sangiorgi *et al.* 2018). During the Quaternary, the history of the Leeuwin Current in the GAB reflects climatically induced changes linked to the glacial–interglacial cyclicality, whereby activity was strongest during interglacial stages (McGowran *et al.* 1997; Wyrwoll *et al.* 2009; Anderskov *et al.* 2010). In contrast, the Flinders Current was probably strengthened during glacial stages because of an intensification and/or northward shift of the glacial atmospheric system in the Southern Ocean (Middleton & Cirano 2002; Hesse *et al.* 2004). At the same time, colder and drier winds might also have augmented the formation of dense water in the inner GAB, including the formation of the South Australian Current which, in the absence of the Leeuwin Current, would probably remain focused at the shelfbreak (Anderskov *et al.* 2010).

2. Data and methods

The stratigraphic interpretation presented in this study is based primarily on a re-examination of regional 2D seismic reflection data and 11 sample stations (eight ODP boreholes and three commercial wells) from the western GAB (Fig. 1). The seismic-reflection lines used in this study were acquired and processed by the Japan National Oil Corporation (JNOC) in 1990 and 1991, and provide a series of N–S transects extending from the Nullarbor Shelf onto the Eyre Terrace (upper continental slope). An additional set of lines covering the central and eastern GAB (Fig. 1) were also referred to and utilised to enable the compilation of the Cenozoic isochron map (Fig. 5). These seismic datasets were loaded into Kingdom seismic and geological interpretation software and can be obtained from the National Offshore Petroleum Information Management System (NOPIMS, <https://www.ga.gov.au/nopims>).

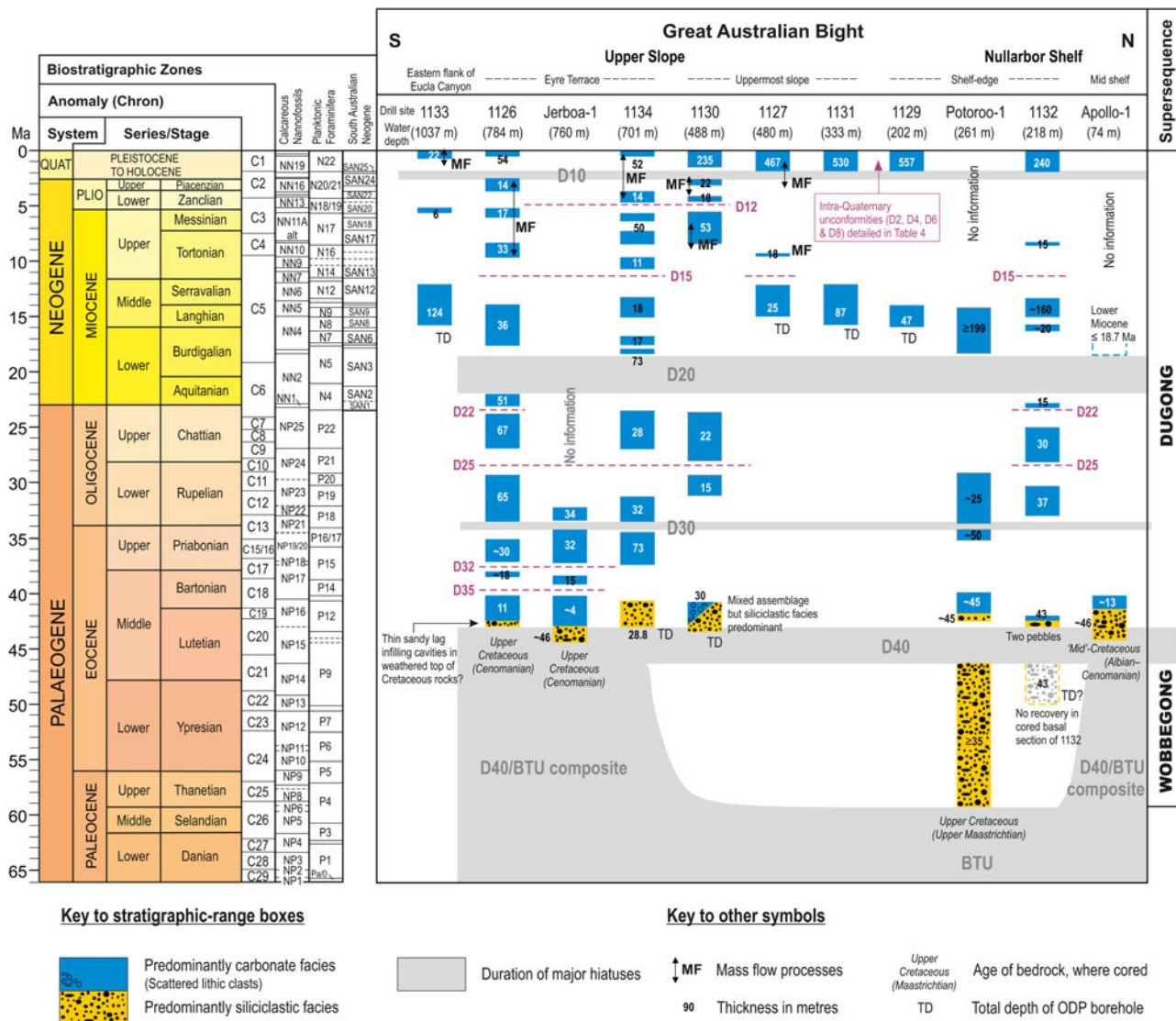


Figure 7 Cenozoic stratigraphy of the western GAB indicating stratigraphical range, thickness, generalised lithofacies of the preserved rocks, major (grey) and minor (purple) unconformities (D10–D40 and BTU) and age of the underlying strata. Timescale and temporal ranges of the standard calcareous nannoplankton and planktonic foraminiferal biozones are those of Gradstein *et al.* (2012); the South Australian Neogene planktonic foraminifer biozonation is from Li *et al.* (2003b, 2004). The biostratigraphic information was sourced as follows: the ODP Leg 182 sites – Feary *et al.* (2000), Shipboard Scientific Party (2000a, b, c, e, f, g, h, i, j) and Li *et al.* (2003a, b, c, 2004); the Jerboa-1, Potoroo-1 and Apollo-1 wells – Well Completion Reports (NOPIMS), Messent (1998), Totterdell *et al.* (2000), Li *et al.* (2003a), Morgan *et al.* (2005) and Hou *et al.* (2006).

The sample data comprise ODP sites 1126, 1127, 1129–1134 and the Jerboa-1, Potoroo-1 and Apollo-1 wells (Fig. 1). In Figure 7, the information derived from these sample sites is presented as a stratigraphic-range chart with the sites arranged as a N–S shelf-to-upper-slope transect and displaying generalised lithofacies, thickness and chronostratigraphic range; the latter is based on biostratigraphic correlation of the sample sites with the planktonic foraminifera and calcareous nannofossil biozonal schemes of Gradstein *et al.* (2012), and the South Australian Neogene (SAN) planktonic foraminifer biozonation of Li *et al.* (2003b, 2004). Whereas Figure 7 represents a revision of previous charts that include the SAN zones, their calibration to the standard zonation of planktonic foraminifers (N zones) is herein maintained. In this study, information on lithology, planktonic foraminifera and calcareous nannofossils for all investigated ODP sites was sourced primarily from the *Initial Results* Volume 182 (Feary *et al.* 2000; Shipboard Scientific Party 2000a, b, c, e, f, g, h, i, j), with additional analysis of the planktonic foraminifera of sites 1126, 1130, 1132 and 1134 provided by the *Scientific Results* Volume 182 (Li *et al.* 2003b, c;

Hine *et al.* 2004) and resulting published papers (Li *et al.* 2003a, 2004). Lithologic and biostratigraphic information for the Jerboa-1, Potoroo-1 and Apollo-1 wells was gathered from the various well completion reports, accessed from NOPIMS, and published information (Messent 1998; Totterdell *et al.* 2000; Li *et al.* 2003a; Morgan *et al.* 2005; Hou *et al.* 2006). Whereas biostratigraphic resolution and correlation is variable across the dataset, Figure 7 depicts stratigraphic calibration that represents *high-confidence* biozone placements – essentially, proven stratigraphic range – based on the identification of ‘common overlap zones’ between calcareous nannofossil and planktonic foraminifera.

The integration of the stratigraphic-range chart with regional 2D seismic reflection lines provided the basis for the appraisal of the seismic stratigraphy of the Nullarbor Shelf and Eyre Terrace (upper slope) described in this paper. Four key seismic reflection lines – Ja90-19, –23, –27 and –31 – were re-interpreted and calibrated with the ODP sites (Figs 6, 8, 9). In the construction of the regional stratigraphic framework, emphasis was placed on the identification of depositional packages bounded by seismically

mappable surfaces of discontinuity according to the criteria established by Mitchum *et al.* (1977). Based on this process, a common set of five major seismic reflectors – representing regional (shelf-to-slope) unconformities – have been identified: D10 (Base Quaternary Unconformity); D20 (Lower Miocene Unconformity); D30 (Base Oligocene Unconformity); D40 (Middle Eocene Unconformity); and BTU (Base Tertiary Unconformity) (Figs 4, 6–9). The prefix ‘D’ denotes those reflectors specific to the Dugong Supersequence, whereas the BTU represents the overall base of the Cenozoic succession and is commonly a composite unconformity surface. In addition, a further ten minor reflectors are identified and calibrated within the Dugong Supersequence (Figs 7–9). These are largely restricted to the upper slope, though the Upper Miocene D15 boundary is locally identifiable on the outer shelf (Figs 8b, c). The four major boundaries, D10–D40, divide the supersequence at *Series* level into, respectively, Quaternary, upper Lower–Upper Miocene, Oligocene–lowest Miocene and Middle–Upper Eocene sequences (Fig. 7). The exception is the Pliocene sequence on the upper slope, which can be identified as a distinct, albeit localised, unit bounded by the D10 and D12 reflectors (Fig. 8b). Summary descriptions of all these unconformities and the stratigraphic sequences are presented in Tables 4 and 5.

Figure 4 shows the relationship between our revised and integrated stratigraphic framework of the Dugong Supersequence compared to the existing and separate seismic stratigraphic and biostratigraphic schemes. Whereas we can broadly recognise the sequence 1–6 stratigraphic subdivision presented by Feary & James (1995, fig. 2; 1998, fig. 5) and Feary *et al.* (2004, fig. F2) our seismic interpretation is perceptibly different in terms of the configuration and extent of depositional units, their chronostratigraphic assignment and their correlation from shelf to slope (*cf.* Fig. 10). Regarding the Middle Palaeogene to Neogene–Quaternary biostratigraphic hiatuses of Li *et al.* (2003a, b, c, 2004) (Fig. 4), we remain cautious of the status and significance assigned to the bulk of the 20 unconformities and three mega-hiatuses proposed by these workers, based on ODP sites 1126, 1130, 1132 and 1134, as nowhere have they presented a correlation of these boundaries with seismic reflection data. Consequently, the existing scheme of unconformities lacks stratigraphic context beyond the limit of the borehole(s) in which they have been identified. Based on our integrated interpretation, we demonstrate that most of their hiatuses have limited expression on the upper slope and argue against the basic premise of Li *et al.* (2003a, 2004) that the hiatuses are all globally correlatable. For purposes of clarification, a tentative correlation between the two schemes is indicated in Table 6, and this issue is further considered in section 5.2 (Discussion).

Vertical thicknesses based on seismic reflection data are presented in msec TWTT. P-wave velocities measured across the Cenozoic succession on the outer shelf/upper slope of the western GAB are generally in the range of 1.5–2.2 km s⁻¹ (Feary *et al.* 2000; Shipboard Scientific Party 2000a). For ease of calibration, a general interval velocity of 2 km s⁻¹ has been applied to the Cenozoic succession on the outer margin, so that thicknesses given here in msec TWTT can be taken as near-maximum estimates in metres (e.g., 500 msec TWTT is ≈500 m). In Figure 5, the distribution of the isochrons is consistent with drilled thicknesses proved by the ODP and IODP boreholes and petroleum exploration wells.

3. Stratigraphical framework of the Dugong Supersequence

The distribution, configuration and stratigraphical range of the Dugong Supersequence in the western GAB are depicted in Figures 5–7. Whereas Figure 5 illustrates the generalised

distribution and thickness of the entire Cenozoic succession on the Nullarbor Shelf and adjacent upper slope, we interpret this pattern to largely reflect the configuration of the Dugong Supersequence for several reasons: the underlying Wobbecong Supersequence is discontinuous across the shelf (Smith & Donaldson 1995); it is largely confined to the outer shelf as a relatively narrow and buried shelf-edge delta (Feary & James 1998; Sharples *et al.* 2014); and it forms only a patchy veneer on the Eyre and Ceduna terraces (*cf.* Totterdell *et al.* 2000; Bradshaw *et al.* 2003; Totterdell & Krassay 2003; Totterdell & Bradshaw 2004) (Figs 3, 6). Although the shelf-edge delta is locally up to 400 msec TWTT in thickness (Sharples *et al.* 2014), this coincides with the thickest (>1000 msec TWTT) part of the shelf-margin succession (Fig. 5). Thus, the mounded and locally wavy pattern of accumulation depicted by the outer shelf–upper slope contours largely reflects margin-shaping processes linked to the Dugong Supersequence, especially the Quaternary sequence (Fig. 6).

On seismic profiles, the base of the Dugong Supersequence is marked by a moderate-to-high-amplitude reflection that represents a regional hiatus (Totterdell *et al.* 2000; Bradshaw *et al.* 2003; Totterdell & Krassay 2003; Totterdell & Bradshaw 2004) (Figs 8, 9). This basal reflection marks a composite unconformity incorporating the merged D40 and BTU unconformities (Table 4). The overlying Middle–Upper Eocene rocks rest on a range of older rocks, including Palaeocene–Lower Eocene (Wobbecong Supersequence), Cretaceous, Permian(?) and Precambrian basement (Totterdell *et al.* 2000; Totterdell & Krassay 2003) (Figs 3, 6). Totterdell *et al.* (2000, 2014) placed the Dugong/Wobbecong supersequence boundary – our D40 reflection – at the Ypresian/Lutetian boundary, whereas Li *et al.* (2003a) suggested an intra-Lutetian age (~43 Ma) for the base of the carbonate succession. Reappraisal of spore pollen and dinoflagellate cyst data from the Potoroo-1 well (*cf.* Morgan *et al.* 2005) indicates that the clastic section equivalent to the Wobbecong Supersequence is no younger than the top of the *Proteacidites asperopolus* spore pollen zone. The top of this zone corresponds to the base of the NP15 calcareous nannofossil zone (Morgan *et al.* 2005, fig. 5.5) which is at ~46.2 Ma (Fig. 7). In consideration of all these data, we have tentatively assigned D40 as an early Lutetian hiatus of up to 3 My duration (43–46.2 Ma) (Table 4).

As noted in section 1.2, the limitations of stratigraphic resolution within the offshore succession continue to present a challenge, especially regarding the Oligocene–Miocene carbonate platform deposits and their deeper-water outer-shelf correlatives. Inspection of the profiles in Figures 6, 8, 9 highlights the inherent complexity within the Oligocene–Miocene succession (the D30–D10 interval), even at *Series* level. Using the criteria of Feary & James (1998), we have tentatively traced the D30 Base Oligocene Unconformity from the outer shelf into the platform succession (Fig. 6); however, recognition of the D20 Lower Miocene Unconformity, which correlates with the hiatus between the Aburakurrie and Nullarbor limestones (Fig. 4), within the carbonate platform succession remains ambiguous (Figs 6, 8c). The absence of Oligocene rocks in the Apollo-1 well (Figs 4, 7) suggests that, at least locally, the boundary separating the upper Lower–Middle Miocene Nullarbor Limestone Formation and the Middle–Upper Eocene Wilson Bluff Limestone Formation is a composite D30/D20 unconformity surface. Notwithstanding this problem of stratigraphic resolution, the key aspects (seismic stratigraphy and lithology) of the stratigraphical framework of the Dugong Supersequence as observed on the western Nullarbor Shelf and Eyre Terrace are presented below, in ascending stratigraphical order. Additional details on seismic reflection configuration patterns and lithological characteristics are summarised in Tables 5 and 7, whereas thicknesses of all drilled sections are indicated in Figure 7.

Table 4 Summary characteristics of the main seismically mappable unconformities (**bold** notation) and the localised minor unconformities (*italicised* notation) in the western GAB. Tentative age of the Pliocene to Palaeocene unconformities is derived from the biostratigraphic data presented in Figure 7, with the approximate stratigraphic range of the hiatus, both chronological and biostratigraphic (calcareous nannofossil and planktonic foraminifera), based on the age of the oldest overlying, and youngest underlying sediments. The dating of the various Quaternary unconformities is based on a combination of biostratigraphic, marine oxygen isotopic and magnetostratigraphic data derived from Brunnur *et al.* (2002), Holbourn *et al.* (2002), Ladner (2002) and Fuller *et al.* (2003).

Name and geographic extent of unconformity	Description	Age (stage) and approx. stratigraphic range of hiatus
<i>D2 (Middle Pleistocene)</i> Upper slope	Forms a moderate- to high-amplitude, planar, convex reflection; varies from a variably erosive, angular unconformity to sub-parallel disconformity; interdigitates upslope with shelf-edge Pleistocene succession; downlaps seaward onto Pliocene/Miocene deposits.	Ionian ~0.45–0.5 Ma
<i>D4 (Middle Pleistocene)</i> Upper slope	Forms a moderate- to high-amplitude, planar, convex-wavy reflection; predominantly erosional angular unconformity; possibly truncated by outer-shelf Pleistocene succession; downlaps seaward onto Pliocene in west and D6 horizon in east.	Ionian ~0.65 Ma
<i>D6 (Lower Pleistocene)</i> Upper slope	Forms a moderate- to high-amplitude, planar, convex-wavy reflection; erosive, angular unconformity in west, sub-parallel disconformity in east; truncated by shelf-edge Pleistocene succession in east, less clear in west; downlaps seaward onto Pliocene in west and Miocene in east.	Calabrian ~1.0 Ma
<i>D8 (Lower Pleistocene)</i> Upper slope	Forms a moderate- to high-amplitude, irregular reflection; erosive, locally concave, angular unconformity in west, sub-parallel disconformity in east; truncated by shelf-edge Pleistocene succession in east, less clear in west; downlaps seaward onto Pliocene in west and Miocene in east.	Calabrian ~1.1–1.7 Ma
D10 – Base Quaternary (Lower Pleistocene) Outer shelf–upper slope	Forms a moderate- to high-amplitude continuous reflection; planar to irregular, erosional angular unconformity that truncates Neogene sediments across the outer shelf and upper slope; landward mappable limit marked by mid-shelf carbonate reef escarpment.	Gelasian ~1.8–2.6 Ma NN17–19/N20–22
<i>D12 (Lower Pliocene)</i> Upper slope	Forms a moderate-amplitude reflection in vicinity of ODP 1130 and Jerboa-1 well; locally composite with Late Neogene Slide glide plane near slide scar; elsewhere, poorly recognised within general accumulation of Pliocene and Upper Miocene mass-flow deposits.	Zanclean ~4.75–5.0 Ma NN13/N18–19
<i>D15 (Upper Miocene)</i> Outer shelf–upper slope	Forms a high-amplitude planar reflection on the upper slope in vicinity of ODP 1126 and 1134, which truncates underlying sediments; less distinct on outer shelf but is planar to irregular and erosive where observed, separating upper hummocky seismic facies (above) from planar facies (below), and terminates by onlap onto carbonate reef escarpment; no clear reflection at ODP 1127 and 1132 but change in internal acoustic character noted.	Serravallian/Tortonian ~10.8–12.0 Ma NN7–8/N12–14
D20 – Lower Miocene Outer shelf–upper slope	Forms a moderate- to high-amplitude, continuous to semi-continuous, sub-planar to irregular reflection; erosive, predominantly angular unconformity; locally terminates at Miocene slide; continuity on upper slope locally poor due to intra-Miocene slumping and erosion; shelfward correlation to carbonate platform succession remains ambiguous; locally composite with D30?	Aquitanian/Burdigalian ~18.7–22.0 Ma NN2/N4–5
<i>D22 (Base Miocene)</i> Upper slope–(?)shelf-edge	Forms a sporadic strong to weak seismic reflection; a localised strong sub-planar to irregular reflection at ODP 1126 on the upper slope is locally erosive; at ODP 1132 on palaeo-shelf-edge, reflection probably lies within a reflective zone that includes Oligocene.	Chattian/Aquitanian ~23.0–23.5 Ma NP25–NN1/N4
<i>D25 ('Mid' Oligocene)</i> Upper slope–(?)shelf-edge	Forms a high-amplitude sub-planar reflection on upper slope that marks an angular unconformity, locally erosive and onlapped; no outstanding reflection on palaeo-shelf-edge where boundary is lost within a reflective zone; landward correlation to carbonate platform succession is unclear.	Late Rupelian ~28.0–29.0 Ma NP24/P21
D30 – Base Oligocene Outer shelf–upper slope	Forms a variable amplitude, continuous to semi-continuous reflection; sub-planar to irregular erosive unconformity on shelf, but locally truncated by D20; beyond palaeo-shelfbreak it is predominantly an onlap surface; a tentative seismic horizon is traced into the carbonate platform succession.	Priabonian/Rupelian ~33.7–34.2 Ma NP21/P18
<i>D32 (Upper Eocene)</i> Upper slope	Internal discordant and lensoid reflections observed in Upper Eocene section but difficult to correlate any specific reflection with biostratigraphic break.	Bartonian/Priabonian ~37.2–38.0 Ma NP17–18/P15
<i>D35 (Middle Eocene)</i> Upper slope	Internal discordant and lensoid reflections observed in Upper Eocene section but difficult to correlate any specific reflection with biostratigraphic break.	Bartonian ~39.2–40.1 Ma NP17/P14
D40 – Middle Eocene Outer shelf–upper slope	Forms a moderate- to high-amplitude, sub-planar, even to slightly irregular reflection along top of Wobbegong Supersequence delta; commonly angular and erosive; landward, generally terminates by	Lutetian ~43.0–46.2 Ma NP15/P9–12

(Continued)

Table 4 Continued.

Name and geographic extent of unconformity	Description	Age (stage) and approx. stratigraphic range of hiatus
	erosional pinch-out; on upper slope, it generally downlaps onto eroded Cretaceous rocks.	
BTU – Base Tertiary Unconformity Outer shelf–upper slope	Forms a strong reflection at the base of the Wobbegong Supersequence, especially beneath the Wobbegong delta; varies from a sub-planar to highly irregular angular unconformity that is eroded into underlying Cretaceous and older strata; commonly forms palaeo-valleys in Basement rocks; over much of the shelf and upper slope, the base of the Cenozoic succession comprises a composite hiatus, incorporating D40.	Danian/Selandian (late Maastrichtian?) ~59.2–≥66.0 Ma NP6/P4 and older

3.1. Middle–Upper Eocene sequence

3.1.1. Seismic stratigraphy. The Middle–Upper Eocene sequence is bounded at its base by the D40 unconformity and at its top by the D30 unconformity, though it locally crops out at seabed on the inner shelf (Feary *et al.* 1993; James *et al.* 1994) (Fig. 6; Table 4). The D40 unconformity commonly forms a composite surface with the BTU where the sequence directly overlies Mesozoic and older rocks. This sequence displays an irregular sheetform geometry of variable thickness (100–200 msec TWTT) across the shelf and upper slope, including the Wilson Bluff Limestone Formation within the lower carbonate platform succession. However, it thins (<100 msec TWTT), largely due to erosion, towards the Early/Mid-Eocene palaeo-shelf-edge where it overlies the Wobbegong Delta, though localised complexes of Middle Eocene bryozoan reef mounds up to 200 m thick are developed atop the delta (Sharples *et al.* 2014) (Figs 6, 8, 9). The sequence is locally absent on the upper slope because of primary depositional pinch-out as well as later erosion where the slope has been incised by canyons (Fig. 6).

Beneath the inner Nullarbor Shelf, the internal seismic reflection configuration of the Wilson Bluff Limestone Formation depicts mounded accumulations separated by sub-horizontal reflections traceable for over 20 km (Feary & James 1995, 1998) (Fig. 6; Table 5). The transition into the acoustically layered outer-shelf Middle–Upper Eocene succession (Table 5) is marked by gently inclined (<0.7°) seaward-dipping surfaces (Figs 6, 8c). The bryozoan mound complexes developed at the Early/Mid-Eocene palaeo-shelf-edge are overlapped by later Mid-Eocene and younger strata (Fig. 9a).

On the upper slope, the Middle–Upper Eocene sequence commonly exhibits a seismically layered character (Table 5) with planar to wavy reflections onlapping onto the Wobbegong delta front and downlapping onto Mesozoic strata downslope (Figs 6a–c, 8, 9). An erosional moat is locally preserved separating the mounded deposits from the delta slope (Fig. 8b). Whereas the sediment record at ODP site 1126 and in the Jerboa-1 well (Fig. 7) indicates the presence of intra-Mid and Mid/Late Eocene unconformities, herein designated as D35 and D32 (Table 4), respectively, their specific resolution on the seismic data remains poorly resolved despite internal discordances being observed (Figs 8b, 9a). A variably disrupted reflection pattern characterises the fill in the Eucla Canyon (Table 5; Fig. 9b).

3.1.2. Lithology. The base of the Middle–Upper Eocene sequence is characterised by a thin but widespread siliciclastic facies that varies from less than 1 m to several tens of metres thick (Fig. 7; Tables 5, 7). On the Nullarbor Shelf, green glauconitic sandstones were drilled in the Apollo-1 and Potoroo-1 wells, whereas two pebbles of calcareous sandstone were recovered from the base of the carbonate succession at ODP site 1132

(Shipboard Scientific Party 2000h), and site 1130 cored a mixed assemblage of siliciclastic and carbonate rocks (Shipboard Scientific Party 2000f; Li *et al.* 2003a). On the upper slope, bioclastic and glauconitic sandstone was recovered at ODP sites 1126 and 1134 (Shipboard Scientific Party 2000b, j) and in the Jerboa-1 well, though ambiguity remains over its stratigraphic setting (*cf.* Table 7).

The overlying carbonate succession on the inner Nullarbor Shelf is characterised by bryozoal limestone in the lower part of the carbonate platform whereas bioclastic wackestone, packstone and grainstone have been recovered on the outer shelf (Table 5). In addition, Sharples *et al.* (2014) report that the Middle Eocene section in the Potoroo-1 well includes a bryozoan mound complex at the base of the carbonate. At ODP site 1132, several firmgrounds were identified near the top of the sequence, including at the level of the D30 unconformity, which also displays brecciation and the presence of possible Neptunian dykes (Shipboard Scientific Party 2000h). Abundant bioturbation includes *Thalassinoides* burrows.

On the upper slope, Middle and Upper Eocene nannofossil chalk/ooze and mudstone is predominant at ODP sites 1126 and 1134 (Shipboard Scientific Party 2000b, j) and in the Jerboa-1 well (Table 5). Intensive bioturbation includes *Zoophycos* and *Chondrites* traces. No obvious lithological change is reported across the intra-Eocene D35 and D32 unconformities at ODP site 1126.

3.2. Oligocene–lowest Miocene sequence

3.2.1. Seismic stratigraphy. The Oligocene–lowest Miocene sequence is bounded at its base and top by the D30 and D20 unconformities, respectively (Fig. 6; Table 4). It displays a variably eroded sheetform geometry across the outer shelf, up to 100 msec thick at the palaeo-shelf-edge but commonly ≤50 msec TWTT thick landward. Correlation with the carbonate platform succession beneath the inner shelf, specifically the Abrakurrie Limestone Formation (Fig. 4), remains ambiguous. Indeed, the Oligocene–lowest Miocene sequence might be locally absent on the inner shelf due to erosion associated with the formation of the D20 unconformity (Fig. 6d). By way of contrast, the sequence is locally up to 200 msec TWTT thick on the upper slope in the vicinity of ODP site 1126. Lower Oligocene, Upper Oligocene and lowest Miocene sediments are all preserved at this site, separated by the D25 and D22 unconformities (Figs 7, 9a; Table 4). Farther west, lowest Miocene sediments are absent on the upper slope at ODP sites 1130 and 1134; their occurrence beyond site 1132 on the outermost shelf is terminated by the escarpment that marks the Late Neogene palaeo-shelf-edge (Fig. 8b).

On the outer Nullarbor Shelf, the Oligocene–lowest Miocene sequence displays an acoustically layered pattern (Table 5) with a hint of low-angle downlap onto the D30 unconformity near

Table 5 Summary of the seismic reflection configuration patterns and lithologies that characterise the Middle Eocene–Quaternary stratigraphic sequences in the western GAB. Seismic reflection patterns based primarily on this study, with additional information derived from Feary & James (1995, 1998) and Sharples *et al.* (2014). Lithological information for ODP sites derived from Shipboard Scientific Party (2000a, b, c, e, f, g, h, i, j) and Well Completion Reports for Apollo-1, Jerboa-1 and Potoroo-1 wells.

Stratigraphy	Seismic reflection configuration patterns	Lithological characteristics
Quaternary sequence	Outer-shelf section displays aggrading, planar-to-irregular, locally hummocky, variable amplitude, semi-continuous, sub-parallel reflection pattern. Shelf-edge configuration includes variable amplitude, hummocky-to-mounded, and sigmoid and oblique prograding reflection patterns. Upper-slope section is dominated by a convex-upward mounded package of low-to-high amplitude, well-layered, sub-parallel, semi-continuous reflections displaying two-way closure (updip/downdip), subdivided by several distinct intraformational unconformities (D2–D8) and locally moulded into upslope-migrating sediment waves (up to 10 km long, 1 km wide and 40 m high), buried and at seabed. Downslope, only uppermost unit (above D2) extends as a sheetform deposit; its layered reflection pattern locally disturbed and chaotic, including on flank of Eucla Canyon.	Outer-shelf section largely untested beneath seabed veneer. On the upper slope, the mounded package has been proved to comprise mostly pale yellow to pale grey bioclastic packstone with subordinate wackestone, grainstone and white to grey calcareous ooze/chalk, e.g., ODP 1126, 1127, 1129, 1130, 1131, 1132 and 1134. Grain size ranges from coarse silt to fine-grained sand in matrix with coarse-grained sand to granule-size bioclasts. Floatstone and rudstone recovered in upper part of section (above D2), including granule- to pebble-grade bryozoan fragments. Strong and pervasive bioturbation; common firmgrounds. Decimetre-scale upwards-coarsening cyclicity at sites 1127 and 1129; sporadic inverse-to-normally graded beds (turbidites) and evidence of soft-sediment deformation and slumping reported at sites 1127, 1130 and 1131. In Eucla Canyon, ODP 1133 proved bioturbated, varicoloured calcareous ooze, deformed by disharmonic and isoclinal folding, on basal grainstone turbidite.
Pliocene sequence	On the upper slope, the Pliocene sequence generally displays weak-to-moderate, semi-continuous, chaotic to lenticular reflections; however, the Upper Pliocene section becomes more strongly layered upslope toward the Late Neogene Slide scar, onto which hummocky to wavy clinofolds display upslope migration, onlap, and eventual burial of the escarpment. At ODP 1130, the boundary between the Lower and Upper Pliocene sections is marked by a moderately reflective, semi-continuous but irregular reflection.	Strongly bioturbated Lower Pliocene calcareous nannofossil chalk and Upper Pliocene olive–pale grey bioclastic packstone occur immediately downslope from late Neogene slide scar at ODP 1130, separated by an unconformity that is marked by slumped bedding. Farther downslope, Lower Pliocene mixed nannofossil ooze and a wackestone–rudstone assemblage at ODP 1134, and Upper Pliocene white–grey calcareous nannofossil ooze at ODP 1126: both sections include varying content of coarse-grained bioclasts, including bryozoans, and matrix-supported pebble-grade intraclasts of nannofossil chalk.
Upper Lower–Upper Miocene sequence	Flat-lying to hummocky reflections within the inner shelf, upper Lower–Middle Miocene carbonate platform (<i>Nullarbor Lst. Fm</i>) are largely discontinuous and of variable amplitude, in contrast to the well-defined prograding reflections in the escarpment zone, and the moderate-amplitude of the more continuous, sub-parallel to wavy reflections of the correlative, aggrading outer-shelf section. The outer shelf, Upper Miocene ‘coalesced mound complex’ comprises individual mounds ranging 30–110 m thick and 0.4–1.5 km across. On upper slope, entire sequence shows variable and generally less coherent reflection configurations, including sub-parallel to wavy and contorted, hummocky to chaotic and structureless, reflection-free patterns; common lensoid packages; internal erosion by channelised incision; and mass-flow activity, including the Late Neogene Slide. Chaotic and hummocky reflection pattern on flanks of Eucla Canyon includes stacked accumulation of lensoid packages.	On the outer shelf, ODP 1132 proved upper Lower–Middle Miocene white to pale grey and olive grey, bioturbated, glauconitic and bioclastic grainstone and grey to black chert overlain by Upper Miocene white to grey calcareous ooze and chalk and minor bioclastic packstone. Upper Lower–Middle Miocene Marl, wackestone, packstone and grainstone recovered at Potoroo-1 well. On western Eyre Terrace, upper Lower–Middle Miocene rocks include bioturbated white to pale grey foraminiferal and calcareous nannofossil ooze and chalk interbedded with chert and glauconitic and bioclastic mudstone to packstone, e.g., ODP 1126 and 1134. Farther east, ODP 1127, 1129, 1131 and 1133 proved Middle Miocene pale grey to olive grey, bioturbated, glauconitic and bioclastic wackestone, packstone and grainstone with interbedded chert/porcellanite. Upper Miocene rocks on upper slope dominated by bioturbated, pale grey, nannofossil ooze/chalk, sporadic bioclastic packstone and grainstone, e.g., ODP 1126, 1127, 1130, 1133 and 1134. These sites also record firmgrounds, intraformational breaks, graded bedding, inclined and folded (slumped) bedding and rotated clasts.
Oligocene–Lowest Miocene sequence	Inner-shelf carbonate platform (<i>Abrakurrie Lst. Fm</i>) lacks resolution. Outer-shelf section is layered with low-to-medium amplitude, sub-planar, sub-parallel reflections. Upper-slope section is mainly layered, sub-parallel reflection pattern that reveals onlap and downlap onto underlying rocks, including progressive burial of Wobbegong delta front by planar and wavy clinofolds; hummocky and lenticular patterns in Upper Oligocene, including downlap onto angular discordance of D25 unconformity, as well as localised channelised incision associated with the D22 unconformity. Chaotic and hummocky reflection patterns elsewhere on slope, including the Eucla Canyon.	Pale yellow/brown, glauconitic, bioclastic and foraminiferal grainstone and packstone with subordinate wackestone and marl recovered from Lower Oligocene–lowest Miocene rocks on outer shelf, e.g., ODP 1132 and Potoroo-1 well. White to pale grey, bioturbated, calcareous nannofossil ooze/chalk is predominant throughout the sequence on the upper slope, e.g., ODP 1126, 1130 and 1134, though lowest Miocene rocks only present at site 1126. Subordinate interbedded lenses and nodules of greenish grey chert/porcellanite also present (excepting the Lower Oligocene section at ODP 1134). The Jerboa-1 well proved Lower Oligocene rocks containing abundant sponge spicules, but no information on younger rocks.

Middle–Upper Eocene sequence	<p>The inner-shelf carbonate platform (<i>Wilson Bluff Lst. Fm</i>) displays mounded units, 10–15 km wide, 100 msec TWTT thick, separated by high-amplitude sub-horizontal reflections; hint of downlap towards seaward edge of platform. Outer-shelf section is mainly layered with variable weak-to-strong, planar-to-wavy reflection configuration; sporadic bryozoan mounds, 5–13 km wide, extend 60–150 km along shelf-edge. The upper-slope section is layered, with moderate amplitude, lensoid to mounded/wavy configuration displaying two-way (updip/downdip) closure and intraterritorial discordances (D32 and D35). Layered to lenticular/hummocky/chaotic reflections in Eucla Canyon.</p> <p>Carbonate facies includes: (1) bryozoal limestone on carbonate platform, e.g., Apollo-1 well; (2) interbedded, bioturbated, grey, yellow, red, white bioclastic wackestone, packstone and grainstone on outer shelf, e.g., ODP 1130 and 1132, and Potoroo-1 well; (3) bioturbated, white to pale grey nanofossil chalk/ooze and mudstone with sporadic lenses of chert/porellanite, and interbedded wackestone and packstone on upper slope, e.g., ODP 1126 and 1134, and Jerboa-1 well. Basal siliciclastic facies includes dark grey–green, red, brown, poorly sorted, very fine- to very coarse-grained bioclastic sandstone, minor mudstone, sporadic pebbles, glauconite, fragments of lignite and benthonic fauna that includes <i>Cibicides</i> spp., e.g., Apollo-1, Potoroo-1 and Jerboa-1 wells, and ODP 1126, 1130, 1132 and 1134.</p>
------------------------------	---

ODP site 1132 (Fig. 8b). The Middle Eocene bryozoan mound complexes were progressively onlapped and buried (Fig. 9). Whereas ODP site 1132 proved Lower Oligocene, Upper Oligocene and lowest Miocene sediments (Fig. 7), there is no obvious seismic expression of the D22 or D25 unconformities on the outer shelf where these boundaries might converge within a highly reflective zone. On the upper slope, seaward of the Wobbe-gong Delta, this sequence mostly comprises acoustically layered Oligocene sediments whose reflection configuration reveals evidence of onlap, downlap and sporadic channel incision, which highlight the angular and locally erosive nature of the D22 and D25 unconformities (cf. Table 5; Figs 8a, 9b). Lowest Miocene sediments at ODP site 1126 are not seismically distinguishable from the overlying upper Lower–Middle Miocene sediments, all of which seem to be part of a disturbed Miocene section (Fig. 9a). Farther downslope, the entire Oligocene–lowest Miocene sequence displays a chaotic signature towards the seaward edge of the upper slope, where the sequence appears to infill a former canyon as well as the Eucla Canyon (Figs 6c, 9b).

3.2.2. Lithology. On the outer Nullarbor Shelf, the Oligocene–lowest Miocene sequence comprises predominantly bioclastic grainstone and packstone (Table 5). At ODP site 1132, the brecciated D30 unconformity is overlain by a basal Oligocene grainstone bed, which contains delicate branching bryozoans and serpulids (Shipboard Scientific Party 2000h). Despite the occurrence of the D25 and D22 biostratigraphic breaks at this site, no obvious lithological changes were observed across these unconformities; however, a sharp change to chert-rich deposits of the overlying Middle–Upper Miocene sequence marks the D20 unconformity. A mixed assemblage of Lower Oligocene marl, wackestone, packstone and grainstone is reported from the Potoroo-1 well.

Calcareous nanofossil ooze/chalk predominates on the upper slope at ODP sites 1126, 1130 and 1134 where Lower and Upper Oligocene rocks were proved at all sites, though lowest Miocene deposits were only present at ODP site 1126 (Shipboard Scientific Party 2000b, f, j) (Fig. 7; Table 5). At all sites, the sediments are pervasively bioturbated with *Zoophycos* and *Chondrites* burrows in abundance. Sporadic firmgrounds are present in the lowest Miocene and Upper Oligocene sections at ODP site 1126. Whereas the D25 and D22 unconformities are recognised biostratigraphically and on seismic reflection profiles from the slope succession, no obvious lithological change is recorded across these boundaries.

3.3. Upper Lower–Upper Miocene sequence

3.3.1. Seismic stratigraphy. On the outer shelf and upper slope, the upper Lower–Upper Miocene sequence is generally bounded at its base by the D20 unconformity, and its top is marked by the D10 unconformity, except where the base Pliocene D12 unconformity is locally recognised (see below) (Figs 6, 8b; Table 4). The sequence is commonly between 140 and 200 msec TWTT in thickness on the outer shelf, whereas, on the upper slope, it is generally thinner due to erosion, ranging from 15 to 140 msec thick (Fig. 6). In the mid to inner shelf region, Upper Miocene sediments are absent, and the upper Lower–Middle Miocene Nullarbor Limestone Formation marks the top of the sequence, which is locally exposed at seabed (James *et al.* 1994). The basal D20 unconformity remains poorly resolved. The intra-Miocene D15 unconformity separates upper Lower–Middle Miocene and Upper Miocene units on the outer shelf and upper slope, though this boundary is not everywhere distinguishable on seismic reflection data (Figs 8, 9). On the mid shelf, this interface is marked by a steeply dipping reef-front escarpment that has been traced for at least 475 km, is up to 300 m high and forms the rimmed edge to the Mid-Miocene carbonate platform (Feary & James 1995), which thins landward and is

Table 6 Tentative correlation of Mid-Palaeogene–Quaternary unconformities utilised in this study with those previously proposed by Li *et al.* (2003a, b, c, 2004). Name of hiatus highlighted in **bold** represents confident correlation between studies; *italic* notation represents hiatuses in existing scheme uncorroborated by present study (see text for further details). Global sequence boundaries are those of Hardenbol *et al.* (1998).

Li <i>et al.</i> (2003a, b, c, 2004)			This study		
Hiatus	Global sequence boundary	Age	Unconformity/other unassigned hiatuses	Age range of hiatus	Comment
<i>H15</i>	Cala1/2	1.5 Ma			Li <i>et al.</i> (2004) state that MH3 ‘...is represented in the Bight by a reflector between seismic sequences 2 and 3 [of Feary & James 1995, 1998]’ – our regional D10 unconformity. The significance of H15 and H14 cannot be corroborated from seismic data. The possibility that H15 is one of several highly localised hiatuses in the basal part of the Eyre Terrace Drift at ODP site 1130 on the upper slope cannot be discounted. The likelihood that H14 – described from a slump deposit at ODP sites 1126 and 1134 – is anything other than a localised upper-slope discordance is questionable.
MH3		1.5–2.5 Ma	D10 Base Quaternary	~1.8–2.6 Ma	
<i>H14</i>	Ge1	2.5 Ma			
H13	Pia1	3.5 Ma	<i>Unassigned ‘Mid’-Pliocene boundary</i>		This ‘Mid’ Pliocene hiatus is seismically identifiable only at ODP site 1130 where Pliocene deposits are divided by a moderately reflective, semi-continuous, irregular reflection that is restricted to the upper slope fill of the Late Neogene Slide.
H12	Za1	4.5 Ma	D12 Lower Pliocene	~4.75–5.0 Ma	The H12 hiatus is seismically identifiable only at ODP site 1130. It correlates with the D12 unconformity, which is restricted to the upper slope, and is locally composite with glide plane of Late Neogene Slide.
<i>H11</i>	Me2	5.7 Ma			Li <i>et al.</i> (2004) state that MH2 ‘...created unconformities up to 15 and 5 Myr in duration...at [ODP] sites 1130 and 1132 [respectively]’. However, inspection of seismic data indicates that sediment removal at former site is related to Late Neogene Slide, whereas hiatus at 1132, 1126 and 1134 is associated with D15 unconformity, i.e., different surfaces. The significance of H9–H11 cannot be confirmed from seismic data. H9 and H10 are probably localised upper-slope hiatuses (ODP sites 1126 and 1134); the status of H11 (reportedly coeval with a slump at site 1126) is uncertain.
<i>H10</i>	Tor3/Me1	7.0 Ma	<i>Unassigned, localised, intra-Upper Miocene hiatuses on upper slope?</i>		
<i>MH2</i>		8–9 Ma			
<i>H9</i>	Tor2	9.3 Ma			
H8	Ser4/Tor1	11.7 Ma	D15 Upper Miocene	~10.8–12.0 Ma	The H8 hiatus is seismically identifiable at ODP sites 1126, 1132 and 1134. It correlates with our D15 unconformity on the outer shelf and upper slope.
<i>H7</i>	Ser2	13.5 Ma			Li <i>et al.</i> (2004) state that MH1 represents an ‘...absence of an almost 8 Myr record from [ODP] site 1132 [which] indicates a significant event from 15–16 Ma’. We correlate the major Early Miocene hiatus at site 1132 with the D20 unconformity (see below). The significance of H5–H7 cannot be confirmed from seismic data. Whereas H5 might coincide with a localised upper slope hiatus at site 1134, the status of H6 and H7 is uncertain.
<i>H6</i>	Lan2/Ser1	14.8 Ma	<i>Unassigned, localised, intra-Lower–Middle Miocene hiatuses on upper slope?</i>		
<i>MH1</i>		15–16 Ma			
<i>H5</i>	Bur5/Lan1	16.4 Ma			
<i>H4</i>	Bur3	18.7 Ma			The status and significance of H2–H4 cannot be confirmed from seismic data. This section is generally an interval of poor recovery and absence of diagnostic species. Our study interprets a major regional erosional gap (D20) at most sites, though possibility of intermittent sedimentation on upper slope (ODP sites 1126 and 1134) cannot be discounted.
<i>H3</i>	Aq3/Bur1	20.5 Ma	D20 Lower Miocene	~18.7–22.0 Ma	
<i>H2</i>	Aq2	22.2 Ma			
H1	Ch4/Aq1	23.8 Ma	D22 Base Miocene	~23.0–23.5 Ma	The H1 hiatus is seismically identifiable at ODP site 1126. It correlates with our D22 unconformity. This boundary has also been proved at site 1132 on outer shelf, though specific reflector is indistinct within a strongly reflective zone.
‘Mid’ Oligocene	Ru4/Ch1	28.5 Ma	D25 ‘Mid’ Oligocene	~28.0–29.0 Ma	The ‘Mid’ Oligocene hiatus is seismically identifiable at ODP sites 1126, 1130 and 1134 on the upper slope. It correlates with our D25 unconformity. This boundary has also been proved at site 1132 on outer shelf, though specific reflector is indistinct within a strongly reflective zone.
D	Pr4/Ru1	33.5–34 Ma	D30 Base Oligocene	~33.7–34.2 Ma	The D hiatus is seismically identifiable across the outer margin at ODP sites 1126, 1132 and 1134, and in wells Jerboa-1 and Potoroo-1. It correlates with our regional D30 unconformity.
C	Pr1	37 Ma	D32 Upper Eocene	~37.2–38.0 Ma	The C hiatus is identified at ODP site 1126 and the Jerboa-1 well but is restricted to the Eocene drift on the upper slope. It correlates with our D32 unconformity.
B	Bart 1	39–40 Ma	D35 Middle Eocene	~39.2–40.1 Ma	The B hiatus is identified at ODP site 1126 and the Jerboa-1 well but is restricted to the Eocene drift on the upper slope. It correlates with our D35 unconformity.
A	Lu4	43 Ma	D40 Middle Eocene	~43.0–46.2 Ma	The A hiatus is seismically identified at ODP sites 1126, 1130, 1132, and 1134, and in wells Jerboa-1, Potoroo-1 and Apollo-1. It correlates with our regional D40 unconformity.

Table 7 Summary of the stratigraphic setting and lithology of the Middle Eocene siliciclastic facies at the base of the Dugong Supersequence. Lithological and thickness data for ODP sites derived from Shipboard Scientific Party (2000a, b, f, h, b, f, b, j) and Li *et al.* (2003a), and Well Completion Reports for Apollo-1, Jerboa-1 and Potoroo-1 wells.

Site/well	Stratigraphic setting	Lithology
ODP 1126	Borehole located seaward (downslope) of the Wobbe-gong delta. Basal cored section unconformably overlies eroded Cretaceous rocks.	Veneer of yellow to brown bioclastic sandstone infilling cm-sized cavities in ferruginous hardground atop brown, ? Cenomanian, cross-bedded sandstone.
ODP 1130	Borehole located above the outer part of the Wobbe-gong delta plain. 30-m-thick basal cored section interpreted (this study) as reworked top of delta plain.	Mixed siliciclastic/carbonate assemblage comprising predominantly red, poorly sorted, fine sand- to granule-grade bioclastic, calcareous sandstone gradational into sandy limestone; subordinate red bioclastic glauconitic wackestone, grey carbonate mudstone and white/red bryozoan grainstone and bivalve grainstone.
ODP 1132	Borehole located above inner part of Wobbe-gong delta plain. No recovery in basal 43 m of borehole, which likely terminated in Wobbe-gong Supersequence.	Two pebbles of coarse sand- to granule-grade calcareous sandstone with abundant bioclastic and lithic fragments recovered at base of carbonate succession. It remains uncertain whether these pebbles form part of the Wobbe-gong delta or represent reworked delta plain material at the base of the Dugong Supersequence.
ODP 1134	Borehole located seaward (downslope) of the Wobbe-gong delta, though proximal to mass-flow deposit. Only upper 0.3 m of 28.8-m-thick basal cored section recovered.	Upper 0.3 m of siliciclastic section comprises coarse-grained, brown limonitic sandstone with glauconite, abundant skeletal grains and minor planktonic foraminifers. It remains uncertain whether any part of this section includes mass-flow material deposited contemporaneous with/or reworked from the Wobbe-gong delta.
Jerboa-1	Borehole located seaward (downslope) of the Wobbe-gong delta. Basal cored section is 46 m thick and unconformably overlies eroded Cretaceous rocks.	Muddy sandstone composed of Fe-stained quartz, lithic fragments, glauconite and bioclastic debris, including bryozoans, benthic foraminifers, sponge spicules and bivalves.
Potoroo-1	Borehole located above the Wobbe-gong delta front. 45-m-thick cored basal siliciclastic section unconformably overlies Wobbe-gong Supersequence.	Poorly sorted, very fine- to very coarse-grained, commonly Fe-stained, green glauconitic and bioclastic sandstones with abraded bryozoal fragments, fluctuating proportions of benthic (especially <i>Cibicides</i> spp.) and planktonic fauna.
Apollo-1	Borehole located on mid-shelf. Basal cored section is 46 m thick and unconformably overlies eroded Cretaceous rocks.	Dark grey to green, medium- to coarse-grained glauconitic sandstone with common fragments of lignite and poorly preserved arenaceous fauna.

absent from the innermost shelf (Feary *et al.* 1993; James *et al.* 1994) (Figs 5, 6).

The internal seismic character of the upper Lower–Upper Miocene sequence is highly variable (Table 5). On the inner Nullarbor Shelf, the Nullarbor Limestone Formation contains an abundance of flat-lying-to-hummocky reflections, which display a stacked aggrading configuration that changes to a sigmoid-oblique pattern at the rimmed edge of the carbonate platform (Feary & James 1995, 1998) (Figs 6, 8c). Downslope of the escarpment, progradational stacking of planar to hummocky and lensoid packages appear to terminate by downlap at the level of the D20 boundary (Figs 6, 8c). The correlative outer-shelf section, bounded by the D15 and D20 unconformities, extends towards the shelf-edge as a predominantly layered sheetform unit ranging from about 20 to 140 msec TWTT thick, with a hint of low-angle downlap onto the D20 unconformity (Fig. 8b). The overlying Upper Miocene unit (above D15) has been described as a ‘coalesced mound complex’ (Table 5), which extends for up to 30 km away from the reef-front escarpment across the outer shelf (Feary & James 1998). The mound complex terminates landward by onlap onto the rimmed escarpment (Fig. 8c); towards the shelf-edge, the reflection pattern becomes more flat-lying (Fig. 6).

All or part of the upper Lower–Upper Miocene sequence on the outer shelf is truncated by a distinct buried erosional escarpment, up to 200 m high, which probably marks the late Neogene palaeo-shelf-edge (Fig. 6). This buried escarpment is most pronounced on seismic profile Ja90-23 where observational evidence for a major slide – herein informally termed the ‘Late Neogene Slide’ – is preserved (see below) (Fig. 8b). Downslope, the upper slope succession preserves elements of the lower and upper outer shelf units. In some areas, these units are traceable across the shelf-edge, in others they are detached; always, the stratigraphy and the internal reflection configuration is generally less coherent on the slope than the shelf.

On seismic profile Ja90-19, a layered upper Lower–Middle Miocene section is locally incised by an erosional channel, up to 6 km wide, whose fill was subsequently truncated by the D15 unconformity; the overlying Upper Miocene unit contains numerous acoustically structureless packages (Fig. 8a). To the east, only the Upper Miocene unit is preserved on the upper slope in the vicinity of ODP site 1130, where it is preserved as a thin (20–60 msec TWTT) irregular deposit with a structureless to chaotic acoustic signature. This deposit directly overlies, and terminates upslope against, Oligocene strata at the base of the buried escarpment at a lower projected stratigraphic level than the upper Lower–Middle Miocene unit on the adjacent shelf. Thus, this boundary might represent the glide plane of the Late Neogene Slide, which can be traced downslope for 15–20 km, and that the escarpment represents the slide scar (Fig. 8b).

A more complete record of upper Lower–Upper Miocene sedimentation on the upper slope is indicated by ODP site 1126 (Fig. 9a). However, whilst the drilled stratigraphic section indicates a degree of continuity with the outer shelf, interpretation of seismic profile Ja90-27 suggests that the Upper Miocene section (above D15), which displays a lensoid form, might be detached from its outer-shelf equivalent. Upslope extrapolation of the D15 unconformity away from ODP site 1126 suggests that it might be cut out at the level of the D10 unconformity. Thus, the bulk of this upper slope succession is probably the upper Lower–Middle Miocene unit, albeit its generally contorted internal reflection pattern differs from its signature on the adjacent shelf. The removal of the Upper Miocene unit from parts of the upper slope is further enhanced on the eastern margin of the study area where ODP sites 1127, 1129, 1131 and 1133 prove a predominantly Middle Miocene record, with thin Upper Miocene deposits only intersected at the deepest-water

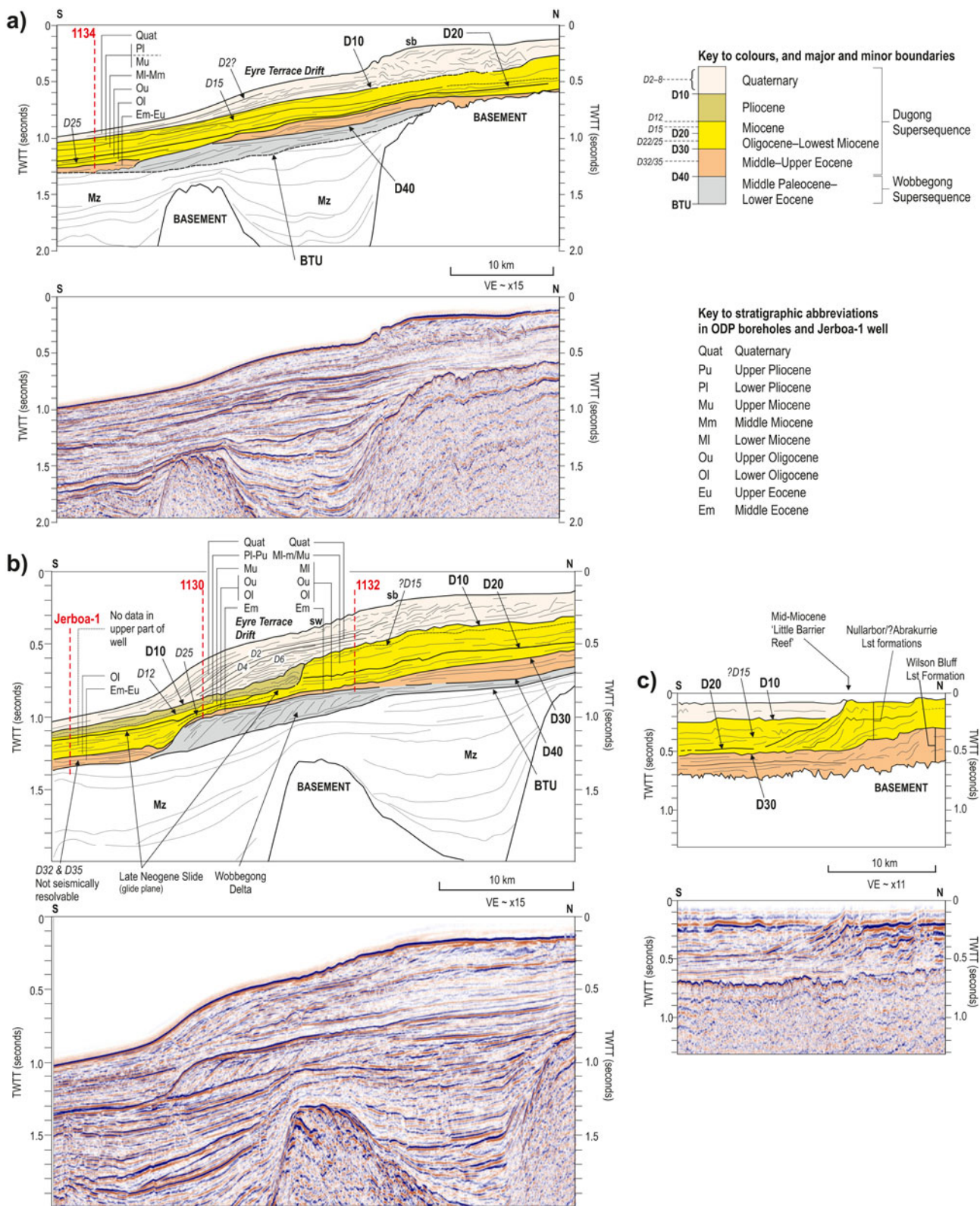


Figure 8 Seismic reflection profiles and accompanying interpretations from the western GAB showing the seismic-stratigraphic architecture of the Dugong Supersequence beneath the outermost shelf–upper slope (a, b) and the mid-shelf region (c), highlighting the main mappable outer shelf–upper slope unconformities (bold) and the more localised minor unconformities (italics) largely restricted to the upper slope. (a) Interpreted and uninterpreted seismic profile Ja90-19 calibrated with ODP borehole 1134. (b, c) Interpreted and uninterpreted seismic profile Ja90-23 calibrated in (b) with ODP boreholes 1130 and 1132, and the Jerboa-1 well. Locations of profiles shown in Figure 6. Abbreviations: Mz, Mesozoic; sb, shelfbreak; sw sediment waves. VE at seabed $\sim \times 15$.

sites (1127 and 1133) (Figs 7, 9b). Whereas the lower part of the upper Lower–Upper Miocene sequence on the outer shelf can be traced onto the upper slope, the internal seismic character changes from acoustically layered on the shelf to chaotic and

hummocky on the lower part of the upper slope and flanks of the Eucla Canyon (Fig. 9b).

3.3.2. Lithology. On the outer Nullarbor Shelf, an upper Lower–Middle Miocene bioclastic wackestone, packstone and

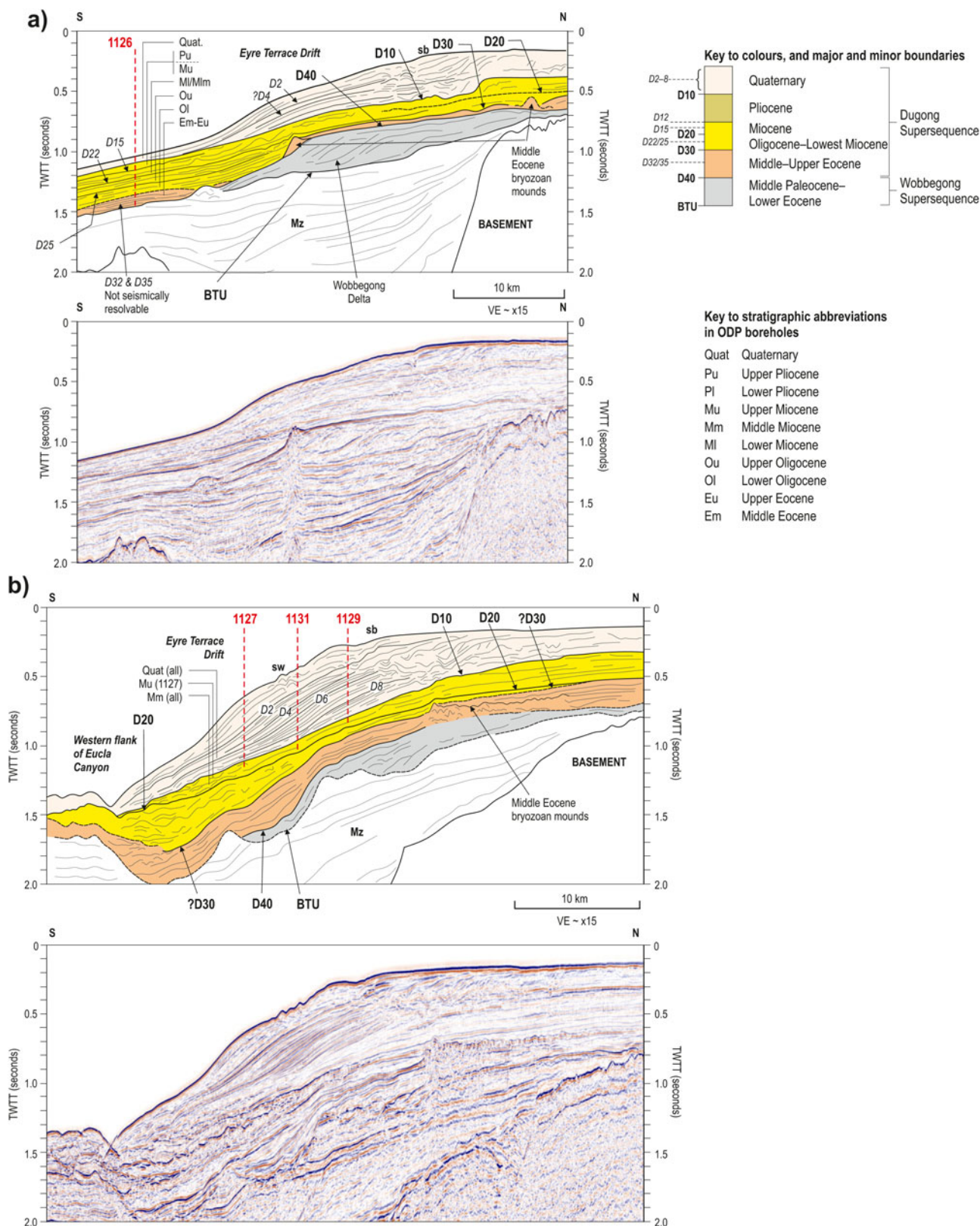


Figure 9 Seismic reflection profiles and accompanying interpretations from the western GAB showing the seismic-stratigraphic architecture of the Dugong Supersequence beneath the outermost shelf–upper slope, highlighting the main mappable outer shelf–upper slope unconformities (bold) and the more localised minor unconformities (italics) largely restricted to the upper slope. (a) Interpreted and uninterpreted seismic profile Ja90-27 calibrated with ODP borehole 1126. (b) Interpreted and uninterpreted seismic profile Ja90-31 calibrated with ODP boreholes 1127, 1129 and 1131. Locations of profiles shown in Figure 6. Abbreviations: Mz, Mesozoic; sb, shelfbreak; sw sediment waves. VE at seabed ~×15.

grainstone succession unconformably overlain by Upper Miocene calcareous ooze/chalk was intersected by ODP site 1132 (Shipboard Scientific Party 2000h) and the Potoroo-1 well (Table 5). ODP site 1132 penetrated the D15 unconformity

(Fig. 8b); although the contact was not cored, the lithological change is sharp.

On the upper slope, a more mixed assemblage of chalk/ooze and bioclastic carbonate rocks prevails throughout the entire

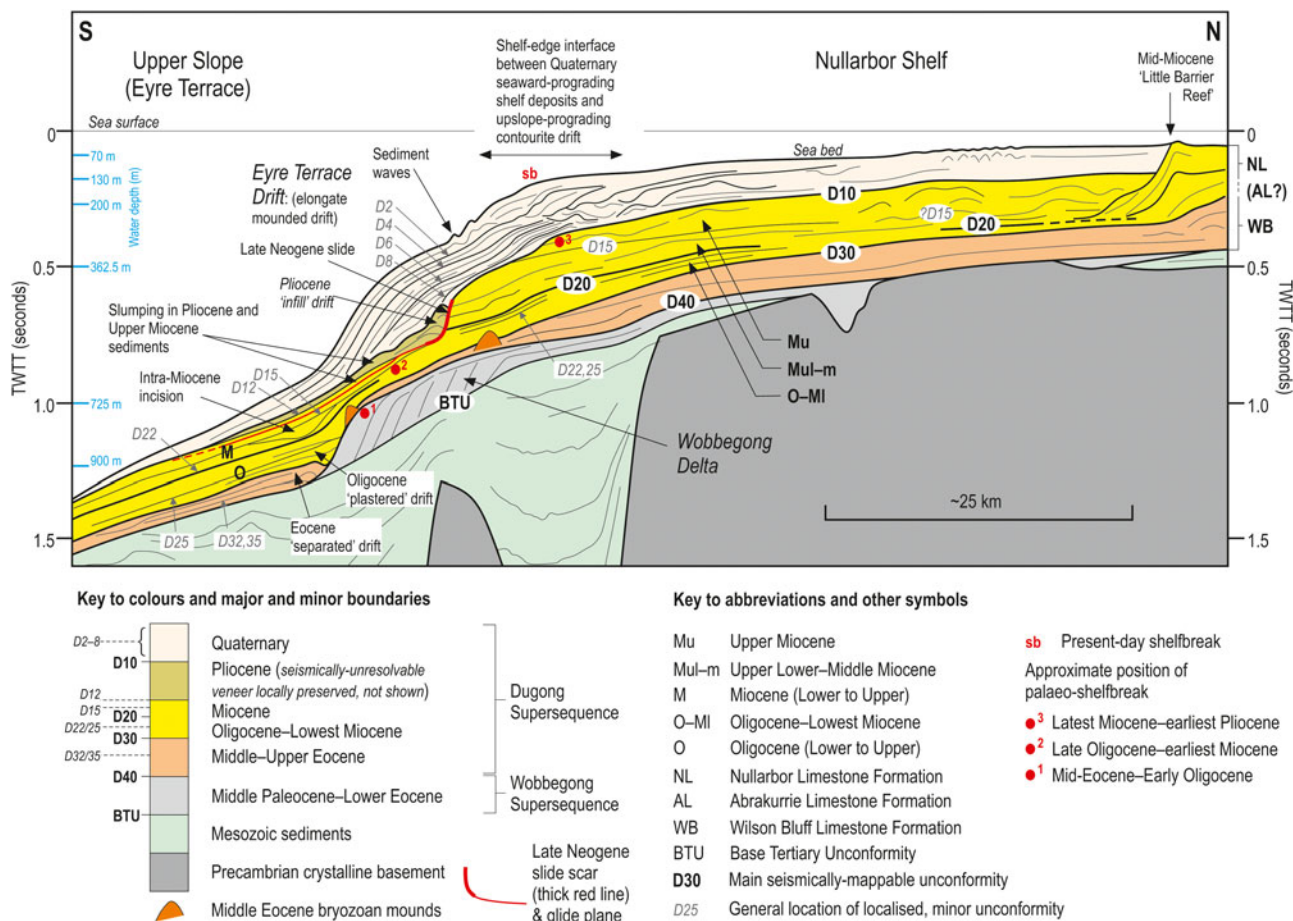


Figure 10 Schematic section summarising the main characteristics of the Cenozoic stratigraphic framework on the western Nullarbor Shelf and adjacent upper slope (see text for details.) VE $\times 30$.

sequence (Table 5). ODP site 1130 proved Upper Miocene sediments unconformable on Upper Oligocene deposits; the contact probably represents the base (glide plane) of the Late Neogene slide (Fig. 8b). The Upper Miocene deposits predominantly comprise bioturbated nannofossil ooze/chalk. The basal 30 m is more varied and includes beds of bioclastic grainstone with sharp bases and sharp-to-gradational tops, inclined and folded bedding in the chalk and the presence of a firmground (Shipboard Scientific Party 2000f). ODP sites 1126 and 1134 cored the entire preserved upper Lower–Upper Miocene sequence, including the D15 unconformity (Figs 8a, 9a). The upper Lower–Middle Miocene section includes calcareous ooze/chalk interbedded with bioclastic wackestone and packstone (Shipboard Scientific Party 2000b, j) (Table 5). Some beds have sharp bases and are normally graded, though much of the section is intensely bioturbated, commonly *Zoophycos* and *Chondrites* burrows, and most bed contacts are transitional. At both sites, the Upper Miocene section comprises nannofossil ooze; however, the section at ODP site 1126 is punctuated by several slumped beds that display inclined and folded bedding, silicified layers comprising irregular to nodular porcellanite and a firmground. This section is also intensely bioturbated, including *Zoophycos*, *Chondrites*, *Planolites*, *Terrabelina* and *Thalassinoides* burrows. At ODP site 1126, the D15 unconformity coincides with the base of the slumped beds; at ODP site 1134, the unconformity broadly coincides with an upward change from partially lithified to unlithified sediment. A further series of local, unassigned biostratigraphic breaks have been identified at both sites (Fig. 7; Shipboard Scientific Party 2000b, j).

Farther east, ODP sites 1127, 1129, 1131 and 1133 all terminated within Middle Miocene rocks that predominantly

comprised bioturbated, bioclastic wackestone, packstone and grainstone interbedded with chert/porcellanite (Shipboard Scientific Party 2000c, e, g, e, i) (Figs 7, 9b; Table 5). Upper Miocene rocks were recovered only at ODP sites 1127 and 1133. At site 1127, the Upper Miocene section comprises bioclastic packstone and minor grainstone beds with rotated intraclasts overlain by strongly bioturbated calcareous ooze/chalk, including *Zoophycos* and *Planolites* burrows (Shipboard Scientific Party 2000c). There is no obvious lithological or textural change in the bioclastic packstone above and below the Middle/Upper Miocene biostratigraphic break, though the Upper Miocene section appears disturbed. ODP site 1133 proved bioturbated Upper Miocene nannofossil ooze with sporadic firmground development, including at the boundary with the underlying Middle Miocene section (Shipboard Scientific Party 2000i). Both these sites display significant amounts of reworking of benthic and planktonic foraminifers and calcareous nannofossils (Shipboard Scientific Party 2000c, i).

3.4. Pliocene sequence

3.4.1. Seismic stratigraphy. Pliocene sediments are restricted to the upper slope of the Eyre Terrace (Fig. 6). They are best preserved where they form part of the infill of the Late Neogene Slide scar (Fig. 6b); elsewhere on the slope (e.g., ODP sites 1126 and 1134), they are largely seismically unresolvable from the underlying Miocene deposits (Figs 6a, c). The top of the sequence is marked by the D10 unconformity, whereas the base is marked by the D12 unconformity; the latter is locally composite with the glide plane of the Late Neogene Slide (Fig. 8b). The Pliocene sequence is thickest (up to 120 msec TWTT) immediately adjacent to the slide scar where well-

developed upslope-migrating clinoforms are identified (Table 5); however, it thins downslope to less than 50 msec TWTT (40 m thick) at ODP site 1130, and might pinch out at the seaward edge of the Eyre Terrace (Figs 6b, 8b). Lower and Upper Pliocene units are proved at ODP site 1130 (Shipboard Scientific Party 2000f) (Fig. 7), separated by a moderate reflection; however, Pliocene reflection patterns are generally weaker and less coherent downslope (Table 5).

3.4.2. Lithology. The Pliocene sequence comprises a mixed, commonly disturbed, upper slope assemblage of calcareous nanofossil ooze/chalk and bioclastic wackestone, packstone, floatstone and rudstone (Shipboard Scientific Party 2000b, f, j) (Table 5). The sediments are strongly bioturbated and include *Chondrites* burrows. At ODP site 1130, Lower Pliocene calcareous nanofossil chalk is unconformably overlain by Upper Pliocene bioclastic packstone (Shipboard Scientific Party 2000f). The top of the Pliocene sequence (D10 unconformity) is marked by a hardground, whereas the base of the Upper Pliocene section is characterised by syn-sedimentary deformation depicted by inclined and disturbed alternating layers of glauconitic bioclastic packstone and white nanofossil bioclastic packstone. The basal D12 unconformity is marked by a sharp textural change from a uniform wackestone texture in Upper Miocene nanofossil chalk to an interbedded mudstone to packstone texture in the overlying Lower Pliocene chalk (Shipboard Scientific Party 2000f). Elsewhere, Lower Pliocene wackestone-to-rudstone and Upper Pliocene calcareous ooze were recovered at ODP sites 1134 and 1126, respectively; both sections contain a wide variety of coarse-grained bioclasts and lithic clasts (Shipboard Scientific Party 2000b, j) (Table 5).

3.5. Quaternary sequence

3.5.1. Seismic stratigraphy. The Quaternary sequence is preserved as a wedge-shaped deposit on the outer shelf and upper slope. Its base is marked by the D10 unconformity; its top is the present-day seabed (Fig. 6). The sequence locally exceeds 550 msec TWTT in thickness (557 m at ODP site 1129) at the shelf-edge, but is more generally between 220 and 300 msec TWTT thick. On the outer Nullarbor Shelf, the thickness generally ranges from 100 to 200 msec TWTT but terminates landward, abruptly, by onlap onto the seaward edge of the rimmed Middle Miocene carbonate platform (Figs 6, 8c). On the carbonate platform, the Quaternary sediments occur as a patchy veneer, below seismic resolution (Feary *et al.* 1993; James *et al.* 1994, 2001, 2006). On the upper slope, the Quaternary sequence gradually thins downslope onto the main part of the Eyre Terrace and on the flanks of the Eucla canyon, and might pinch-out, locally.

The internal seismic character of the Quaternary sequence is variable and can be described as three distinct zones: outer shelf, shelf-edge and upper slope (Table 5). On the outer shelf, the sequence displays a predominantly aggrading, layered internal reflection configuration as well as areas characterised by hummocky reflections (Fig. 6). Towards the shelf-edge, the outer-shelf reflections transition into a more complex configuration that displays a disrupted pattern, which includes hummocky-to-mounded and prograding reflection configurations (Figs 6, 8, 9). Complex reflector-truncation patterns within the shelf-edge section produce a locally hummocky–contorted configuration (e.g., Fig. 9b).

By way of contrast, the slope section displays a convex-up mounded external form and a strongly layered internal reflection configuration that exhibits two-way closure in the core of the mound (Figs 6, 8, 9; Table 5). The axis of the mounded section can be traced for over 200 km along the length of the Eyre Terrace (Figs 5, 6). Four internal boundaries have been identified – D2 (youngest), D4, D6 and D8 – and provisionally correlated along strike of the Eyre Terrace (Figs 8, 9). Reflections D2, D6

and D8 essentially correlate with reflections A, B and C previously described by the Shipboard Scientific Party (2000c, e, g), whereas D4 is introduced in this study. These reflections represent intra-Pleistocene unconformities, including erosional truncation surfaces, which delineate up-to-five subsequences that locally and individually exceed 100 m thick (Fig. 9b; Table 4). Upslope, the relationship of the mounded deposit with the shelf-edge section appears to be complex and marked by erosional truncation patterns as well as interdigitation, especially with the younger part of the prograding shelf-edge where onlap of seaward-prograding clinoforms by upslope-migrating wavy clinoforms is locally observed (e.g., Fig. 9b). The latter are observed throughout the Quaternary sequence on the Eyre Terrace, buried and at seabed, and have been previously described as sediment waves (Huuse & Feary 2005; Anderskov *et al.* 2010) (e.g., Figs 8b, 9b). Multibeam bathymetry data from the eastern part of the Terrace (Anderskov *et al.* 2010, fig. 4) shows a sediment wave field oriented subparallel to slightly oblique to the bathymetric contours, and migrating upslope to the NW. Downslope, only the uppermost part of the Quaternary sequence (above D2) extends as a sheetform deposit to the edge of the Eyre Terrace (Figs 6, 8, 9).

3.5.2. Lithology. On the Nullarbor Shelf, the Quaternary sequence remains largely untested, other than in dredge and grab samples, and short cores (<2 m), which proved a surface veneer of mixed uppermost Pleistocene bioclastic and lithic sand, and Holocene gravel lag deposits and patches of quartzose-bioclastic palimpsest sand (Feary *et al.* 1993; James *et al.* 1994, 2001). On the upper slope, the Quaternary sequence has been tested at all ODP sites (Figs 6–9): sites 1127, 1129, 1130, 1131 and 1132 cored the main part of the convex-up mounded deposit, with sites 1129 and 1132 close to the interface with the shelf-edge succession; sites 1126 and 1134 cored the slope veneer seaward of the core of the mound; site 1133 cored the eastern flank of the Eucla Canyon (Fig. 1). In general, the mounded deposit comprises bioclastic packstone with subordinate bioclastic wackestone, grainstone, floatstone and rudstone (Table 5). Calcareous nanofossil ooze predominates in the slope veneer and on the flank of the Eucla Canyon.

The upper slope mounded deposit has been tested at ODP sites 1127, 1129, 1130, 1131 and 1132 (Figs 6, 8b, 9b). The lithology at all five sites is dominated by bioclastic packstone in association with subordinate wackestone, grainstone and sporadic interbeds of calcareous ooze/chalk (Shipboard Scientific Party 2000c, e, f, g, h) (Table 5). By way of contrast, an association of floatstone and rudstone occurs in the uppermost part (above the D2 unconformity) of the mound at ODP sites 1129, 1131 and 1132 (Anderskov *et al.* 2010). The entire sequence is thoroughly bioturbated, predominantly by a *Zoophycos* ichnofauna (*Zoophycos*, *Chondrites*, *Planolites*) and *Thalassinoides* burrows. Bed contacts are commonly gradational. An upwards-coarsening cyclicity over tens of metres in the uppermost part of the mound (above the D2 unconformity) has been reported from sites ODP 1127 and 1129, with beds at these sites grading from ooze to grainstone, and packstone to floatstone/rudstone, respectively (Shipboard Scientific Party 2000c, e). At ODP site 1130, normal- to inversely graded turbidite beds are sporadically recorded throughout the Quaternary sequence (Shipboard Scientific Party 2000f; Simo & Slatter 2002).

Lithological indicators for unconformable contacts across the D2–D8 boundaries are provided by evidence of lithological change, firmgrounds and increased down-core lithification associated with these boundaries at all sites (Shipboard Scientific Party 2000c, e, f, g, h). The D8 boundary at ODP sites 1127 and 1131 forms a concave, eroded top to the oldest part of the mound; downslope of this erosion surface there is lithological evidence of slumping. At ODP site 1127, this includes rotated

blocks of mudstone, deformed bedding and a chaotic mix of fine-grained packstone, coarse-grained grainstone and mudstone (Shipboard Scientific Party 2000c). At ODP site 1131, the section below the D8 unconformity includes a thin layer of deformed chalk and a few thin celestite-filled cracks (Shipboard Scientific Party 2000g). Lithological changes and firmgrounds across the D2–D6 boundaries are also reported from ODP sites 1130 and 1132 (Shipboard Scientific Party 2000f, h).

ODP sites 1126 and 1134 lie seaward of the axis of the mounded deposit, towards the outer part of the Eyre Terrace, where the preserved Quaternary sequence correlates wholly with the sequence above the D2 unconformity (Figs 8a, 9a). Both sites proved calcareous nannofossil ooze (Shipboard Scientific Party 2000b, j) (Table 5). Bioturbation is strong and includes *Thalassinoides* burrows. Some variation is noted at site 1134, in the lower part of the section, which contains sporadic grainstone-rudstone interbeds that comprise a variety of coarse components, including bryozoan fragments, as well as indications of soft sediment deformation. The latter include pebble-sized lumps of calcareous nannofossil ooze interpreted as clasts reworked by slump activity (Shipboard Scientific Party 2000j). On the eastern flank of the Eucla Canyon, ODP site 1133 recovered deformed calcareous ooze overlying a grainstone turbidite (Shipboard Scientific Party 2000i) (Table 5).

4. Interpretation

The Middle Eocene siliciclastic rocks are broadly correlatable with the Hampton Sandstone and Upper Pidinga formations (Fig. 4), which represent established transgressive facies at the base of the carbonate succession (Benbow *et al.* 1995; Smith & Donaldson 1995; Totterdell *et al.* 2000). Collectively, the poorly sorted, bioclastic and glauconitic nature of the sandstones, together with a benthonic fauna that includes *Cibicides* spp. and worn and abraded bryozoan fragments, are consistent with a mid to inner neritic high-energy setting. This lag deposit is represented in varying degrees in all ODP boreholes and wells that penetrated the base of the Dugong Supersequence (Fig. 7; Table 6) and implies a basin-wide transgressive phase of sedimentation.

The overlying carbonate succession has been widely promoted as an aggradational–progradational, predominantly cool-water carbonate platform with a distally steepened carbonate ramp that downlaps onto the Eyre Terrace (upper slope) (James & von der Borch 1991; Feary & James 1995, 1998; Feary *et al.* 2004). It is well established that the Middle Eocene–Middle Miocene carbonate platform succession beneath the inner shelf represents the aggradational accumulation of inner ramp (Middle–Upper Eocene Wilson Bluff Limestone Formation) and rimmed shelf (upper Lower–Middle Miocene Nullarbor Limestone Formation) sediments (Feary & James 1995, 1998; Feary *et al.* 2004); as such, these are not considered further in this section. However, our study reveals significant seismic and sedimentary evidence for separate, albeit overlapping, sedimentary systems operating on the outer shelf (seaward of the carbonate platform) and upper slope. Whereas the outer shelf deposits largely display characteristics common to a mid to outer ramp/shelf setting, the upper slope succession includes indicators of both downslope and alongslope processes. The main seismic-stratigraphic characteristics of the outer shelf and upper slope successions are highlighted in Figure 10, whereas a summary of key indicators of sedimentary transport processes on the upper slope is presented in Table 8. The contrast between these successions is demonstrated below through reference to their bounding surfaces, sediment body geometry, seismic facies, sedimentary characteristics and other paleoenvironmental

Table 8 Summary of indicators of sedimentary transport processes responsible for shaping the upper slope (Eyre Terrace), and the nature of the interface between the outer shelf and upper slope successions, including the approximate position of the contemporary shelfbreak.

Stratigraphy	Indicators of downslope processes	Indicators of alongslope process	Interface with outer-shelf succession and approximate position of the contemporary shelfbreak
Quaternary sequence	ET: sporadic beds of sediment flow deposits. EC: mass flow deposits	ET: elongate mounded 'Eyre Terrace' drift with sediment waves; internal erosional discontinuities; compatible contourite sedimentary facies	Varies between interdigitation and erosional truncation. Shelfbreak has prograded seaward (locally up to 15 km) from its latest Miocene–earliest Pliocene position
Pliocene sequence	ET: sporadic beds of sediment flow deposits	ET: infill drift; compatible contourite sedimentary facies	(Pliocene absent on shelf). Earliest Pliocene shelfbreak profile marked by erosional scarp (including slide) cut into Miocene succession
Upper Lower–Upper Miocene sequence	ET: Late Neogene Slide; sporadic sediment gravity flow deposits; localised channel incision EC: mass flow deposits	ET: up to five localised intra-sequence biostratigraphic breaks – uncertain whether alongslope, downslope or mixed origin	Dislocation and erosional truncation across Late Neogene Slide; interdigitation linked to reworking and mass flow activity, including Eucla Canyon. Shelfbreak inflection point remains generally above Wobbeong Delta in Mid-Miocene but has migrated landward (10–20 km) by latest Miocene, with an increased gradient partly enhanced by sliding
Oligocene–Lowest Miocene sequence	ET: localised slumping and channel incision. EC: mass flow deposits	ET: contourite sheet drift (plastered); compatible contourite sedimentary facies	Non-deposition/erosion on Wobbeong Delta-front; interdigitation linked to reworking and mass flow activity, including Eucla Canyon; despite burial of Wobbeong Delta in the Late Oligocene, and lessening of slope gradient, shelfbreak inflection point remained generally above delta top
Middle–Upper Eocene sequence	EC: mass flow deposits	ET: elongate mounded drift (separated); internal discordances; compatible contourite sedimentary facies	Non-deposition/erosion on Wobbeong Delta-front; interdigitation linked to reworking and mass flow activity, including Eucla Canyon; clinof orm at front of delta marks shelfbreak

Abbreviations: EC, Eucla Canyon; ET, Eyre Terrace.

indicators. The interface between the outer shelf and upper slope systems varies from sharp (absent through erosion and/or non-deposition) to transitional (including through interdigitation). Although the general location of the shelfbreak has remained relatively constant since the Mid-Eocene (Figs 2b, 3), minor fluctuations in its position demarcate the contemporary interface between the two domains (Fig. 10; Table 8). The combination of the primary depositional processes to erode, rework and shape the morphology of the shelf-margin will be considered further in the Discussion (section 5).

4.1. Outer shelf

Middle Eocene–Middle Miocene sediment packages (D40–D15 interval) – coeval with the carbonate platform succession – extend seaward from the escarpment and reef complex of the inner shelf as a series of regionally extensive, unconformity-bounded, sheetform deposits with an acoustically bedded internal reflection pattern (Fig. 10; Tables 4, 5). The reflections are generally sub-horizontal and sub-parallel, but with indications of seaward low-angle downlap in the Oligocene–lowest Miocene sequence (Figs 6, 8, 9). These packages comprise a variably interbedded succession of bioclastic wackestone to grainstone (Table 5) that preserves a predominantly neritic to upper bathyal benthic foraminiferal assemblage, and is extensively burrowed, including *Thalassinoides* (Shipboard Scientific Party 2000a, h). As might be expected from the stratigraphic setting, these sedimentary and microfaunal characteristics are generally consistent with a shelf environment that encompasses the mid-to-outer ramp/shelf setting – that is, below fair-weather/storm wave base (Wetzel 1984; Bosence & Wilson 2003). The predominance of grainstone on the outermost shelf (*cf.* Table 5) might be indicative of the removal of finer-grained material from the shelf by current activity at the seabed and spill-over onto the upper slope. The gradual onlap and burial of the Middle Eocene bryozoan mound complexes by Upper Eocene and Oligocene sediments (Fig. 9) indicates the activity of traction currents; however, the general preservation of delicate branching bryozoans and serpulids suggests that current reworking was probably intermittent – for example, storm-induced currents.

The Upper Miocene unit on the outer shelf, above the D15 unconformity, displays an aggradational parallel-to-mounded seismic reflection configuration, comprises calcareous ooze and chalk with minor packstone (Table 5) and onlaps the escarpment marking the edge of the rimmed carbonate platform (Figs 6, 8c, 10). The latter implies a lowstand deposit that developed following a relative fall in sea level, which exposed the upper Lower–Middle Miocene rimmed carbonate platform – the Mid-Miocene ‘Little Barrier Reef’. The seaward transition from mounded to parallel and flat-lying reflections might represent a much narrower and more confined carbonate ramp on the outer shelf, incorporating an inner coalesced carbonate mound complex (Feary & James 1998) and flat-lying outer ramp deposits.

The Quaternary sequence similarly represents a lowstand deposit that is largely confined to the outer shelf, unconformable on the D10 unconformity and terminates landward by onlap onto the upper part of the Mid-Miocene ‘Little Barrier Reef’ escarpment. Towards the shelf-edge, the Quaternary sequence displays a laterally prograding reflection configuration, which includes sigmoid and oblique progradational clinoforms, and complex reflector-truncation patterns that produce a locally mounded-to-chaotic acoustic signature at seabed and buried (Figs 8–10). The ‘mounded’ signature was originally interpreted by Feary & James (1995, 1998) to be indicative of autochthonous biogenic mound growth, and subsequently labelled as a shelf-edge bryozoan reef mound complex (Shipboard Scientific Party 2000a; Feary *et al.* 2004), though Huuse & Feary (2005)

and Anderskov *et al.* (2010) rejected this interpretation in favour of sediment waves, with which we concur (see below). Our appraisal of the complex internal reflection terminations within the entire shelf-edge section leads us to suggest that this reflection configuration resembles a large-scale interference pattern between a shelf-edge cut-and-fill complex and a sediment wave field (Fig. 9b). The formation of these features might thus be attributed to a combination of coeval scour and deposition; the expression of some type of high-energy system (see Discussion: section 5.1).

4.2. Upper slope

The identification of downslope mass-movement deposits in the sediment record is generally clear cut as they are single event deposits with well-defined characteristics. Identifying alongslope contourite deposits, however, is more complex as bottom currents affect to a greater or lesser extent the longer-term accumulation of sediment by other processes (pelagic, hemipelagic, turbiditic) so that a blend of characteristics is necessary for their recognition.

4.2.1. Indicators of alongslope processes. The Quaternary sequence on the upper slope is preserved as a large-scale elongate sediment mound that exceeds 500 m in thickness and can be traced for over 200 km along the length of the Eyre Terrace (Figs 5, 6). Certain specific seismic and sedimentary features of this mound are characteristic of contourite drifts (*cf.* Faugeres *et al.* 1999; Stow *et al.* 2002; Faugères & Stow 2008). These include: the basin-scale convex-upward geometry and margin-parallel elongation of the sediment mound; erosional discontinuities at the base and within the mound (D2–D10 unconformities) that extend across the accumulation as a whole; an internal reflection configuration that varies from sub-parallel and continuous to wavy and irregular, including upslope-migrating clinoforms that resemble sediment waves (Huuse & Feary 2005; Anderskov *et al.* 2010); reflector terminations that include downlap, onlap and two-way closure; sediment that is predominantly fine-grained (silt to very fine sand) but with sporadic interbeds of coarser bioclastic deposits in the upper part of the mound; gradational bed contacts, and textural variation on several scales (tens of centimetres to tens of metres), including inversely-to-normally graded units; and pervasive bioturbation, characterised by a *Zoophycos* ichnofauna.

The sedimentary characteristics of the Quaternary sequence imply that a relatively stable environmental setting where burrowing activity was able to keep pace with sedimentation predominated throughout the deposition of the sediment mound. However, fluctuations in bottom current strength are indicated by several features on different scales, which arguably reflect increasing energy levels, ranging from small, centimetre-scale graded beds, through the development of medium-scale sediment wave fields, to the deposition of up to five large-scale (locally >100 m thick) unconformity-bounded subsequences (separated by the D2–D8 boundaries) (Figs 8, 9) that comprise the large-scale drift. Whereas some authors (e.g., Simo & Slatter 2002; Brooks *et al.* 2003; Feary *et al.* 2004) have suggested that the observed textural and grain-size cyclicity in the graded beds is a function of a varying relative sea level, the influence of alongslope currents offers an alternative mechanism whereby such variation reflects fluctuation in bottom-current strength; coarser-grained sediments are associated with strong currents, finer-grained material with low current strength. Thus, the coarsening-upward couplets assigned by Simo & Slatter (2002) to a fluctuating sea level might equally be assigned to the C1–C3 division, which represents the negatively graded part of the composite contourite facies model of Stow *et al.* (2002); the C3 division representing the coarser fraction related to bottom-current velocity increase. The occurrence of erosive

basal and internal hiatuses (D10–D2) is most probably related to episodes of particularly vigorous bottom currents (Stow *et al.* 2002). Based on all this evidence, we suggest that the Eyre Terrace sediment mound represents a contourite drift (Huuse & Feary 2005), which we have termed the Eyre Terrace Drift. Its overall geometry and association with sediment waves is comparable with *elongate mounded drifts* observed elsewhere in the world, including the Rockall Trough in the NE Atlantic (Stoker *et al.* 1998; Masson *et al.* 2002). Such drifts may occur anywhere from the outer shelf/upper slope to the abyssal plains depending on the depth at which the bottom current flows (Stow *et al.* 2002). Given that the main development of the drift lies between 200 and 700 m water depth, the Quaternary upper slope succession can be further classed as a *shallow water contourite drift* (*sensu* Stow *et al.* 2002). Its complex relationship with the outer-shelf Quaternary section is considered elsewhere (see Discussion: section 5.1).

Sediment mounds in the Pliocene, Oligocene and Middle–Upper Eocene deposits also display seismic features diagnostic of contourite drifts. The large-scale seismic geometry of the Pliocene sequence is one that has clearly moulded to onlap the headwall scarp of the Late Neogene Slide (see below) and to fill progressively the topographic depression of its evacuation hollow (Figs 8b, 10). The setting and relative confinement of this deposit is characteristic of an *infill drift* (Stow *et al.* 2002), examples of which have been recognised in association with several major slides on the NW European margin (Evans *et al.* 2005). In the Middle Eocene–Oligocene section, sub-parallel to wavy and mounded sediments display a progressive, upslope onlap of the front of the Wobbecong Delta (Figs 8, 9b, 10). The erosional moat associated with the mounded Middle–Upper Eocene sequence (Fig. 8b) is characteristic of a *separated drift*, whereas the sheet-like Oligocene accumulation is more typical of a *plastered drift* (Faugères *et al.* 1999; Stow *et al.* 2002; Faugères & Stow 2008). This interpretation contrasts with that of Feary & James (1995, 1998) who described the Middle Eocene–Oligocene section as an ‘*aggrading*’ and ‘*multi-lobed, deep-water slope sediment apron*’ comprising sediment derived directly downslope from the adjacent shelf and deposited as ‘*a series of gently seaward-dipping reflectors*’. However, the sedimentary characteristics throughout this section are consistent with a contourite origin, being predominantly fine-grained, strongly bioturbated and containing a benthic and planktonic foraminiferal association characteristic of an upper to middle bathyal (200–800 m) environment (Shipboard Scientific Party 2000b, f, j). The abundance of *Zoo-phycos* and *Chondrites* biogenic traces is commonly associated with stable environmental conditions, and the slow, continuous accumulation of sediment (Wetzel 1984).

Although the intra-Middle and Upper Eocene D32 and D35 unconformities are not readily identifiable on the seismic data, their identification solely within the Middle–Upper Eocene separated drift (Figs 8b, 9a) suggests that they formed as an integral part of drift accumulation and might reflect fluctuations in the strength of the bottom currents during its deposition. In contrast, the ‘Mid’ Oligocene D25 and Base Miocene D22 unconformities are identified from the shelf-edge on to the upper slope; thus, their formation might be indicative of a more widespread erosive regime (see Discussion: section 5.2).

The origin of several unassigned biostratigraphic breaks in the upper Lower–Upper Miocene sequence specific to ODP sites 1126 and 1134, on the outer edge of the Eyre Terrace, remains uncertain due to their localisation and lack of obvious correlation between the two sites (Fig. 7). Local scouring of the strongly bioturbated sediments by bottom currents cannot be discounted, though there is also evidence for the activity of sporadic mass flow processes (see below).

4.2.2. Indicators of downslope processes. On the Eyre Terrace, the Neogene succession preserves most evidence for

downslope processes ranging from large-scale sliding and channel incision to small-scale interbeds of sediment gravity flow deposits (Table 8). The largest and most prominent indicator of downslope processes is the Late Neogene Slide recognised by the major erosional scour that truncates the entire outer shelf succession of upper Lower–Upper Miocene sediments. The preserved Upper Miocene section on the upper slope is detached from the outer shelf succession, displays a structureless to chaotic acoustic character and rests unconformably – via the base of the slide – on Upper Oligocene deposits (Fig. 8b). At site 1130, the basal ~15 m of the 53-m-thick Upper Miocene section is a mixed assemblage of undisturbed nannofossil chalk, slumped nannofossil chalk and thin-to-medium-bedded turbidites (Shipboard Scientific Party 2000f). The timing of the slide event is inferred as late Tortonian based on the comparison between the biostratigraphic range of the displaced Upper Miocene sediments at site 1130 (SAN17–19/NN10–12) and the undisturbed, slightly older, outer shelf section at site 1132 (SAN17/NN10) (Figs 6, 7).

Farther downslope, the upper Lower–Upper Miocene sequence is punctuated by several biostratigraphic breaks (Fig. 7) which, together with seismic-stratigraphic evidence for channel incision (e.g., Fig. 8a) and generally contorted internal reflection pattern (Fig. 9a), might be indicative of intermittent downslope traction-currents, though the action of alongslope bottom currents cannot be discounted (see above). A background sedimentary record dominated by strongly bioturbated calcareous ooze punctuated by discrete slumped beds that display inclined and folded bedding, turbidites, thin silty layers with rotated intraclasts and much reworked biogenic material implies sporadic mass flow activity on the upper slope throughout the Miocene (Shipboard Scientific Party 2000c, i, j). Whereas the gross external form of the overlying Pliocene sequence is of an *infill drift* (see above), indications of chaotic to lensoid seismic unit’s downslope from the Late Neogene Slide combined with lithological evidence for sporadic syn-sedimentary deformation, including inclined bedding and rip-up clasts, implies episodic reworking and/or instability. At ODP site 1134, the Lower Pliocene bioclastic deposits (Table 5) are described as ‘*neritically influenced*’ (Shipboard Scientific Party 2000j), which suggests derivation of material from the outer shelf.

The remainder of the upper slope succession preserves only sporadic indicators of downslope processes. In the Quaternary sequence, downslope of the concave erosional top of the oldest part of the Eyre Terrace Drift marked by the D8 unconformity (Fig. 9b), ODP sites 1127 and 1131 contain evidence of slumping, including deformed bedding and rotated intraclasts. This might represent localised failure and redeposition of the drift deposits (e.g., Stoker *et al.* 2001). Similar intermittent syn-sedimentary deformation characteristics are also seen in the upper part of the Quaternary sequence (above D2 at site 1134) seaward of the main axis of the Eyre Terrace Drift. In the Palaeogene succession, the possibility has already been raised that the basal Middle Eocene siliciclastic section at ODP site 1134 might be linked to a localised mass flow deposit at the foot of the Wobbecong Delta (Table 7; Fig. 8a). The borehole record for the remainder of the Palaeogene succession suggests a relatively stable upper-to-middle bathyal setting on the Eyre Terrace (see above); however, towards the seaward edge of the Terrace, the entire Oligocene–lowest Miocene sequence locally displays a chaotic seismic reflection signature where the sequence appears to infill a former canyon (Fig. 6c). Moreover, localised channel incision and erosion associated with the D22 (Base Miocene) unconformity (Fig. 9a) might be further indicative of sporadic downslope processes.

By way of contrast, on the eastern side of the study area, seismic and sedimentary observations indicate that the Eucla Canyon has been an active downslope sediment transport route

since at least the Mid-Eocene (Tables 5, 8). On seismic profiles, the fill of the canyon is characterised by a lenticular to hummocky and chaotic seismic reflection pattern, including stacked accumulations of lensoid packages, characteristic of mass flow deposits (Mitchum *et al.* 1977; Nardin *et al.* 1979). Although lithological data are restricted to the Neogene–Quaternary section, the occurrence of scoured bedding surfaces, turbidites, soft sediment deformation structures (rotated intraclasts, slumped and folded bedding) and much reworked biogenic material within this section are consistent with mass flow processes.

5. Discussion

The revised stratigraphic framework of the Dugong Supersequence presented in Figure 10 provides an observational basis upon which to appraise the post-breakup development of the Eucla Basin in the western GAB since the Mid-Eocene. Whereas we recognise some compatibility with the established stratigraphic model of Feary & James (1995, 1998) and Feary *et al.* (2004) – specifically, the architecture of the carbonate platform succession on the inner Nullarbor Shelf – the large-scale sediment-body geometry of the upper slope succession indicates a predominance of contourite deposits beneath the Eyre Terrace; this represents a significant departure from the established model, which proposed a shelf-margin succession dominated by downslope processes. Our revised framework also distinguishes between major unconformities, which are mappable from the shelf to the upper slope, and minor unconformities that are largely restricted to the upper slope. The major unconformities delineate second- to third-order (2–13 My) frequencies of change in relation to sedimentary cycles across the margin, whereas the minor slope hiatuses locally punctuate these depositional packages giving rise to higher frequency third- to fourth-order (<1–2.5 My) cycles (periodicities based on Fulthorpe 1991). The major unconformities are all characteristically angular and erosional (Table 4) and mark abrupt changes in the stratigraphic architecture of the outer margin. On the upper slope, we attribute the increased complexity of the Dugong Supersequence – manifested by the minor hiatuses and other unassigned discordances identified herein (Fig. 7) – largely to bottom-current erosional processes and sporadic mass wasting. Our results conflict with existing models of Mid-Palaeogene to Neogene–Quaternary unconformity formation on the Eyre Terrace (*cf.* Li *et al.* 2003a, b, c, 2004), which predict that they all represent ‘local manifestations of major third-order boundaries’ (as defined by Hardenbol *et al.* 1998) and that global eustasy was ‘a dominant control’ on Cenozoic sedimentation in the Eucla Basin. Whilst we recognise some correlation between the different schemes (*cf.* Table 6), our stratigraphic interpretation challenges the status and significance of many of the hiatuses – especially within the Neogene succession – described by Li *et al.* (2003a, 2003b, 2003c, 2004). Thus, in the following text, we focus on the shelf-margin and assess the likely processes that are responsible for these observations and interpretations and consider the implications in terms of the main geologic and oceanographic controls on the development of the Dugong Supersequence and concomitant shaping of the western GAB shelf-margin since the Mid-Eocene.

5.1. A revised shelf-margin stratigraphic model: implications for sedimentary and oceanographic processes shaping the western GAB

Over the last three to four decades, the notion that the shelf-edge in the western part of the GAB extended onto the Eyre Terrace as a series of extensive prograding clinoforms, especially during the Quaternary, has been widely promoted (Bein & Taylor 1991;

James & von der Borch 1991; James *et al.* 1994, 2006; Feary & James 1995, 1998; Shipboard Scientific Party 2000a; Saxena & Betzler 2002; Feary *et al.* 2004; Anderskov *et al.* 2010). It is the interpretation of the Quaternary sequence that has guided the currently accepted model whereby progradation is envisaged to have resulted from episodic off-shelf sediment transport by wave action combined with *in situ* deep-water carbonate production (James & von der Borch 1991; James *et al.* 1994). The term ‘shaved shelf’ has been applied to this style of continental shelf (*cf.* James *et al.* 1994), whilst the relatively passive process of ‘autogenic progradation’ (*cf.* Boreen & James 1993) has been applied to the formation of the ‘stacked, shelf-margin system tracts’ (James *et al.* 1994). However, the schematic depiction of this process does not represent the seismic-stratigraphic expression of the Quaternary shelf-margin succession as presented in this study (Fig. 10). In the original model depiction of a shaved shelf presented by James *et al.* (1994), and in a subsequent paper by Saxena & Betzler (2002), all the prograding clinoform packages are shown to terminate by top lap at a single horizontal surface. Inspection of the seismic profiles in Figures 6, 8, 9 shows that this is not the case; nor do we recognise the geometrical continuity of clinoforms from the shelf to the slope as depicted by previous authors (e.g., James & von der Borch 1992; James *et al.* 1994; Feary & James 1995, 1998; Feary *et al.* 2004). In our view, the established seismic stratigraphic model does not adequately address the internal complexity of the Quaternary sequence and older shelf-margin succession of the Dugong Supersequence. In particular, the potential significance of along-slope currents in shaping the upper slope succession has been largely ignored.

Instead, our observations suggest that the Quaternary sequence on the upper slope provides a spectacular example of a current-controlled sediment body – the Eyre Terrace Drift. The scale (>500 m thick) and continuity (200 km long) of this elongate sediment drift suggests that relatively stable conditions prevailed in the bottom current regime and/or oceanographic setting during the last 2 My, notwithstanding episodic fluctuations in bottom-current strength and direction expressed in terms of grain-size variation, development of upslope-migrating sediment waves and erosional discontinuities (D2–D8 unconformities). The variability in current activity is generally a function of the complexity of the hydrodynamic regime, which in the GAB is well documented and includes: the presence of eastward- and westward-flowing boundary currents; large-scale eddies that distort the E–W flow patterns (Cresswell & Griffin 2004); and the periodic upflow of cold, nutrient-rich waters of the westward-flowing Flinders Current onto the Nullarbor Shelf, via the Eyre Terrace (*cf.* James *et al.* 2001 and references therein) (Figs 1, 11). Anderskov *et al.* (2010) proposed that the sediment waves were driven by downslope density currents and dense water cascades originating on the shelf; however, their association with a contourite sediment drift and their subparallel-to-oblique orientation to the regional slope (Fig. 11; *cf.* Anderskov *et al.* 2010, fig. 4) suggest that an alongslope bottom-current origin cannot be discounted (Faugères *et al.* 1999; Masson *et al.* 2002). In a comparable upper-slope setting on the SE Brazilian margin, the Brazil Current – a southward-flowing boundary current – locally generates eddies on an upper slope terrace whose activity interferes with shelf currents; the sedimentary consequences include the formation of clinoform patterns imprinted with sediment waves migrating along the trend of the current (Viana *et al.* 2002a; Schattner *et al.* 2019). Huuse & Feary (2005) attributed the formation of both the drift and the sediment waves on the Eyre Terrace to activity of the Leeuwin Current; however, we would suggest that the bulk of the drift lies within the core of the zone of influence of the Flinders Current (Fig. 11; Table 3).

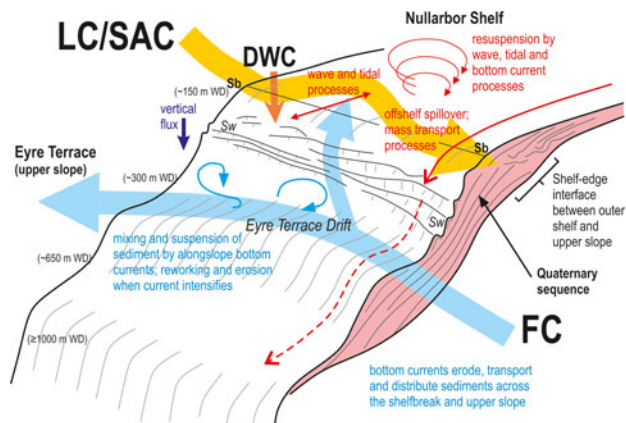


Figure 11 Schematic perspective model of Quaternary shelf-margin setting under the potential influence of a variety of bottom current and downslope gravity processes, as well as vertical (hemipelagic) flux (see text for details). Sediment wave pattern based on Anderskov *et al.* (2010, fig. 4). Abbreviations: DWC, dense water cascades; FC, Flinders Current; LC/SAC, Leeuwin Current/South Australian Current; Sb, shelf-break; Sw, sediment waves; WD, water depth.

The complexity of the hydrographic regime is also likely responsible for the variable internal reflection configuration that marks the interface between the upper slope drift and the equivalent aggrading-to-prograding outer-shelf section of the Quaternary sequence. The outer-shelf succession is interpreted to represent a pattern of alternating sedimentation and erosion driven by the high-amplitude, short-period sea-level fluctuations during the Quaternary (Boren & James 1993; Feary & James 1998; Feary *et al.* 2004): the laterally prograding deposits on the outer shelf represent a lowstand system, when much of the shelf was exposed and contained large hypersaline lagoons with the coastline near the shelf-edge; in contrast, the present highstand system represents a flooded shelf with wave abrasion largely restricted to the inner shelf. Whereas during glacial periods the Leeuwin Current might have been much weaker, the South Australian Current probably remained active, and the Flinders Current may have intensified leading to conditions more favourable to upwelling; dense water cascades might also have persisted (Anderskov *et al.* 2010 and references therein). Nevertheless, uncertainty remains regarding the likely ‘downward shifting’ of the core of the boundary currents, in response to sea-level fall. Offshore SE Brazil, the core of the upper slope Brazil Current and its ‘depth of action’ both shifted downwards by several hundred metres during the Last Glacial Maximum; however, during sea-level rise, the boundary-current core shifted landward, bedforms developed on the uppermost slope and a shelf/slope front was (re-)established at the shelf-edge (Viana & Faugères 1998; Viana *et al.* 2002b). The distinction and significance of any such temporal and spatial variation in boundary current activity on the southern Australian slope remains unclear. Our interpretation of the shelf-edge interface as depicted in Figures 8–10 shows that the deposits of the Eyre Terrace Drift aggraded upslope to the contemporary shelf-edge throughout its development. For the most part, the contact with the outer shelf prograding system remains unclear, albeit resembling a large-scale coeval interference pattern between a prograding shelf-edge cut-and-fill complex and an aggrading sediment drift/wave field, though the low resolution of the seismic data precludes certainty. Although the details of the shelf-edge interface need to be better clarified, this reflection pattern might suggest that sedimentation mechanisms related to retreating-shore dynamics and outer shelf bottom-current reworking – essentially reflecting a shelf/slope hydrodynamic interface – are responsible for its complexity. In the Canterbury Basin, offshore New

Zealand, a comparable, disturbed seismic-stratigraphic architecture on the outer shelf has been attributed to the effect of along-slope current activity by creating mounded morphologies and disrupting reflection terminations (Lu & Fulthorpe 2004). Much further detailed work in the GAB is required to address this issue.

Although the predominance of alongslope processes in the construction of the Quaternary upper slope succession conflicts with the established model of shelf-margin progradation via downslope processes of resedimentation, it does not necessarily negate the contribution of shelf-derived material to the build-up of the contourite drift. Whereas in abyssal drifts along many continental margins the provenance of sediment can often be traced to areas thousands of kilometres upstream of the drift (e.g., the Greater Antilles Outer Ridge: Tucholke 2002), the Eyre Terrace Drift is a relatively shallow water deposit, and the occurrence of neritically derived benthic foraminifers and well-preserved bryozoan fragments, together with sporadically interbedded turbidite and slump deposits, suggests that at least some of its sediment was derived from the adjacent shelf (Feary *et al.* 2000; James *et al.* 2000, 2004). Eddies and storm- and tide-driven currents commonly induce off-shelf spillover of material onto the slope, which might induce the generation of mass transport processes (Fig. 11). Farther to the SE, it has been demonstrated that regularly occurring dense water cascades throughout the Quaternary contributed to the formation of the Bass Canyon of the Gippsland Basin, offshore SE Australia (Mitchell *et al.* 2007). By analogy, a similar process may have been important in the development of canyons in the GAB. However, based on the generally subordinate presence of sediment gravity flow deposits proved within the Quaternary upper slope succession, it is probable that any muddy and fine-sand grade material (at least) derived from the adjacent shelf and/or more distant sources (located either E or W), including off-shelf spillover or vertical (hemipelagic) flux, was prone to current-controlled redistribution along the slope (Fig. 11). Velocities associated with the eastward- and westward-flowing boundary currents commonly range between 0.2 and 0.5 ms⁻¹, and are strong enough to winnow and entrain the sediment and shape the clinoform geometry of the Eyre Terrace Drift (Black *et al.* 2003; Masson *et al.* 2004).

In assessing the longer-term importance of alongslope and downslope processes on the upper slope, our observations are considered together with data from the wider southern Australian margin (Fig. 12). The abundant seismic-stratigraphic evidence for sediment drift development during the Mid–Late Eocene, Oligocene and Pliocene, as well as the overall fine-grained and strongly bioturbated background sedimentary character to the entire Middle Eocene–Pliocene succession, demonstrates a longevity to alongslope processes extending back into the Palaeogene. These observations are consistent with the discovery of an upper Middle Eocene–Recent succession of contourite deposits and bottom current erosional features on the deep-water Ceduna Terrace, located to the SE of the study area (Jackson *et al.* 2019) (Fig. 1). Collectively, these data add to the growing belief that an oceanic circulation pattern has existed offshore southern Australia since the mid-Palaeogene, which has led some workers to speculate the presence of an eastward-flowing proto-Leeuwin Current (e.g., McGowran *et al.* 1997; Stickley *et al.* 2004; Sauermilch *et al.* 2019) (Fig. 12). It remains unclear as to what role, if any, the westward-flowing Flinders Current might have played during the development of the Palaeogene oceanic circulation. Its link to the Tasman Outflow (Wijeratne *et al.* 2018) and its association with the ACC suggest that it might have been instigated in the Early Oligocene (Exon *et al.* 1999; Norvick & Smith 2001). Although the detail remains to be worked out, this general scenario supports our

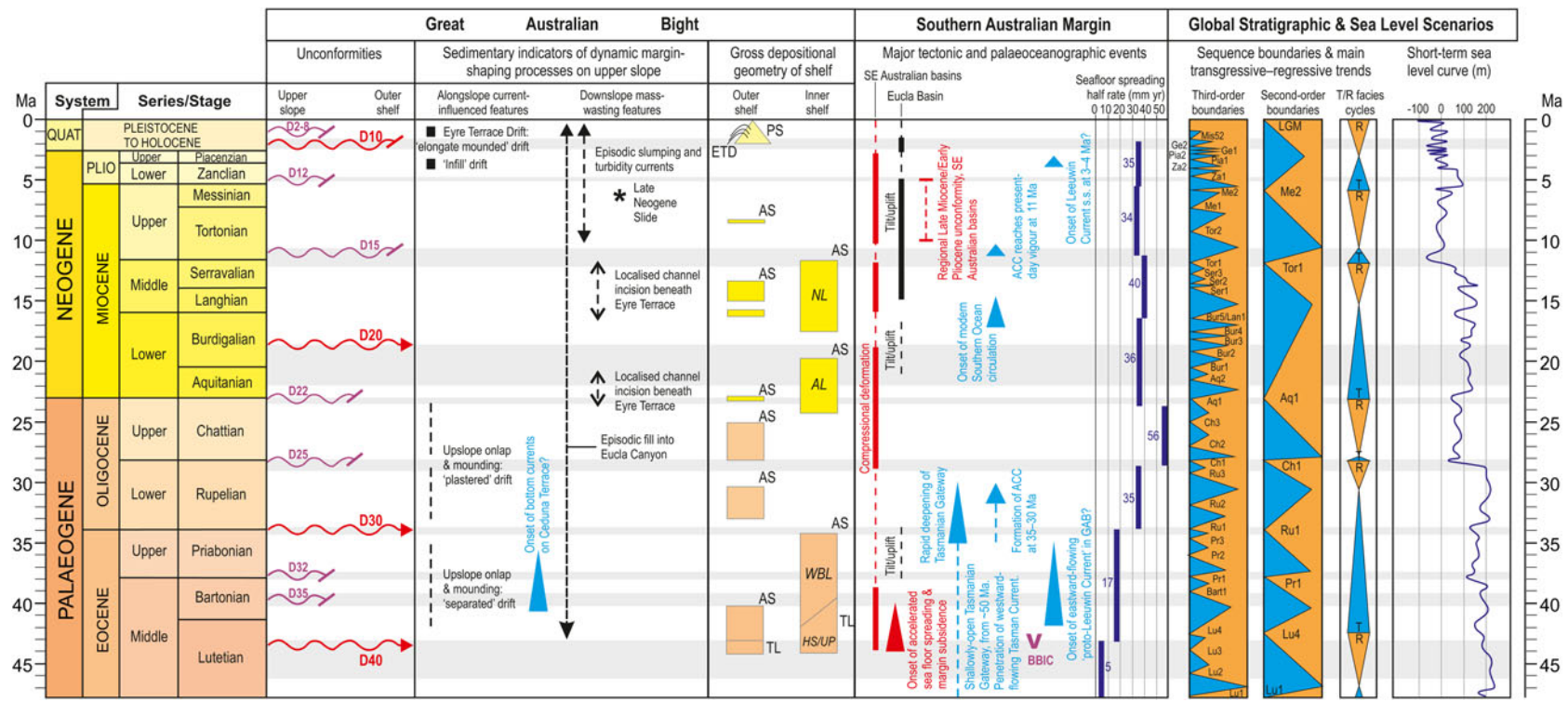


Figure 12 Middle Eocene–Pleistocene tectonostratigraphy for the Dugong Supersequence in the western GAB. The compilation of the unconformities (red, main seismically mappable surfaces on shelf; purple, minor, mostly localised to upper slope; grey bands, approximate range of hiatus), upper slope margin-shaping processes and depositional geometry of the shelf from the GAB is from this study, except ‘Ceduna Terrace bottom currents’ from Jackson *et al.* (2019); the representation of the shelf succession is based on ODP site 1132 and the Apollo-1 well, as presented in Figure 7. Additional information is derived from the following sources: under the ‘South Australian Margin’ column, tectonic events and sea floor spreading rates are adapted from Totterdell *et al.* (2000), Norvick & Smith (2001), Sayers *et al.* (2003), Li *et al.* (2004), Hou *et al.* (2008), Holford *et al.* (2011a, 2014), Mahon & Wallace (2020) and Reynolds *et al.* (2017), and palaeoceanographic data are from McGowran *et al.* (1997), Stickley *et al.* (2004), Wyrwoll *et al.* (2009); Bijl *et al.* (2013, 2018), Scher *et al.* (2015), Sangiorgi *et al.* (2018) and Sauermilch *et al.* (2019); under the ‘Global Stratigraphic & Sea Level Scenarios’ column, sequence boundaries are from Gradstein *et al.* (2012), T/R facies cycles are from Hardenbol *et al.* (1998), and the short-term sea level curve is derived from Haq & Al-Qahtani (2005) and Totterdell *et al.* (2014). Abbreviations: ACC, Antarctic Circumpolar Current; AL, Abrakurrie Limestone Formation; AS, aggrading shelf; BBIC, Bight Basin Igneous Complex; ETD, Eyre Terrace Drift; HS, Hampton Sandstone; NL, Nullarbor Limestone Formation; PS, prograding shelf; TL, transgressive lag; UP, Upper Pidinga Formation; WBL, Wilson Bluff Limestone Formation. (See Table 4 for key to unconformities.) Timescale is based on Gradstein *et al.* (2012).

interpretation that the development of the Middle Eocene–Oligocene sequences on the Eyre Terrace were, at least in part, influenced by bottom currents.

An increased prevalence of mass movement processes characterises the Neogene succession on the upper slope. Whereas the Eucla Canyon has been a conduit for mass-flow deposits since the Mid-Eocene, the Miocene–Pliocene appears to have witnessed an increased general instability on the shelf-margin. The most significant expression of this instability is the Late Neogene slide that resulted in a major slump deposit (of Upper Miocene sediment) on the central part of the Eyre Terrace (Figs 8b, 10). An increase in tectonic activity on the SE Australian margin is apparent from the Late Miocene onwards (Fig. 12), manifested by widespread fault reactivation, uplift and folding, accelerated uplift of highlands (including the Mt. Lofty Range of South Australia) and the development of a regional Late Miocene–Early Pliocene unconformity observed in basins such as the Otway, Torquay and Gippsland basins (Dickinson *et al.* 2002; Holford *et al.* 2011a, and references therein). Although the Eucla Basin is largely undeformed, regional west-up tilting of the basin occurred in the late Mid-Miocene (Benbow *et al.* 1995; Feary & James 1998) after the deposition of the Nullarbor Limestone Formation (Sandiford 2007). Moreover, the Late Neogene slide, tentatively dated as late Tortonian (this study), fits within the 10–5 Ma best estimate for the age of the regional unconformity (Holford *et al.* 2011b). It should be noted that vigorous contour currents can erosively undercut submarine slopes, which might result in or enhance the inherent gravitational instability of the margin, thereby generating slides and slumps. It is interesting to note that the present-day vigour of the ACC was established since ~11 Ma (Fig. 12), which might have implications for a strengthening of the Flinders Current during the Late Neogene and Quaternary and its impact on the southern Australian margin. Any potential link between tectonics, gravitational instability and contour currents in this area remains to be established.

The Late Neogene Slide scar was subsequently buried beneath a Pliocene ‘infill drift’ (Figs 8b, 10). The scale of this accumulation combined with the thick Quaternary Eyre Terrace Drift suggest a significant increase in the influence of bottom currents since about 5 Ma offshore southern Australia, and especially since 2 Ma when, following a major phase of erosion on the shelf and slope (the D10 unconformity), the Eyre Terrace Drift accumulated rapidly (as described above). Factors influencing a general change in ocean dynamics (including the Leeuwin, South Australian and Flinders currents) since the late Neogene also remain to be assessed.

5.2. Appraising the significance of unconformities on the outer margin: implications for their causal mechanism

Li *et al.* (2003a, 2004) interpreted their series of Middle Palaeogene to Neogene–Quaternary hiatuses (Fig. 4; Table 6) as an indicator that global eustasy was ‘a dominant control’ on the Cenozoic sedimentary development of the southern Australian continental margin, especially during the Neogene. This hypothesis was predicated on the assumption that all their hiatuses coincided with third-order global sequence boundaries as delineated by Hardenbol *et al.* (1998) (Table 6). The Palaeogene hiatuses (A–D) were interpreted to record regional sea-level changes driven by a series of rapid changes in Southern Ocean seafloor spreading rates (Li *et al.* 2003a), whereas the Neogene–Quaternary unconformities (H1–H15) were attributed primarily to a glacio-eustatic control, and the three ‘mega-hiatuses’ (MH1–MH3) that more likely represented sediment removal rather than non-deposition were interpreted as being caused by large-scale slope failure driven by differential uplift and subsidence (Li *et al.* 2004). Notwithstanding the general uncertainty surrounding putative schemes that purport to the existence of a

globally correlatable suite of eustatic cycles (*cf.* Miall 1997), we find their hypothesis to be inconsistent with the stratigraphic results presented here. Our reasons are summarised below.

As previously noted, the existing scheme of unconformities lacks stratigraphic context beyond the limit of the boreholes (ODP sites 1126, 1130, 1132 and 1134) in which they have been identified. The correlation chart and resultant schematic fence diagram presented both for the Palaeogene (Li *et al.* 2003a, fig. 5) and Neogene–Quaternary (Li *et al.* 2004, fig. 3) successions in these boreholes bear no resemblance to the actual geology of their shelf-margin setting as determined in this study by seismic interpretation. In particular, the existing scheme does not recognise the Late Neogene Slide between sites 1132 and 1130; nor the physical separation of the Eocene sequence on the outer shelf (site 1132) and upper slope (sites 1130, 1126 and 1134); nor the seismic expression of surfaces of discontinuity common throughout the upper-slope succession. Based on these observations, an appraisal of the existing scheme shows that MH2 of Li *et al.* (2004) correlates with our Late Neogene Slide surface at site 1130, and with the Upper Miocene D15 unconformity at sites 1126, 1132 and 1134 – that is, MH2 as previously defined does not represent a single surface of slope failure. We note also that MH3 of Li *et al.* (2004) correlates with our regional Base Quaternary D10 unconformity, whilst MH1 correlates with our Lower Miocene D20 unconformity (probably a composite D20/D15 hiatus at site 1130) (Table 6); again, neither of these hiatuses are the result of large-scale slope failure. Moreover, the discontinuous nature of many of the unconformities in the existing scheme is exemplified by the intra-Eocene hiatuses B and C (Li *et al.* 2003a), and the bulk of the Neogene–Quaternary hiatuses (H2–H7, H9–H11, H14–15) (Li *et al.* 2004). Our preferred interpretation of the former is that they represent erosional hiatuses associated with the development of the Eocene elongate mounded sediment drift on the upper slope; the latter discontinuities are mostly associated with discrete slump deposits and current-scoured erosion surfaces that commonly vary stratigraphically between sites (Table 6; Fig. 7). In our view, these results are consistent with highly localised discontinuities of restricted extent on the upper slope.

Logically, eustatic sea-level changes should leave their impact on the sedimentary architecture of strata, especially on continental shelves. However, we find no expression of these hiatuses (B, C, H2–H7, H9–H11, H14–15) on the adjacent shelf. According to Lu & Fulthorpe (2004), the limited areal distribution of unconformities is generally an indicator that such unconformities are not sequence boundaries. Thus, we would urge caution when considering the consequences of global correlations made by Li *et al.* (2003a, 2004) to these specific sets of hiatuses on the upper slope. The abundant evidence presented in this study, and from Jackson *et al.* (2019), for oceanographic current activity in the GAB since the Mid-Eocene (Fig. 12) presents a new variable, previously not considered in the established model of southern margin development, that the formation of some of the hiatuses on the upper slope is simply a result of intermittent erosion and/or non-deposition in response to fluctuations in alongslope bottom-current strength.

There is no doubt that the unconformity-bounded stratigraphic architecture of the Dugong Supersequence beneath the Nullarbor Shelf reflects significant changes in relative sea level across the Eucla Basin. However, the angular, erosional character of the major margin-wide unconformities together with the abrupt changes in sequence architecture are not consistent with generation by passive sea-level changes (Galloway 1989; Embry 1990). Inspection of Figure 12 shows no clear correlation of our major sequence-bounding unconformities to the global cycle charts. Instead, they appear to be most closely related to tectonic events, which are summarised below:

- The Middle Eocene D40 unconformity (\equiv A of Li *et al.* 2003a) is generally attributed to subsidence of the southern Australian margin in response to an acceleration of the seafloor spreading rate at \sim 43 Ma (Totterdell *et al.* 2000). This reflects a margin-wide event that elsewhere included a strong phase of Mid-Eocene inversion, uplift and exhumation in SE Australian basins (McGowran *et al.* 2004; Holford *et al.* 2011a).
- A further acceleration in spreading rate at \sim 34 Ma coincides with the Base Oligocene D30 unconformity (\equiv D of Li *et al.* 2003a). The onset of west-up–east-down uplift and tilting – ‘dynamic topographic tilting’ – of the Eucla Basin is also recorded from the onshore sedimentary succession around this time (\sim 37–35 Ma) (Sandiford 2007; Hou *et al.* 2008).
- A combination of further changes in spreading rate (Li *et al.* 2004), continued intermittent compressional deformation offshore SE Australia (Holford *et al.* 2011a) and dynamic tilting of the Eucla Basin following the deposition of the Abrakurrie Limestone Formation (Hou *et al.* 2008) span the Mid-Oligocene D25 (\equiv Mid-Oligocene of Li *et al.* 2003c), Base Miocene D22 (\equiv H1 of Li *et al.* 2004) and Early Miocene D20 unconformities.
- As noted above (section 5.1), a significant increase in tectonic activity is recorded from the Late Miocene onwards. The onshore Eucla Basin succession preserves a record of several hundred metres of differential vertical movement after the deposition of the Nullarbor Limestone Formation, which resulted in seaward tilting and localised faulting of the basin (Feary & James 1998; Sandiford 2007; Hou *et al.* 2008). On the Nullarbor Shelf, the Upper Miocene D15 (\equiv H8 of Li *et al.* 2004) unconformity marks the base of an Upper Miocene–Quaternary offlapping succession that is restricted to the outer shelf and upper slope (Fig. 10). A general instability along the shelf-margin is indicated by the formation of the Late Neogene Slide and associated mass-flow deposits. That this area of instability is part of a larger region of late Neogene deformation is supported by evidence of widespread uplift, folding and unconformity development in many SE Australian basins (Dickinson *et al.* 2002; Holford *et al.* 2011a, 2014).
- The Base Quaternary D10 (\equiv MH1 of Li *et al.* 2004) unconformity represents the most dramatic angular unconformity on the outer margin, characterised by significant erosion of the underlying Middle–Upper Miocene and Pliocene rocks on the outer shelf and upper slope (Figs 6, 8, 9). Onshore, the preservation of the Upper Pliocene–Lower Pleistocene Roe Calcarenite (Fig. 4) has been attributed by James *et al.* (2006) to uplift immediately after deposition; they further suggested that the uplift correlated with the MH1 hiatus of Li *et al.* (2004), our D10 unconformity, and inferred a widespread Pliocene/Pleistocene boundary uplift event. The intense erosional scouring associated with D10 on the upper slope followed by the deposition of the Eyre Terrace Drift suggests that the formation of this unconformity was, at least in part, generated by vigorous bottom-current activity.

Arguably, the availability of tectonic mechanisms to explain our major (second- to third-order) stratigraphic cyclicity negates the requirement for global eustasy as a primary mechanism in the generation of the stratigraphic architecture in the Eucla Basin. Whereas we note the close comparison between our D25 and D15 unconformities with significant ‘global’ drops of sea level as presented on the short-term sea level curve of Haq & Al-Qahtani (2005) (Fig. 12), it cannot be ignored that these unconformities also correspond with regional tectonic events. Nevertheless, the restricted preservation of the post-D15 Upper Miocene succession to the outer margin might be a function of the generally low global sea level throughout the Late Miocene exposing the bulk of the Eucla Basin (to the north). Although

Li *et al.* (2003a, 2004) acknowledged the contribution of tectonic activity in the formation of their Palaeogene and Late Neogene hiatuses, their primary emphasis was on eustatic control ‘complicated by local tectonics’. In our appraisal of their unconformities, we have demonstrated that the bulk of their hiatuses on the upper slope were most probably the result of localised sedimentary processes with no direct correlation to global cyclicity.

There is a strong temporal correspondence of our major unconformities (including also D25, D22 and D15) with periods of enhanced tectonic activity in SE Australian basins, which themselves correspond with major reconfigurations of the Indo-Australian Plate (Holford *et al.* 2011a). Compressional deformation is pervasive on the SE Australian margin whereas the Eucla Basin is characterised by differential vertical movements during these periods (Fig. 12). Despite this tectonic variability along the margin, the correlation of events suggests a coordinated geodynamic response to the late post-breakup transmission of plate boundary stresses into the plate interior. The absence of inversion structures from the Eucla Basin is commonly regarded as an indication that the overall geodynamic response was much less in this basin than farther east; however, the outer-margin succession of the Dugong Supersequence preserves a record of the sensitivity to plate boundary processes that cannot be ignored in consideration of the control of the late post-breakup vertical motions across the Eucla Basin.

By way of contrast, the intra-Quaternary D2–D8 unconformities reflect a fourth-order or higher frequency cyclicity (Table 4). These unconformities are inextricably linked to the development of the Eyre Terrace Drift, and most probably correspond to episodes of increased bottom current circulation linked to hydrological fluctuation. In the Quaternary, such fluctuations are probably linked to global climate fluctuations and glacio-eustatic sea-level changes, which can determine changes in ocean surface temperatures, the nature and generation of different water masses (surface and deep) and the oceanic circulation pattern (wind-driven and thermohaline) (Faugères *et al.* 1999; Faugères & Stow 2008). However, at present, there is no clear link between the timing of formation of the D2–D8 unconformities and hydrological fluctuation at the scale of interglacial–glacial cycles. Anderskov *et al.* (2010) have demonstrated that formation and accretion of sediment waves in the upper part of the Eyre Terrace Drift occurred during both glacial and interglacial phases. Such uncertainty in attempting to relate particular climatic conditions (and, hence, sea level) to particular intensities of bottom currents is further echoed by a number of studies in the northern and southwestern Atlantic Ocean (*cf.* Faugères *et al.* 1999; Faugères & Stow 2008 and references therein) that show more or less random variation in drift development related to current intensity. Further speculation on this issue is beyond the scope of this paper.

6. Conclusions

This study has presented an appraisal of the stratigraphic framework of the Dugong Supersequence in the western GAB. By combining seismic reflection and sedimentary data, it has been possible to identify the large-scale pattern of sedimentation and basin development on the outer part of the Eucla Basin. The following key points should be noted:

- A revised seismic-stratigraphic framework for the Dugong Supersequence on the shelf-margin of the Eucla Basin is characterised by four main depositional packages – Middle–Upper Eocene, Oligocene–lowest Miocene, upper Lower–Upper Miocene and Quaternary – bounded by four regionally mappable unconformities, D10–D40. Pliocene deposits are restricted to the upper slope. These depositional packages

are further divided on the outer shelf and upper slope by localised unconformities of more limited extent.

- Whereas the shelf succession comprises a predominantly aggrading-to-prograding succession of carbonate platform and ramp deposits, the sediments at the shelf-edge and on the upper slope are dominated by contourites. The Quaternary Eyre Terrace Drift is an elongate mounded drift and represents the most conspicuous seismic-stratigraphic expression of alongslope sedimentation, though smaller-scale manifestations of contourite drifts are preserved in the Eocene (separated drift), Oligocene (plastered drift) and Pliocene (infill drift) rocks.
- The Neogene succession on the upper slope displays evidence of instability on the margin, best expressed by the Late Neogene Slide (Late Miocene) and associated mass movement deposits. Nevertheless, the Miocene sequence is dominated by fine-grained and strongly bioturbated material comparable with the underlying and overlying sequences, suggesting that alongslope processes might have prevailed as background sedimentation.
- The tectonostratigraphic setting of the Dugong Supersequence indicates that the late post-breakup development of the Eucla Basin was characterised by long-term tectonic instability and differential vertical motions. This is expressed by a series of angular and erosive unconformities that mark abrupt changes in sequence architecture consistent with tectonic activity. Correlation with periods of enhanced tectonic activity in SE Australian basins suggests that this instability was an integral part of the regional geodynamic response of the southern Australian margin to late post-breakup transmission of intra-plate stresses.

Our results have profound implications for the Cenozoic sedimentary and tectonic development of the southern Australian margin. The influence of alongslope currents on sedimentary processes on the shelf-margin since the Mid-Eocene has not previously been considered for the western GAB, whilst the availability of tectonic mechanisms, combined with our critical appraisal of previously defined hiatuses on the upper slope as third-order global sequence boundaries, challenges putative models (e.g., Li *et al.* 2003a, 2004) that cite global eustasy as the primary control on the stratigraphic architecture of the Eucla Basin. Thus, there is much scope for the development of a new and more comprehensive model of late post-breakup continental margin development, offshore southern Australia, which considers how the stratigraphic and sedimentological information presented in this paper can contribute to a better understanding of the tectonic and oceanographic development of the wider Australian–Antarctic Basin. In particular, this study and others (e.g., Jackson *et al.* 2019) provide a geological record of erosional and depositional contourite bedforms that can be used to assess and constrain the long-term influence of alongslope currents that have shaped the southern Australian margin. Whereas the role of boundary currents that currently bathe this margin, such as the Leeuwin, South Australian and Flinders currents, is well known, their palaeoceanographic significance and interaction remains uncertain, as does the configuration of palaeo-circulation patterns. Establishing exactly what configuration of boundary currents and water masses would best explain the style, pattern and distribution of the preserved bedforms should be a key objective of future work.

7. Acknowledgements

The authors would like to thank Jane Blevin for her constructive review of this paper. Seismic reflection data were supplied by

Petroleum Geo-Services (PGS) as part of their Southern Australian Margin Digital Atlas, which we gratefully acknowledge. We also thank IHS Markit for provision of Kingdom software. Martyn Stoker and Jennifer Totterdell gratefully acknowledge the award of Visiting Research Fellow titles in the Australian School of Petroleum and Energy Resources. Simon Holford gratefully acknowledges funding support from the South Australian Department for Energy and Mining.

8. References

- Alley, N. F., Clarke, J. D. A., MacPhail, M. M. & Truswell, E. M. 1999. Sedimentary infillings and development of major Tertiary palaeo-drainage systems of south-central Australia. *International Association of Sedimentologists, Special Publication* **27**, 337–66.
- Anderskov, K., Surlyk, F., Huuse, M., Lykke-Andersen, H., Bjerager, M. & Tang, C. D. 2010. Sediment waves with a biogenic twist in Pleistocene cool water carbonates, Great Australian Bight. *Marine Geology* **278**, 122–39.
- Bein, J. & Taylor, M. L. 1991. The Eyre Sub-basin: recent exploration results. *APEA Journal* **21**, 91–98.
- Benbow, M. C., Lindsay, J. M. & Alley, N. F. 1995. Eucla basin and palaeo-drainage. In Drexel, J. F. & Preiss, W. V. (eds.) *The geology of South Australia: vol. 2. The Phanerozoic*, Bulletin **54**, 178–86. South Australia Geological Survey.
- Bijl, P. K., Bendle, J. A. P., Bohaty, S. M., Pross, J., Schouten, S., Tauxe, L., Stickley, C. E., McKay, R. M., Röhl, U., Olney, M., Slijs, A., Escutia, C., Brinkhuis, H. & Expedition 318 Scientists. 2013. Eocene cooling linked to early flow across the Tasmanian Gateway. *Proceedings of the National Academy of Sciences* **110**, 9645–50.
- Bijl, P. K., Houben, A. J., Hartman, J. D., Pross, J., Salabarnada, A., Escutia, C. & Sangiorgi, F. 2018. Palaeoceanography and ice sheet variability offshore Wilkes Land, Antarctica – Part 2: insights from Oligocene–Miocene dinoflagellate cysts. *Climate of the Past* **14**, 1015–33.
- Black, K. S., Peppe, O. C. & Gust, G. 2003. Erodibility of pelagic carbonate ooze in the northeast Atlantic. *Journal of Experimental Marine Biology and Ecology* **285**, 143–63.
- Boreen, T. D. & James, N. P. 1993. Holocene sediment dynamics on a cool-water carbonate shelf: Otway, Southeastern Australia. *Journal of Sedimentary Petrology* **63**, 574–88.
- Bosence, D. W. J. & Wilson, R. C. L. 2003. Part 4. Carbonates: 11. Carbonate depositional systems. In Coe, A. L. (ed.) *The sedimentary record of sea-level change*, 209–33. Cambridge: Cambridge University Press.
- Bradshaw, B. E., Rollet, N., Totterdell, J. M. & Borissova, I. 2003. *A revised structural framework for frontier basins on the Southern and Southwestern Australian Continental Margin*. Geoscience Australia Record 2003/03.
- Brooks, G. R., Hine, A. C., Mallinson, D. & Drexler, T. M. 2003. Data report: Texture and composition of upper-slope sediments in the Great Australian Bight: sites 1130 and 1132. In Hine, A. C., Feary, D. A. & Malone, M. J. (eds) *Proceedings of the Ocean Drilling Program, scientific results*, vol. 182. College Station, Texas (Ocean Drilling Program), 1–21. <https://doi.org/10.2973/odp.proc.sr.182.003.2002>.
- Brown, B. J., Müller, R. D. & Struckmeyer, H. I. M. 2001. Anomalous tectonic subsidence of the southern Australian passive margin: response to Cretaceous dynamic topography or differential lithospheric stretching? In Hill, K. C. & Bernecker, T. (eds.) *Eastern Australian Basins Symposium I*, 563–70. Petroleum Exploration Society of Australia, Special Publication.
- Brunn, C. A., Andres, M., Holbourn, A. E., Siedlecki, S., Brooks, G. R., Molina-Garza, R. S., Fuller, M. D., Ladner, B. C., Hine, A. C. & Li, Q. 2002. Quaternary planktonic foraminiferal biostratigraphy, ODP Leg 182 sites. In Hine, A. C., Feary, D. A. & Malone, M. J. (eds) *Proceedings of the Ocean Drilling Program, scientific results*, vol. 182, 1–16. College Station, Texas: Ocean Drilling Program. <https://doi.org/10.2973/odp.proc.sr.182.011.2002>.
- Cirano, M. & Middleton, J. F. 2004. The mean wintertime circulation along Australia's Southern Shelves: a numerical study. *Journal of Physical Oceanography* **34**, 668–84.
- Clarke, J. D. A., Gammon, P. R., Hou, B. & Gallagher, S. J. 2003. Middle to Upper Eocene stratigraphic nomenclature and deposition in the Eucla Basin. *Australian Journal of Earth Sciences* **50**, 231–48.
- Clarke, J. D. A. & Hou, B. 2000. Eocene coastal barrier evolution in the Eucla Basin. *MESA Journal* **18**, 36–41.

- Cockshell, C. D., Hill, A. J. & McKirdy, D. M. 1990. *Final report APIRA project P298 Bight Duntroon basins study*. Department of Mines and Energy South Australia, Oil, Gas and Coal Division, DME 129/88.
- Cresswell, G. R. & Dominguez, C. M. 2009. The Leeuwin Current south of Western Australia. *Journal of the Royal Society of Western Australia* **92**, 83–100.
- Cresswell, G. R. & Griffin, D. A. 2004. The Leeuwin Current, eddies and sub-Antarctic waters off south-western Australia. *Marine and Freshwater Research* **55**, 267–76.
- Cresswell, G. R. & Petersen, J. L. 1993. The Leeuwin Current of Western Australia. *Australian Journal of Marine and Freshwater Research* **44**, 285–303.
- Dickinson, J. A., Wallace, M. W., Holdgate, G. R., Gallagher, S. J. & Thomas, L. 2002. Origin and timing of the Miocene–Pliocene unconformity in southeast Australia. *Journal of Sedimentary Research* **72**, 288–303.
- Duran, E. R., Phillips, H. E., Furue, R., Spence, P. & Bindoff, N. L. 2020. Southern Australia Current System based on a gridded hydrography and a high-resolution model. *Progress in Oceanography* **181**, 1–20. doi: 10.1016/j.pocean.2019.102254
- Embry, A. F. 1990. A tectonic origin for third-order depositional sequences in extensional basins – implications for basin modelling. In Cross, T. A. (ed.) *Quantitative dynamic stratigraphy*, 491–501. Englewood Cliffs: Prentice-Hall.
- Evans, D., Harrison, Z., Shannon, P. M., Laberg, J. S., Nielsen, T., Ayers, S., Holmes, R., Hoult, R. J., Lindberg, B., Hafliadason, H., Long, D., Kuijpers, A., Andersen, E. S. & Bryn, P. 2005. Palaeoslides and other mass failures of Pliocene to Pleistocene age along the Atlantic continental margin of NW Europe. *Marine and Petroleum Geology* **22**, 1131–48.
- Exon, N., Kennett, J. & Malone, M. & the Leg 189 Shipboard Scientific Party. 1999. The opening of the Tasmanian Gateway drove global paleoclimatic and palaeoceanographic changes: results of Leg 189. *Journal of Marine Research* **57**, 11–18.
- Fairclough, M. C., Benbow, M. C. & Rogers, P. A. 2007. Explanatory notes for the OOLDEA 1:250 000 geological map, sheet SH52-12, South Australia. Department of Primary Industries and Resources. Report Book, 2007/11, 44p.
- Faugères, J.-C. & Stow, D. A. V. 2008. Contourite drifts: nature, evolution and controls. In Rebesco, M. & Camerlenghi, A. (eds) *Contourites. Developments in sedimentology*, vol. **60**, 259–88. Amsterdam: Elsevier.
- Faugères, J.-C., Stow, D. A. V., Imbert, P. & Viana, A. 1999. Seismic features diagnostic of contourite drifts. *Marine Geology* **162**, 1–38.
- Feary, D. A., Birch, G., Boreen, T. et al. 1993. *Geological sampling in the Great Australian Bight: Scientific post-cruise report – R/V Rig Seismic Cruise 102*. Australian Geological Survey Organisation Record 1993/18, 140 pp.
- Feary, D. A., Hine, A. C., James, N. P. & Malone, M. J. 2004. Leg 182 synthesis: exposed secrets of the Great Australian Bight. In Hine, A. C., Feary, D. A. & Malone, M. J. (eds) *Proceedings of the Ocean Drilling Program, scientific results*, vol. **182**. College Station, Texas: Ocean Drilling Program. <https://doi:10.2973/odp.proc.sr.182.017.2004>.
- Feary, D. A., Hine, A. C., Malone, M. J. et al. 2000. *Proceedings of the ocean drilling program, initial reports*, vol. **182**. College Station, Texas: Ocean Drilling Program. <https://doi:10.2973/odp.proc.ir.182.2000>.
- Feary, D. A. & James, N. P. 1995. Cenozoic biogenic mounds and buried Miocene(?) barrier reef on a predominantly cool-water carbonate continental margin – Eucla Basin, western Great Australian Bight. *Geology* **23**, 427–30.
- Feary, D. A. & James, N. P. 1998. Seismic stratigraphy and geological evolution of the Cenozoic, cool-water Eucla Platform, Great Australian Bight. *American Association of Petroleum Geologists Bulletin* **82**, 792–816.
- Feng, M., Waite, A. & Thompson, P. 2009. Climate variability and ocean production in the Leeuwin Current system off the west coast of Western Australia. *Journal of the Royal Society of Western Australia* **92**, 67–81.
- Fuller, M., Molina-Garza, R., Antretter, M. & Lichowski, F. 2003. Magnetostratigraphy of the Plio-Pleistocene carbonate section of the Great Australian Bight. *Australian Journal of Earth Sciences* **50**, 447–66.
- Fulthorpe, C. S. 1991. Geological controls on seismic sequence resolution. *Geology* **19**, 61–65.
- Galloway, W. E. 1989. Genetic stratigraphic sequences in basin analysis II: application to northwest Gulf of Mexico Cenozoic basin. *American Association Petroleum Geologists Bulletin* **73**, 143–54.
- Gradstein, F. M., Ogg, J. G., Schmitz, M. D. & Ogg, G. M. 2012. *The geologic time scale 2012*. Amsterdam: Elsevier, 1144 pp.
- Haq, B. U. & Al-Qahtani, A. M. 2005. Phanerozoic cycles of sea-level change on the Arabian Platform. *GeoArabia* **10**, 127–60.
- Hardenbol, J., Thierry, J., Farley, M. B., Jacquiu, T., De Graciansky, P.-C. & Vail, P. R. 1998. Cenozoic sequence chronostratigraphy. In De Graciansky, P.-C., Hardenbol, J., Jacquiu, T. & Vail, P. R. (eds.) *Mesozoic and Cenozoic sequence chronostratigraphic framework of European Basins*, vol. **60**, 3–13. Tulsa, Oklahoma: SEPM (Society for Sedimentary Geology) Special Publication.
- Hegarty, K. A., Weissel, J. K. & Mutter, J. C. 1988. Subsidence history of Australia's southern margin: constraints on basin models. *American Association of Petroleum Geologists Bulletin* **72**, 615–33.
- Hesse, P. P., Magee, J. W. & van der Kaars, S. 2004. Late Quaternary climates of the Australian arid zone: a review. *Quaternary International* **118–119**, 87–102.
- Hill, A. J. 1995. Bight basin. In Drexel, J. F. & Preiss, W. V. (eds.) *The geology of South Australia, volume 2, The Phanerozoic*, Bulletin **54**, 133–49. South Australia Geological Survey.
- Hillis, R. R., Sandiford, M., Reynolds, S. D. & Quigley, M. C. 2008. Present-day stresses, seismicity and Neogene-to-recent tectonics of Australia's 'passive' margins: intraplate deformation controlled by plate boundary forces. In Johnson, H., Doré, A. G., Gatliff, R. W., Holdsworth, R., Lundin, E. R. & Ritchie, J. D. (eds) *The nature and origin of compression in passive margins*, vol. **306**, 71–90. London: Geological Society, Special Publications.
- Hine, A. C., Feary, D. A. & Malone, M. J. (eds) 2004. *Proceedings of the Ocean Drilling Program, scientific results*, vol. **182**. College Station, Texas: Ocean Drilling Program. <https://doi:10.2973/odp.proc.sr.182.2004>.
- Hocking, R. M. 1990. Eucla basin. In *Geology and Mineral Resources of Western Australia: Geological Survey of Western Australia, Memoir* **3**, 548–61. Geological Survey of Western Australia.
- Holbourn, A., Kuhnt, W. & James, N. 2002. Late Pleistocene bryozoan reef mounds of the Great Australian Bight: isotope stratigraphy and benthic foraminiferal record. *Paleoceanography* **17**, 1–15. doi: 10.1029/2001PA000643
- Holford, S. P., Hillis, R. R., Duddy, I. R., Green, P. F., Stoker, M. S., Tuit, A. K., Backé, G., Tassone, D. R. & MacDonald, J. D. 2011a. Cenozoic post-breakup compressional deformation and exhumation of the southern Australian margin. *APPEA Journal* **51**, 613–38.
- Holford, S. P., Hillis, R. R., Duddy, I. R., Green, P. F., Tassone, D. R. & Stoker, M. S. 2011b. Paleothermal and seismic constraints on late Miocene–Pliocene uplift and deformation in the Torquay sub-basin, southern Australian margin. *Australian Journal of Earth Sciences* **58**, 543–62.
- Holford, S. P., Tuit, A. K., Hillis, R. R., Green, P. F., Stoker, M. S., Duddy, I. R., Sandiford, M. & Tassone, D. R. 2014. Cenozoic deformation in the Otway Basin, southern Australian margin: implications for the origin and nature of post-breakup compression at rifted margins. *Basin Research* **26**, 10–37.
- Hou, B., Alley, N. F., Frakes, L. A., Stoian, L. & Cowley, W. M. 2006. Eocene stratigraphic succession in the Eucla Basin of South Australia and correlation to major sea-level events. *Sedimentary Geology* **183**, 297–319.
- Hou, B., Frakes, L. A., Sandiford, M., Worrall, L., Keeling, J. & Alley, N. F. 2008. Cenozoic Eucla Basin and associated palaeovalleys, southern Australia – climatic and tectonic influences on landscape evolution, sedimentation and heavy mineral accumulation. *Sedimentary Geology* **203**, 112–30.
- Huber, B. T., Hobbs, R. W., Bogus, K. A., Batenburg, S. J., Brumsack, H.-J., do Monte Guerra, R., Edgar, K. M., Edvardson, T., Garcia Tejada, M. L., Harry, D. L., Hasegawa, T., Haynes, S. J., Jiang, T., Jones, M. M., Kuroda, J., Lee, E. Y., Li, Y.-X., MacLeod, K. G., Maritati, A., Martinez, M., O'Connor, L. K., Petrizzo, M. R., Quan, T. M., Richter, C., Riquier, L., Tagliaro, G. T., Wainman, C. C., Watkins, D. K., White, L. T., Wolfgring, E. & Xu, Z. 2019. Site U1512. In Hobbs, R. W., Huber, B. T., Bogus, K. A. & Expedition 369 Scientists (eds) *Australia Cretaceous Climate and Tectonics*. Proceedings of the International Ocean Discovery Program, 369: College Station, Texas (International Ocean Discovery Program). <https://doi.org/10.14379/ioidp.proc.369.103.2019>.
- Huuse, M. & Feary, D. A. 2005. Seismic inversion for acoustic impedance and porosity of Cenozoic cool-water carbonates on the upper continental slope of the Great Australian Bight. *Marine Geology* **215**, 123–34.
- Jackson, C. A. L., Magee, C. & Hunt-Stewart, E. R. 2019. Cenozoic contourites in the eastern Great Australian Bight, offshore southern Australia: implications for the onset of the Leeuwin Current. *Journal of Sedimentary Research* **89**, 199–206.
- Jagodzinski, E. A., Bodorkos, S., Crowley, J. L., Pawley, M. J. & Wise, T. W. 2019. *PACE Copper Coompana Drilling Project: U-Pb dating of*

- basement and cover rocks. Geological Survey of South Australia. Report Book, 2018/00028, 211p.
- James, N. P. & Bone, Y. 1991. Origin of a cool-water, Oligo-Miocene deep shelf limestone, Eucla Platform, southern Australia. *Sedimentology* **38**, 323–41.
- James, N. P., Bone, Y., Carter, R. M. & Murray-Wallace, C. V. 2006. Origin of the Late Neogene Roe Plains and their calcarenite veneer: implications for sedimentology and tectonics in the Great Australian Bight. *Australian Journal of Earth Sciences* **53**, 407–19.
- James, N. P., Bone, Y., Collins, L. B. & Kyser, T. K. 2001. Surficial sediments of the Great Australian Bight: facies dynamics and oceanography on a vast cool-water carbonate shelf. *Journal of Sedimentary Research* **71**, 549–67.
- James, N. P., Boreen, T. D., Bone, Y. & Feary, D. A. 1994. Holocene carbonate sedimentation on the west Eucla Shelf, Great Australian Bight: a shaved shelf. *Sedimentary Geology* **90**, 161–77.
- James, N. P., Feary, D. A., Betzler, C., Bone, Y., Holburn, A. E., Li, Q., Machiyama, H., Simo, T. J. A. & Surlyk, F. 2004. Origin of late Pleistocene bryozoan reef mounds; Great Australian Bight. *Journal of Sedimentary Research* **74**, 20–48.
- James, N. P., Feary, D. A., Surlyk, F., Simo, T. J. A., Betzler, C., Holburn, A. E., Li, Q., Matsuda, H., Machiyama, H., Brooks, G. R., Andres, M. S., Malone, M. J. & ODP Leg 182 Scientific Party. 2000. Quaternary bryozoan reef mounds in cool-water upper slope environments, Great Australian Bight. *Geology* **28**, 647–50.
- James, N. P. & von der Borch, C. C. 1991. Carbonate shelf edge off southern Australia: A prograding open-platform margin. *Geology* **19**, 1005–08.
- Ladner, B. C. 2002. Data report: Calcareous nannofossil biostratigraphy of site 1127, Ocean Drilling Program Leg 182. In Hine, A. C., Feary, D. A. & Malone, M. J. (eds) *Proceedings of the Ocean Drilling Program, scientific results*, vol. 182. College Station, Texas (Ocean Drilling Program), 1–11. <https://doi.org/10.2973/odp.proc.sr.182.013.2002>.
- Li, Q., James, N. P., Bone, Y. & McGowran, B. 1996. Foraminiferal biostratigraphy and depositional environments of the mid-Cenozoic Abrakurrie Limestone, Eucla Basin, southern Australia. *Australian Journal of Earth Sciences* **43**, 437–450.
- Li, Q., James, N. P. & McGowran, B. 2003a. Middle and Late Eocene Great Australian Bight lithobiostratigraphy and stepwise evolution of the southern Australian continental margin. *Australian Journal of Earth Sciences* **50**, 113–28.
- Li, Q., McGowran, B. & Brunnur, C. A. 2003b. Neogene planktonic foraminiferal biostratigraphy of Sites 1126, 1128, 1130, 1132, and 1134, ODP Leg 182, Great Australian Bight. In Hine, A. C., Feary, D. A. & Malone, M. J. (eds) *Proceedings of the Ocean Drilling Program, scientific results*, vol. 182. College Station, Texas (Ocean Drilling Program), 1–67. <https://doi.org/10.2973/odp.proc.sr.182.005.2003>.
- Li, Q., McGowran, B. & James, N. P. 2003c. Eocene–Oligocene planktonic foraminiferal biostratigraphy of Sites 1126, 1130, 1132, and 1134, ODP Leg 182, Great Australian Bight. In Hine, A. C., Feary, D. A. & Malone, M. J. (eds) *Proceedings of the Ocean Drilling Program, Scientific Results*, vol. 182. College Station, Texas (Ocean Drilling Program), 1–28. <https://doi.org/10.2973/odp.proc.sr.182.006.2003>.
- Li, Q., Simo, J. A., McGowran, B. & Holbourn, A. 2004. The eustatic and tectonic origin of Neogene unconformities from the Great Australian Bight. *Marine Geology* **203**, 57–81.
- Lowry, D. C. 1970. *Geology of the Western Australian part of the Eucla Basin*, Bulletin 122. Geological Survey of Western Australia.
- Lu, H. & Fulthorpe, C. S. 2004. Controls on sequence stratigraphy of a middle Miocene–Holocene current-swept, passive margin: offshore Canterbury Basin, New Zealand. *Geological Society of America Bulletin* **116**, 1345–66.
- Mahon, E. M. & Wallace, M. W. 2020. Cenozoic structural history of the Gippsland Basin: Early Oligocene onset for compressional tectonics in SE Australia. *Marine and Petroleum Geology* **114**, 104243.
- Masson, D. G., Howe, J. A. & Stoker, M. S. 2002. Bottom-current sediment waves, sediment drifts and contourites in the northern Rockall Trough. *Marine Geology* **192**, 215–37.
- Masson, D. G., Wynn, R. B. & Bett, B. J. 2004. Sedimentary environment of the Faroe-Shetland and Faroe Bank Channels, north-east Atlantic, and the use of bedforms as indicators of bottom current velocity in the deep ocean. *Sedimentology* **51**, 1207–41.
- McCartney, M. S. & Donohue, K. A. 2007. A deep cyclonic gyre in the Australian–Antarctic Basin. *Progress in Oceanography* **75**, 675–750.
- McGowran, B., Holdgate, G. R., Li, Q. & Gallagher, S. J. 2004. Cenozoic stratigraphic succession in southeastern Australia. *Australian Journal of Earth Sciences* **51**, 459–96.
- McGowran, B., Li, Q., Cann, J., Padley, D., McKirdy, D. M. & Shafik, S. 1997. Biogeographic impact of the Leeuwin Current in southern Australia since the late middle Eocene. *Palaeogeography, Palaeoclimatology, Palaeoecology* **136**, 19–40.
- Messent, B. E. J. 1998. *Great Australian Bight well audit*. AGSO Record 1998/37.
- Messent, B. E. J., Wilson, C. & Flynn, K. 1996. Assessment of the seal potential of Tertiary carbonates, Duntroon Basin, South Australia. *APPEA Journal* **1996**, 233–47.
- Miall, A. D. 1997. *The Geology of Stratigraphic Sequences*. Berlin, Heidelberg, New York: Springer-Verlag, 433 pp.
- Middleton, J. F. & Bye, J. A. T. 2007. A review of the shelf-slope circulation along Australia's southern shelves: Cape Leeuwin to Portland. *Progress in Oceanography* **75**, 1–41.
- Middleton, J. F. & Cirano, M. 2002. A northern boundary current along Australia's southern shelves: the Flinders Current. *Journal of Geophysical Research* **107**, 1–11. doi: 10.1029/2000JC000701 Article No. 3129.
- Mitchell, J. K., Holgate, G. R., Wallace, M. W. & Gallagher, S. J. 2007. Marine geology of the Quaternary Bass Canyon system, southeast Australia: a cool-water carbonate system. *Marine Geology* **237**, 71–96.
- Mitchum, R. M., Vail, P. R. & Sangree, J. B. 1977. Seismic stratigraphy and global changes of sea level, part 6: stratigraphic interpretation of seismic reflection patterns in depositional sequences. In Payton, C. E. (ed.) *Seismic stratigraphy – applications to hydrocarbon exploration*, memoir 26, 117–33. Tulsa, Oklahoma: American Association of Petroleum Geologists.
- Morgan, R., Rowett, A. I. & White, M. R. 2005. Biostratigraphy. In O'Brien, G. W., Paraschivoiu, E. & Hibbert, J. E. (eds.) *Petroleum geology of South Australia*, vol. 5: *Great Australian Bight*, 1–46. Primary Industry and Resources of South Australia.
- Mounsher, L. C. 2016. Evolution and deformation of the onshore Eucla Basin during the Cenozoic. Honours Manuscript 2013. Curtin University, Department of Applied Geology, Geological Survey of Western Australia. Record, 2016/10, 61p.
- Nardin, T. R., Hein, F. J., Gorsline, D. S. & Edwards, B. D. 1979. A review of mass movement processes, sediment and acoustic characteristics, and contrasts in slope and base-of-slope systems v. Canyon-fan-basin floor systems. In Doyle, L. J. & Pilkey, O. H. (eds.) *Geology of continental margins*, Special Publication 27, 61–73. Tulsa, Oklahoma: Society of Economic Palaeontologists and Mineralogists.
- Norvick, M. S. & Smith, M. A. 2001. Mapping the plate tectonic reconstruction of southern and southeastern Australia and implications for petroleum systems. *APPEA Journal* **41**, 15–35.
- O'Connell, L. G. 2011. *Sedimentology of the Miocene Nullarbor Limestone: southern Australia*. East Perth: Geological Survey of Western Australia, Report 111, 211p.
- O'Connell, L. G., James, N. P. & Bone, Y. 2012. The Miocene Nullarbor Limestone, southern Australia; deposition on a vast subtropical epeiric platform. *Sedimentary Geology* **253–54**, 1–16.
- Petruševics, P., Bye, J. A. T., Fahlbusch, V., Hammat, J., Tippins, D. R. & van Wijk, E. 2009. High salinity winter outflow from a mega inverse-estuary – the Great Australian Bight. *Continental Shelf Research* **29**, 371–80.
- Reynolds, P., Holford, S., Schofield, N. & Ross, A. 2017. The shallow depth emplacement of mafic intrusions on a magma-poor rifted margin: an example from the Bight Basin, southern Australia. *Marine and Petroleum Geology* **88**, 605–16.
- Richardson, L. E., Middleton, J. F., Kyser, T. K., James, N. P. & Opdyke, B. N. 2019. Shallow water masses and their connectivity along the southern Australian continental margin. *Deep-Sea Research Part 1*, 103083.
- Ridgeway, K. R. & Condie, S. A. 2004. The 5500-km-long boundary flow off western and southern Australia. *Journal of Geophysical Research* **109**, C04017.
- Robson, A. G., King, R. C. & Holford, S. P. 2017. Structural evolution of a gravitationally detached normal fault array: analysis of 3D seismic data from the Ceduna Sub-Basin, Great Australian Bight. *Basin Research* **29**, 605–624.
- Ryan, W. B. F., Carbotte, S. M., Coplan, J., O'Hara, S., Melkonian, A., Arko, R., Weissel, R. A., Ferrini, V., Goodwillie, A., Nitsche, F., Bonczkowski, J. & Zensky, R. 2009. Global Multi-Resolution Topography (GMRT) synthesis data set. *Geochemistry, Geophysics, Geosystems* **10**, Q03014.
- Sandiford, M. 2007. The tilting continent: a new constrain of the dynamic topographic field from Australia. *Earth and Planetary Letters* **261**, 152–63.
- Sangiorgi, F., Bijl, P. K., Passchier, S., Salzmann, U., Schouten, S., McKay, R. *et al.* 2018. Southern Ocean warming and Wilkes Land ice sheet retreat during the mid-Miocene. *Nature Communications* **9**, 317.
- Sauermilch, I., Whittaker, J. M., Bijl, P. K., Totterdell, J. M. & Jokat, W. 2019. Tectonic, oceanographic, and climatic controls on the

- Cretaceous–Cenozoic sedimentary record of the Australian–Antarctic Basin. *Journal of Geophysical Research: Solid Earth* **124**, 7699–7724.
- Saxena, S. & Betzler, C. 2002. Genetic sequence stratigraphy of cool water slope carbonates (Pleistocene Eucla Shelf, southern Australia). *International Journal of Earth Science (Geologische Rundschau)* **92**, 482–93.
- Sayers, J., Bernardel, G. & Parumes, R. 2003. *Geological framework of the central Great Australian Bight and adjacent areas*. Geoscience Australia Record 2003/12, 140 pp.
- Schattner, U., Lobo, F. J., López-Quirós, A., dos Passos Nascimento, J. L. & de Mahiques, M. M. 2019. What feeds shelf-edge clinoforms over margins deprived of adjacent land sources? An example from southeastern Brazil. *Basin Research* **32**, 293–301.
- Scher, H. D., Whittaker, J. M., Williams, S. E., Latimer, J. C., Kordesch, W. E. C. & Delaney, M. L. 2015. Onset of Antarctic Circumpolar Current 30 million years ago as Tasmanian Gateway aligned with westerlies. *Nature* **523**, 580–83.
- Schofield, A. & Totterdell, J. M. 2008. *Distribution, timing and origin of magmatism in the Bight and Eucla basins*. Geoscience Australia Record 2008/24, 19 pp.
- Sharples, A. G. W. D., Huuse, M., Hollis, C., Totterdell, J. M. & Taylor, P. D. 2014. Giant middle Eocene bryozoan reef mounds in the Great Australian Bight. *Geology* **42**, 683–86.
- Shipboard Scientific Party. 2000a. Leg 182 Summary: Great Australian Bight – Cenozoic Cool-Water Carbonates. In Feary, D. A., Hine, A. C. & Malone, M. J., et al. (eds) *Proceedings of the Ocean Drilling Program, initial reports*, vol. 182. College Station, Texas (Ocean Drilling Program), 1–58.
- Shipboard Scientific Party. 2000b. Site 1126. In Feary, D. A., Hine, A. C. & Malone, M. J., et al. (eds) *Proceedings of the Ocean Drilling Program, initial reports*, vol. 182. College Station, Texas (Ocean Drilling Program), 1–110.
- Shipboard Scientific Party. 2000c. Site 1127. In Feary, D. A., Hine, A. C. & Malone, M. J., et al. (eds) *Proceedings of the Ocean Drilling Program, initial reports*, vol. 182. College Station, Texas (Ocean Drilling Program), 1–90. <https://doi:10.2973/odp.proc.ir.182.105.2000>.
- Shipboard Scientific Party. 2000d. Site 1128. In Feary, D. A., Hine, A. C. & Malone, M. J., et al. (eds) *Proceedings of the Ocean Drilling Program, initial reports*, vol. 182. College Station, Texas (Ocean Drilling Program), 1–113. <https://doi:10.2973/odp.proc.ir.182.106.2000>.
- Shipboard Scientific Party. 2000e. Site 1129. In Feary, D. A., Hine, A. C. & Malone, M. J., et al. (eds) *Proceedings of the Ocean Drilling Program, initial reports*, vol. 182. College Station, Texas (Ocean Drilling Program), 1–86. <https://doi:10.2973/odp.proc.ir.182.107.2000>.
- Shipboard Scientific Party. 2000f. Site 1130. In Feary, D. A., Hine, A. C. & Malone, M. J., et al. (eds) *Proceedings of the Ocean Drilling Program, initial reports*, vol. 182. College Station, Texas (Ocean Drilling Program), 1–98. <https://doi:10.2973/odp.proc.ir.182.108.2000>.
- Shipboard Scientific Party. 2000g. Site 1131. In Feary, D. A., Hine, A. C. & Malone, M. J., et al. (eds) *Proceedings of the Ocean Drilling Program, initial reports*, vol. 182. College Station, Texas (Ocean Drilling Program), 1–82. <https://doi:10.2973/odp.proc.ir.182.109.2000>.
- Shipboard Scientific Party. 2000h. Site 1132. In Feary, D. A., Hine, A. C. & Malone, M. J., et al. (eds) *Proceedings of the Ocean Drilling Program, initial reports*, vol. 182. College Station, Texas (Ocean Drilling Program), 1–87. <https://doi:10.2973/odp.proc.ir.182.110.2000>.
- Shipboard Scientific Party. 2000i. Site 1133. In Feary, D. A., Hine, A. C. & Malone, M. J., et al. (eds) *Proceedings of the Ocean Drilling Program, initial reports*, vol. 182. College Station, Texas (Ocean Drilling Program), 1–51. <https://doi:10.2973/odp.proc.ir.182.111.2000>.
- Shipboard Scientific Party. 2000j. Site 1134. In Feary, D. A., Hine, A. C. & Malone, M. J., et al. (eds) *Proceedings of the Ocean Drilling Program, initial reports*, vol. 182. College Station, Texas (Ocean Drilling Program), 1–80. <https://doi:10.2973/odp.proc.ir.182.112.2000>.
- Simo, J. A. & Slatter, N. M. 2002. Data report: sedimentology of a Pleistocene middle slope cool-water carbonate platform. In Hine, A. C., Feary, D. A. & Malone, M. J. (eds) *Proceedings of the Ocean Drilling Program, Scientific Results*, vol. 182. College Station, Texas (Ocean Drilling Program), 1–15. <https://doi:10.2973/odp.proc.sr.182.016.2002>.
- Smith, M. A. & Donaldson, I. F. 1995. The hydrocarbon potential of the Duntroon Basin. *APPEA Journal* **1995**, 203–19.
- Stagg, H. M. J., Cockshell, C. D., Willcox, J. B., Hill, A. J., Needham, D. V. C., Thomas, B., O'Brien, G. W. & Hough, L. P. 1990. *Basins of the Great Australian Bight region – geology and petroleum potential, folio 5, continental margins program*. Canberra: Bureau of Mineral Resources, Geology and Geophysics.
- Stickley, C. E., Brinkhuis, H., Schellenberg, S. A., Sluijs, A., Röhl, U., Fuller, M., Grauert, M., Huber, M., Warnaar, J. & Williams, G. L. 2004. Timing and nature of the deepening of the Tasmanian Gateway. *Paleoceanography* **19**, PA001022.
- Stoker, M. S., Akhurst, M. C., Howe, J. A. & Stow, D. A. V. 1998. Sediment drifts and contourites on the continental margin off NW Britain. *Sedimentary Geology* **115**, 33–51.
- Stoker, M. S., van Weering, T. C. E. & Svaerdborg, T. 2001. A Mid- to Late Cenozoic tectonostratigraphic framework of the Rockall Trough. In Shannon, P. M., Houghton, P. D. W. & Corcoran, D. V. (eds) *The petroleum exploration of Ireland's offshore basins*, vol. **188**, 411–38. London: Geological Society, Special Publications.
- Stow, D. A. V., Faugères, J.-C., Howe, J. A., Pudsey, C. J. & Viana, A. R. 2002. Bottom currents, contourites and deep-sea sediment drifts: current state-of-the-art. In Stow, D. A. V., Pudsey, C. J., Howe, J. A., Faugères, J.-C. & Viana, A. R. (eds) *Deep-water contourite systems: modern drifts and ancient series, seismic and sedimentary characteristics*, vol. **22**, 7–20. London: Geological Society, Memoirs.
- Talukder, A., Ross, A. S., Trefry, C., Pickard, A. & Tam, T. 2021. Large scale seabed processes in a deep cool water carbonate ramp system: a case study of the Great Australian Bight. *Marine and Petroleum Geology* **125**, 1–14. doi: 10.1016/j.marpetgeo.2020.104793
- Tikku, A. A. & Cande, S. C. 1999. The oldest magnetic anomalies in the Australian–Antarctic Basin: are they isochrons? *Journal of Geophysical Research* **B1**, 661–77.
- Totterdell, J. M., Blevin, J. E., Struckmeyer, H. I. M., Bradshaw, B. E., Colwell, J. B. & Kennard, J. M. 2000. A new sequence framework for the Great Australian Bight: starting with a clean slate. *APPEA Journal* **2000**, 95–117.
- Totterdell, J. M. & Bradshaw, B. E. 2004. The structural framework and tectonic evolution of the Bight Basin. In Boulton, P. J., Johns, D. R. & Lang, S. C. (eds.) *Eastern Australasian Basins Symposium II*, 41–61. Petroleum Exploration Society of Australia, Special Publication.
- Totterdell, J. M., Bradshaw, B. E. & Willcox, J. B. 2005. Chapter 4 – structural and tectonic setting. In O'Brien, G. W. & Hibbert, J. E. (eds.) *Petroleum geology of South Australia*, vol. 5: *Great Australian Bight*, 1–57. Primary Industry and Resources of South Australia.
- Totterdell, J. M. & Krassay, A. A. 2003. *Sequence stratigraphic correlation of onshore and offshore Bight Basin successions*. Geoscience Australia Record 2003/02, 45 pp.
- Totterdell, J. M., Struckmeyer, H. I. M., Bernecker, T. & Kelman, A. P. 2014. *Bight basin, biozonation and stratigraphy*, 2013, chart 35. Geoscience Australia, Australian Government.
- Totterdell, J. M., Struckmeyer, H. I. M., Boreham, C. J., Mitchell, C. H., Monteil, E. & Bradshaw, B. E. 2008. Mid-Late Cretaceous organic-rich rocks from the eastern Bight Basin: Implications for prospectivity. In Blevin, J. E., Bradshaw, B. E. & Uruski, C. (eds.) *Eastern Australian Basins Symposium III*, 137–58. Petroleum Exploration Society of Australia, Special Publication.
- Tucholke, B. E. 2002. The Greater Antilles outer ridge: development of a distal sedimentary drift by deposition of fine-grained contourites. In Stow, D. A. V., Pudsey, C. J., Howe, J. A., Faugères, J.-C. & Viana, A. R. (eds) *Deep-water contourite systems: modern drifts and ancient series, seismic and sedimentary characteristics*, vol. **22**, 39–55. London: Geological Society, Memoirs.
- Viana, A. R., De Almeida Jr, W. & De Almeida, C. W. 2002a. Upper slope sands: late Quaternary shallow-water sandy contourites of Campos Basin, SW Atlantic Margin. In Stow, D. A. V., Pudsey, C. J., Howe, J. A., Faugères, J.-C. & Viana, A. R. (eds) *Deep-water contourite systems: modern drifts and ancient series, seismic and sedimentary characteristics*, vol. **22**, 261–70. London: Geological Society, Memoirs.
- Viana, A. R. & Faugères, J.-C. 1998. Upper slope sand deposits: the example of Campos Basin, a latest Pleistocene–Holocene record of the interaction between alongslope and downslope currents. In Stoker, M. S., Evans, D. & Cramp, A. (eds.) *Geological processes on continental margins: sedimentation, mass-wasting and stability*, vol. **129**, 287–316. London: Geological Society, Special Publications.
- Viana, A. R., Hercos, C. M., De Almeida Jr, W., Magalhães, J. L. C. & De Andrade, S. B. 2002b. Evidence of bottom current influence on the Neogene to Quaternary sedimentation along the northern Campos Slope, SW Atlantic margin. In Stow, D. A. V., Pudsey, C. J., Howe, J. A., Faugères, J.-C. & Viana, A. R. (eds) *Deep-water contourite systems: modern drifts and ancient series, seismic and sedimentary characteristics*, vol. **22**, 249–59. London: Geological Society, Memoirs.
- Wetzel, A. 1984. Bioturbation is deep-sea fine-grained sediments: influence of sediment texture, turbidite frequency and rates of environmental change. In Stow, D. A. V. & Piper, D. J. W. (eds.) *Fine-Grained sediments: deep-water processes and facies*, vol. **15**, 595–608. London: Geological Society, Special Publications.

- Wijeratne, S., Pattiaratchi, C. & Proctor, R. 2018. Estimates of surface and subsurface boundary current transport around Australia. *Journal of Geophysical Research: Oceans* **123**, 3444–66.
- Wyrwoll, K.-H., Greenstein, B. J., Kendrick, G. W. & Chen, G. S. 2009. The palaeogeography of the Leeuwin Current: implications for a future world. *Journal of the Royal Society of Western Australia* **92**, 37–51.
- Yao, W. & Shi, J. 2017. Pacific-Indian interocean circulation of the Antarctic Intermediate Water around South Australia. *Acta Oceanologica Sinica* **36**, 4–14.
-

MS received 26 November 2021. Accepted for publication 3 July 2022. First published online 12 October 2022